Synthesis and Characterization of Quantum Size Metal Oxide Colloidal Particles. Photocatalytic Peroxide Formation on ZnO and TiO_2

Thesis by

Claudius Kormann

In Partial Fulfilment of the Requirements
for the Degree of
Doctor of Philosophy

California Institute of Technology
Pasadena, California
1989

(Submitted 8 November 1988)

Meinen Eltern gewidmet.

Licht!

ACKNOWLEDGEMENTS

I would like to express my gratitude and appreciation for the help and friendship I have received from my friends and colleagues during the course of my research. I am deeply grateful to my advisor, Michael Hoffmann, for his encouragement, his advice, and the extremely tolerant guidance through these three years of our collaboration. This work would not have been possible without the warm friendship, the refreshing optimism and active support of Detlef Bahnemann to whom I am very grateful. I am also very grateful to the other members of the Hoffmann group.

I would like to thank my co–advisor, Harry Gray, for his encouragement and the other members of my examination committee for numerous useful suggestions: Henry Weinberg, Nathan Lewis, and Jim Morgan. I will never forget the stimulating discussions I was lucky to share with Jim Morgan who introduced me to the concepts of a molecular view of oxide surfaces.

Sandy Brooks, Joe Fontana and Rich Eastvedt played an invaluable role in creating an extremely friendly and efficient work environment in the Keck Laboratories; many thanks to them. Special thanks to Gabor Faludi from the glass shop for having shaped some very fine quartz reactors.

Financial support from a grant from the Environmental Protection Agency is acknowledged.

Finally, there are a number of friends behind the scenes who I consider the source of my enthusiasm, motivation, and strength for life – not only as a chemist. In particular, I am profoundly grateful to Antoinette Van Neste, Wera Eickelmann, and Ingeborg Mayr for having shared with me so many moments, adventures, feelings, insights, for having put so much faith in me, for having encouraged me ...

ABSTRACT

The syntheses of transparent colloidal solutions of extremely small ZnO (d< 5nm) and TiO_2 (d< 3 nm) particles in water, alcohol, and acetonitrile are presented. Quantum size effects are observed during particle growth and at final stages of synthesis. They are qualitatively and quantitatively (TiO_2) interpreted by using a simple molecular orbital (MO) picture and a quantum mechanical model developed by Brus. The optical absorption and fluorescence properties as well as the surface acid–base properties are characterized in detail. The two materials are shown to be active photocatalysts in the formation and degradation of H_2O_2 and organic peroxides and in the degradation of chlorinated hydrocarbons. Quantum yields and steady state concentrations are given as function of various reaction parameters such as the oxygen concentration, the nature and concentration of electron donor, pH, and charge of the electron donor. Rates of reaction are correlated with surface speciation as calculated by the SURFEQL computer code. Transparent colloidal solutions of Fe_2O_3 (hematite) have also been prepared, however only negligible photocatalytic activity is found when compared to ZnO and TiO_2. Evidence is presented for $OH^{\bullet}$ radical activity when aqueous TiO_2 suspensions are illuminated at high pH.

TABLE OF CONTENTS

OVERVIEW

The main objectives of this thesis are to elucidate the principles of the photocatalytic formation of hydrogen peroxide and to study the transformations of organic molecules in suspensions of metal oxides that are relevant to the environment. For this purpose three metal oxide systems (ZnO, TiO_2, and Fe_2O_3) have been prepared in transparent colloidal form.

Rates of formation and steady–state concentrations of hydrogen peroxide generated via the photocatalytic reduction of molecular oxygen and the concomitant oxidation of organic molecules (such as acetate or 2–propanol) have been obtained for ZnO, TiO_2, Fe_2O_3 and a sample of desert sand.

The fate of photogenerated valence band holes has been explored by studying the photocatalytic oxidation of organic anions (acetate and its chloro deratives) and cations (chloroethylammonium). The product spectra obtained for surficial photochemical oxidations have been compared with the product spectra from corresponding oxidation studies in homogeneous solution. These experiments have shown that the $OH^{\bullet}$ radical is a likely intermediate in photocatalytic oxidations of suspensions of TiO_2.

Transparent colloids offer several advantages for the study of heterogeneous photocatalysis. In addition to providing a high specific surface area for the adsorption of solutes, the transparency of such suspensions aids in the direct observation of transient and stable absorbent or fluorescent species (i.e., molecules in the homogeneous phase, surface complexes, or colloidal particles). The well defined optical properties of transparent colloidal suspensions allow photochemical quantum yields to be calculated with a high degree of accuracy.

To study the photochemical and photophysical properties of these metal oxide particles turns out to be an interesting subject. In fact, due to the small size of colloidal particles (e.g., r ≈ 25 Å for ZnO colloids, r ≈ 15 Å for TiO_2), electrostatic perturbations (from such sources as excess charge carriers) have an enhanced effect on absorption and fluorescence spectra of the crystallites.

In the course of the metal oxide synthesis (ZnO, TiO_2) characteristic spectroscopic changes are observed that accompany the particle growth which starts with molecular species ($Zn(CO_2CH_3)_2$, $TiCl_4$) and yields measurable (by transmission electron microscopy) crystallites. These effects are due to the "quantum sized" nature of the particles at early growth stages and can be interpreted using quantum mechanical models that were recently described in the literature. In addition, a molecular (MO) model has been proposed to explain the observed spectroscopic properties of extremely small particles.

Recently, it has been shown that ceramics can be made ductile at low temperature, allowing plastic deformations once a polycrystalline material was generated with a crystal size of a few nanometers. The synthetic methods developed during this thesis research for the preparation of large quantities of oxide particles (e.g., TiO_2) of extremely small sizes appear to be much less costly and energy consuming than previous methods of synthesis.

Chapter 1

INTRODUCTION

Photocatalysis on colloidal semiconductor particles has become a recognized research field over the last decade. The main impetus for much of the research has been the potential use of simple semiconductors for solar energy conversion.[1] Extremely small colloidal semiconductor particles, that fall into the transition range between molecular and bulk properties (i.e., 20 to 500 Å) have been found to exhibit properties not found in the bulk phase materials.[2–5] Colloidal semiconductors have been used as heterogenous catalysts for selected synthetic reactions.[6] In environmental systems, the potential importance of photochemically active metal oxides has not been fully recognized. For example, the photochemically induced transformation of small organic molecules and the production of hydrogen peroxide in cloudwater may be mediated by photochemically active particles.

Hydrogen peroxide, H_2O_2, appears to be the most effective oxidant in haze aerosols, clouds, and hydrometeors at low pH.[7–8] Jacob and Hoffmann have shown that the predominant pathway for the formation of sulfuric acid in humid atmospheres below pH 5 is the oxidation of sulfur dioxide by H_2O_2.[8]

Hydrogen peroxide in cloudwater has a number of gas–phase sources,[9] however, heterogeneous photosynthesis of H_2O_2 may prove to be an important source in haze aerosols, fogs, and cloudwater. Various metal oxides, some of which are abundant in natural environments, are known to act as photocatalysts for a variety of reactions.[1] The photocatalytic formation of H_2O_2 in suspensions of zinc oxide for instance is well established (see Chapter 4), however little is known about the mechanism or the nature of reactive intermediates. The photochemical formation of H_2O_2 on TiO_2 particles has been postulated,[10–11] although direct chemical evidence for the photocatalytic H_2O_2

production in colloidal suspensions of TiO_2 has not been obtained. The photochemical activity of Fe_2O_3 sols has also been established.[12–13]

Semiconductors such as Fe_2O_3, TiO_2 and ZnO are often found in aerosol samples (e.g., from desert sands [14–15]). Rates of the photochemical formation and destruction of H_2O_2 needed to be established. Furthermore, the potential role of these minerals in the photochemical transformation of organic molecules needed to be explored.

In addition, the mechanism of oxidation by photogenerated holes needed to be established. For example, oxidation of an electron donor may proceed either by direct electron transfer to a hole or via the intermediate formation of $OH^{\bullet}$ radicals on the surface (cf. Figure 1).

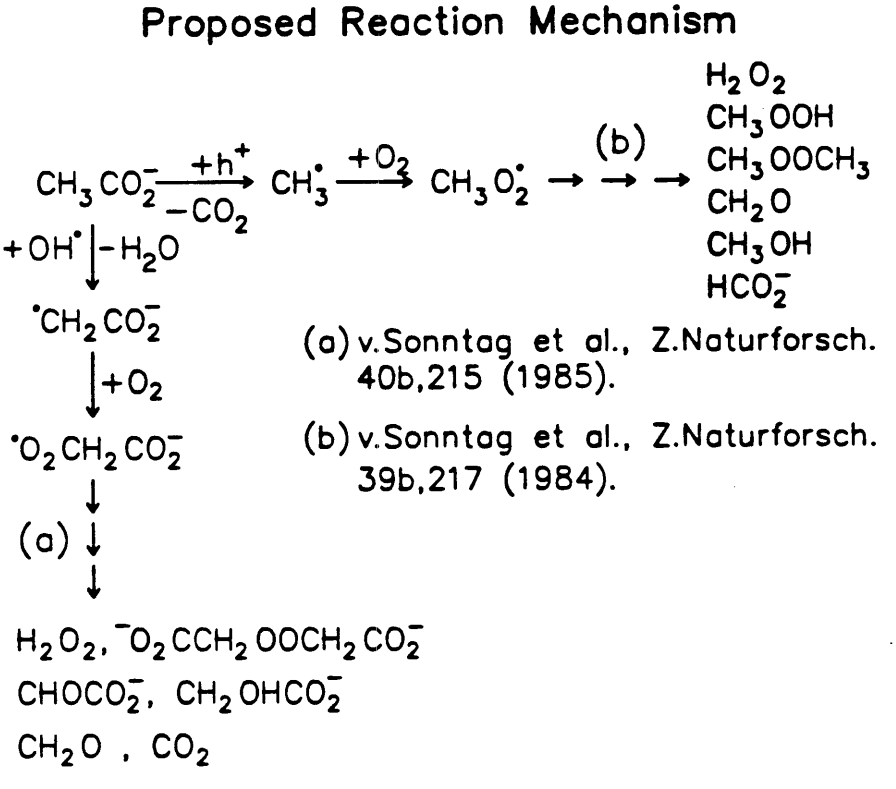

Figure 1

Oxidation of Acetate

Charge–transfer reactions at the interface between a semiconductor and the aqueous medium may provide a route for the conversion of solar energy through water photolysis. While the reduction process initiated by transfer of conduction band electrons is fairly well understood, the fate of the highly oxidizing valence band holes, generated upon illumination of wide bandgap semiconductors such as TiO_2, ZnO, and Fe_2O_3 is less well known. By determining the photo–oxidation products starting from small organic molecules and by comparing the results obtained with those from γ– and pulse– radiolytic studies performed in homogeneous solutions,[16–17] evidence will be obtained for likely reaction intermediates (Figure 2).

The synthesis of transparent aqueous ZnO colloids has been reported only recently (Chapter 2), yet there are no reports about detailed mechanistic studies of photochemically induced H_2O_2 formation on semiconductor particles in the literature.

General concepts of semiconductor redox–chemistry

In general, the photoinduced redox chemistry of semiconductor surfaces can be represented simply as

$$\text{semiconductor} \quad \underset{h\nu/\text{heat}}{\overset{h\nu}{\rightleftharpoons}} \quad e^-(cb) + h^+(vb) \qquad (1)$$

Absorption of a photon with an energy equal to or greater than the bandgap energy [19] (cf. Figure 2) leads to the formation of an electron/hole pair in the semiconductor particle. It should be noted that under steady state illumination with an actinometry on the order of 5×10^{-6} Einstein/l·s (assuming 100% absorption) and a particle concentration of about 10^{-6} mol/l the average time lag

between two effective hits is on the order of 0.2 s. The lifetime of an electron–hole pair depends on the energetic structure of the semiconductor particle (e.g. the density of states in the bandgap and the density of non–reactive vibrational relaxation channels) and was found to be (30 ± 15) ns in a 120 Å sized TiO_2 particle.[20]

It is assumed that the solution surrounding the semiconductor particle contains electron acceptors A (e.g., O_2 or methylviologen) and electron donors D (e.g., 2–propanol, acetate) as shown in Figure 2. There are two conceptionally different ways in which an overall redox reaction between a donor D and an acceptor A can be driven by illuminated semiconductor particles.

$$D + A \longrightarrow D^{+\bullet} + A^{-\bullet} \qquad (2)$$

If the overall reaction is endothermic ($\Delta G^0 > 0$) like, for example, the splitting of H_2O in H_2 and O_2, no material will be able to catalyze this process under normal (thermal) conditions (i.e., 25 ^{0}C and 1 atm). Under these circumstances, a semiconductor would act as a photosensitizer generating chemical molecules on a higher energy level than the parent compounds (see left side of Fig. 2). Since the back reaction in this case is exothermic it is crucial for continuous photosynthetic activity to separate the products. If reaction (2) is exothermic ($\Delta G^0 < 0$) but kinetically hindered by high activation energies (E_a) then semiconductors act as photocatalysts (see right side of Fig. 2) resulting in an overall lowering of E_a. Actually, in many systems one encounters two subsequent one–electron transfers, where the first transfer is slightly endothermic and the second step is strongly exothermic, resulting in an overall exothermic redox reaction. This behavior is illustrated in Figure 3 for an idealized photoassisted redox reaction between oxygen and acetate.

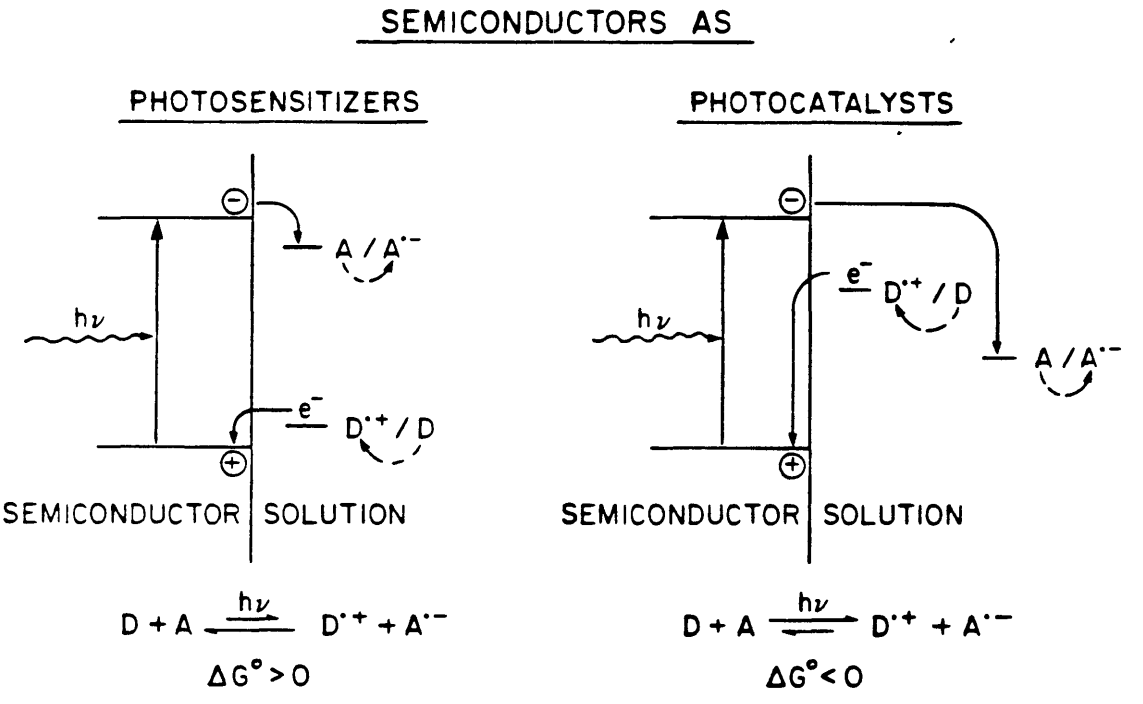

Figure 2

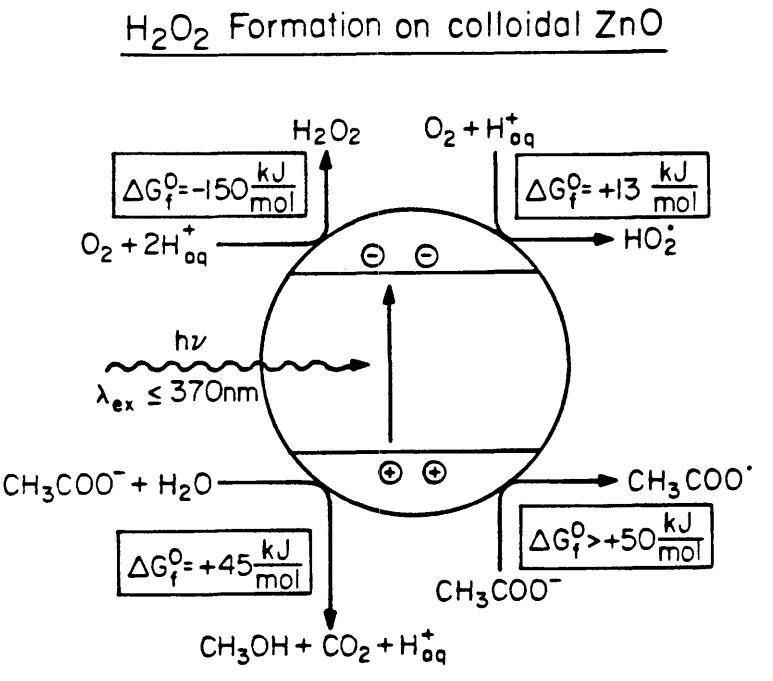

Figure 3

On the right side of Fig. 3 the enthalpy change for the first electron transfer is found to be endothermic. The left side of Fig. 3 shows the free enthalpy changes for two–electron transfers. The overall change (–150+45) kJ/mol = –105 kJ/mol indicates that the reaction of O_2 with acetate is exothermic. The majority of reactions studied as a part of this research can be classified as overall exothermic and hence photocatalytic.

Objectives: In order to study photocatalytic transformations of molecules, i.e., the formation of hydrogen peroxide by oxygen reduction and the oxidation of organic molecules the oxide catalysts had to be synthesized in a well defined form that also allows fast spectroscopic measurements. The synthesis and characterization of colloidal zinc oxide which exhibits quantum size properties is described in Chapter 2. Titanium dioxide colloids were also shown to exhibit quantum size effects once the synthesis was carried out under tightly controlled conditions (Chapter 3). Special emphasis was laid on the characterization of the surface acid–base chemistry that determines the surface charge of the particles. Photochemical experiments were conducted to obtain quantitative insight into the factors that determine the rates of formation and degradation of H_2O_2 and organic peroxides in aqueous suspensions of selected metal oxides (Chapter 4). Chapter 5 which has been published in the ACS symposium series 349 gives a broad overview of the principles that govern the fate of hydrogen peroxide in the atmospheric environment. The objectives of Chapter 6 are to compare the photocatalytic activity of three metal oxide systems: ZnO, TiO_2, and Fe_2O_3. Chapter 7 is a contribution to the ongoing discussion on how the oxidizing species behaves that is generated after photoexcitation of TiO_2 particles. Does it have the reactivity of a hole or an $OH^{\bullet}$ radical? Chapter 8 concludes this thesis with recommendations for future research.

REFERENCES

1. Fendler, J. H. *J. Phys. Chem.* 1985, **89**, 2730.
2. Brus, L. E. *J. Phys. Chem.* 1986, **90**, 2555.
3. Henglein, A. *Pure Appl. Chem.* 1984, **56**, 1215.
4. Rossetti, R.; Ellison, J. L.; Gibson, J. M.; Brus, L. E. *J. Chem. Phys.* 1984, **80**, 4464.
5. Fojtik, A.; Weller, H.; Koch, U.; Henglein, A. *Ber. Bunsenges. Phys. Chem.* 1984, **88**, 969.
6. Fox, M. A. *Acc. Chem. Res.* 1983, **16**, 314.
7. McArdle, J. V.; Hoffmann, M. R. *J. Phys. Chem.* 1983, **87**, 5425.
8. Jacob, D. J.; Hoffmann, M. R. *J. Geophys. Res.* 1983, **88**, 6611
9. McElroy, W. J. *Atmos. Environ.* 1986, **20**, 427.
10. Kraeutler, B.; Bard, A. J. *J. Am. Chem. Soc.* 1978, **100**, 5985.
11. Jaeger, C. D.; Bard, A. J. *J. Phys. Chem.* 1979, **83**, 3146.
12. Moser, J.; Grätzel, M. *Helv. Chim. Acta* 1982, **65**, 1436.
13. Faust, B. C.; Hoffmann, M. R. *Environ. Sci. Technol.* 1986, **20**, 943.
14. Schrauzer, G. N.; Strampach, N.; Nan Hui, L.; Palmer, M. R.; Salehi, J. *Proc. Natl. Acad. Sci. USA* 1983, **80**, 3873.
15. Schütz, L.; Rahn, K. A. *Atmosph. Environ.* 1982, **16**, 171
16. Schuchmann et al. *Z. Naturforsch.* 1985, **40b**, 215.
17. Schuchmann, H.–P.; von Sonntag, C. *Z. Naturforsch.* 1984, **39b**, 217.
18. Bahnemann, D.; Henglein, A.; Spanhel, L. *Faraday Discuss. Chem. Soc.* 1984, **78**, 151.
19. Gerischer, H. *Topics in Applied Physics* 1979, **31**, 121.
20. Rothenburger et al. *J. Am. Chem. Soc.* 1985, **107**, 8054.

Chapter 2

PREPARATION AND CHARACTERIZATION OF QUANTUM SIZE ZINC OXIDE: A DETAILED SPECTROSCOPIC STUDY

[The text of this chapter appeared in: Detlef W. Bahnemann, Claudius Kormann, and Michael R. Hoffmann, J. Phys. Chem., 1987, **91**, 3789.]

J. Phys. Chem. 1987, 91, 3789-3798

Preparation and Characterization of Quantum Size Zinc Oxide: A Detailed Spectroscopic Study

Detlef W. Bahnemann,† Claudius Kormann, and Michael R. Hoffmann*

W. M. Keck Laboratories, California Institute of Technology, Pasadena, California 91125
(Received: November 5, 1986; In Final Form: March 18, 1987)

We report the synthesis of transparent colloidal suspensions of small zinc oxide particles in water, 2-propanol, and acetonitrile. Quantum (Q)-size effects are observed during particle growth and qualitatively interpreted by using a simple molecular orbital (MO) picture. The particles at the final stage of growth are approximately spherical in shape and consist of 2000–3000 ZnO molecules. They exhibit many of the photophysical properties of bulk zinc oxide. However, pronounced shifts in the absorption spectrum during the illumination of anoxic suspensions of ZnO reveal a distinctively different behavior of these small particles. Fluorescence spectra of the ZnO sols suggest that adsorbed electron relays are necessary to shuttle electrons from the conduction band into lower lying traps. Two fluorescence maxima are observed at the final growth stage of the ZnO particles. The bandgap fluorescence at 365 nm has an extremely short lifetime ($\tau < 100$ ps), while the visible luminescence at 520 nm exhibits a slower biexponential decay (i.e., $\tau = 14$ and 190 ns). The latter fluorescence is attributed to photogenerated electrons tunneling to preexisting, trapped holes. The low overall fluorescence quantum yield of $\Phi = 0.03$ measured in these zinc oxide suspensions is indicative of radiationless transitions accompanying the emissions. A pronounced pH dependence of the Stern–Volmer constants obtained with various ionic substances, that effectively quench the 520-nm emission, is explained by specific adsorption to the charged particle surface. The zero point of charge (pH_{zpc}) of the aqueous colloidal suspension was determined to be 9.3 ± 0.2 by several independent methods.

Introduction

The photoelectrochemistry of small semiconductor particles has been an area of active research.[1-3] Recently, there has been a growing interest in ultrasmall particles[4-28] that fall into the transition range between molecular and bulk properties (i.e., with diameters from 1 to 10 nm).[4] Bulk semiconductors exhibit a pronounced increase in light absorption when photon energies exceed the bandgap energy (E_g); however, the photophysics of ultrasmall semiconductor particles is substantially different. Quantum mechanical calculations[4-6] and experimental observations[7-28] suggest that the energy level of the first excited state of the exciton increases with decreasing particle size thus leading to a blue shift in the absorption spectrum. Particle growth results in spectral shifts from an absorption onset (λ_{os}) in the UV for dimers and oligomers to a λ_{os} for the bulk material in the visible or near-IR. In several cases, a concomitant shift in the visible fluorescence (i.e., with $\lambda_{em} > \lambda_{os}$) has been noted.[14-17,19,21] Koch et al.[21] have reported a shift of the onset of absorption of ZnO colloids from 310 to 360 nm during particle growth in 2-propanol, while at the same time the maximum of the fluorescence peak shifted from 460 to 540 nm. Their paper also describes the preparation of an aqueous colloidal suspension of ZnO which, however, requires the presence of a colloid stabilizer, e.g., hexametaphosphate.[21]

α-Fe_2O_3,[29-31] WO_3,[32] and TiO_2[33-35] can be synthesized as transparent colloids in water; however, synthesis of ZnO in H_2O is not readily achieved (e.g., $\Delta G_f° = -0.39$ kJ mol^{-1} for reaction 1 at 25 °C; $\Delta G_f° = -2.79$ kJ mol^{-1} at 100 °C, $\Delta G_f° = 0$ at 13 °C).[36]

$$Zn(OH)_2 \rightleftharpoons ZnO + H_2O \qquad (1)$$

Furthermore, Schindler et al.[37-39] have shown that the dissolution rate of ZnO increases with decreasing particle size. In this respect we report a novel method for the synthesis of transparent ZnO colloids that are stable both in organic and in aqueous suspensions in the absence of stabilizers. In addition, we provide an analysis of the dynamic changes in spectral properties of transparent colloidal suspensions of ZnO that take place during particle growth.

Crystalline ZnO exhibits a characteristic fluorescence spectrum with two maxima around 380 and 500 nm.[40-51] The emission at $\lambda_{em} = 380$ nm has been attributed to the exciton band;[44,51] however, no conclusive interpretation for the visible fluorescence

† Permanent address: Bereich Strahlenchemie, Hahn-Meitner Institut Glienicker Strasse 100, D1000 Berlin 39, West Germany.

(1) Grätzel, M. *Acc. Chem. Res.* **1981**, *14*, 376.
(2) Fendler, J. H. *J. Phys. Chem.* **1985**, *89*, 2730.
(3) Bockris, J. O'M.; Dandapani, B.; Cocke, D.; Ghoroghchian, J. *Int. J. Hydrogen Energy* **1985**, *10*, 179.
(4) Brus, L. E. *J. Phys. Chem.* **1986**, *90*, 2555.
(5) Brus, L. E. *J. Chem. Phys.* **1983**, *79*, 5566.
(6) Brus, L. E. *J. Chem. Phys.* **1984**, *80*, 4403.
(7) Ekimov, A. I.; Onushchenko, A. A. *JETP Lett.* **1981**, *34*, 345.
(8) Ekimov, A. I.; Onushchenko, A. A. *JETP Lett.* **1984**, *40*, 1136.
(9) Ekimov, A. I.; Efros, Al. L.; Onushchenko, A. A. *Solid State Commun.* **1985**, *56*, 921.
(10) Rossetti, R.; Nakahara, S.; Brus, L. E. *J. Chem. Phys.* **1983**, *79*, 1086.
(11) Rossetti, R.; Ellison, J. L.; Gibson, J. M.; Brus, L. E. *J. Chem. Phys.* **1984**, *80*, 4464.
(12) Rossetti, R.; Hull, R.; Gibson, J. M.; Brus, L. E. *J. Chem. Phys.* **1985**, *82*, 552.
(13) Rossetti, R.; Hull, R.; Gibson, J. M.; Brus, L. E. *J. Chem. Phys.* **1985**, *83*, 1406.
(14) Chestnoy, N.; Harris, T. D.; Hull, R.; Brus, L. E. *J. Phys. Chem.* **1986**, *90*, 3393.
(15) Weller, H.; Koch, U.; Gutiérrez, M.; Henglein, A. *Ber. Bunsen-Ges. Phys. Chem.* **1984**, *88*, 649.
(16) Fojtik, A.; Weller, H.; Koch, U.; Henglein, A. *Ber. Bunsen-Ges. Phys. Chem.* **1984**, *88*, 969.
(17) Weller, H.; Fojtik, A.; Henglein, A. *Chem. Phys. Lett.* **1985**, *117*, 485.
(18) Fischer, Ch.-H.; Weller, H.; Fojtik, A.; Lume-Pereira, C.; Janata, E.; Henglein, A. *Ber. Bunsen-Ges. Phys. Chem.* **1986**, *90*, 46.
(19) Fojtik, A.; Weller, H.; Henglein, A. *Chem. Phys. Lett.* **1985**, *120*, 552.
(20) Baral, S.; Fojtik, A.; Weller, H.; Henglein, A. *J. Am. Chem. Soc.* **1986**, *108*, 375.
(21) Koch, U.; Fojtik, A.; Weller, H.; Henglein, A. *Chem. Phys. Lett.* **1985**, *122*, 507.
(22) Weller, H.; Schmidt, H. M.; Koch, U.; Fojtik, A.; Baral, S.; Henglein, A.; Kunath, W.; Weiss, K.; Dieman, E. *Chem. Phys. Lett.* **1986**, *124*, 557.
(23) Henglein, A.; Kumar, A.; Janata, E.; Weller, H. *Chem. Phys. Lett.* **1986**, *132*, 133.
(24) Tanaka, T.; Iwasaki, M. *J. Photogr. Sci.* **1983**, *31*, 13.
(25) Tanaka, T.; Iwasaki, M. *J. Imaging Sci.* **1985**, *29*, 86.
(26) Itoh, T.; Kirihara, T. *J. Lumin.* **1984**, *31&32*, 120.
(27) Nozik, A. J.; Williams, F.; Nenadović, M. T.; Rajh, T.; Micic, O. I. *J. Phys. Chem.* **1985**, *89*, 397.
(28) Sandroff, C. J.; Hwang, D. M.; Chung, W. M. *Phys. Rev. B* **1986**, *33*, 5953.
(29) Stramel, R. D.; Thomas, J. K. *J. Colloid Interface Sci.* **1986**, *110*, 121.
(30) Penners, N. H. G.; Koopal, L. K. *Colloids Surf.* **1986**, *19*, 337.
(31) Bahnemann, D. W.; Kern, J.; Hoffmann, M. R., manuscript in preparation.
(32) Suda, H.; Imai, N. *J. Colloid Interface Sci.* **1985**, *104*, 204.
(33) Duonghong, D.; Ramsden, J.; Grätzel, M. *J. Am. Chem. Soc.* **1982**, *104*, 2977.
(34) Bahnemann, D.; Henglein, A.; Lilie, J.; Spanhel, L. *J. Phys. Chem.* **1984**, *88*, 709.

0022-3654/87/2091-3789$01.50/0 © 1987 American Chemical Society

peak has been given previously.[43,45-50] A detailed study of the fluorescence behavior of the zinc oxide sols thus affords further insight into its mechanism.

Experimental Section

Chemicals and solvents were of reagent grade and used without further purification. The water employed in all preparations was purified by a Milli-Q/RO system (Millipore) resulting in a resistivity of >18 MΩ cm. Reflectance spectra of powder samples with $BaSO_4$ as a reference were obtained with a Shimadzu MPS-2000 spectrophotometer equipped with an integrating sphere. The same instrument and a HP 8451A diode array spectrophotometer were used to measure UV/vis absorption spectra. Fluorescence spectra were recorded using a Shimadzu RF 540 spectrofluorometer. Appropriate filters to avoid second-order contributions were installed in the excitation and emission light paths. Fluorescence quantum yields were measured with 6×10^{-5} M quinine sulfate in 1 N H_2SO_4 as a reference standard.[52] All steady-state spectra were measured at 25 °C.

Particle sizes were determined by transmission electron microscopy (TEM). To prepare the TEM samples a drop of the colloidal suspension was applied for 30 s to a copper mesh covered with a carbon film and subsequently removed with a paper tip. Adhesion of the particles was promoted by exposing the carbon film to a glow discharge prior to this procedure.

The irradiation apparatus consisted of an Osram XBO 450-W xenon lamp in a Müller LX 1450-2 lamp housing and a GM 252 (Kratos) monochromator with the appropriate UV filters. Actinometry was performed with (*E*)-2-(2,5-dimethyl-3-furylethylidene)(isopropylidene)succinic anhydride in toluene according to the method of Heller.[53]

In order to assess the fluorescence yield of the colloidal suspensions under various oxygen partial pressures 3-mL aliquots were bubbled for 20 min with an O_2/N_2 gas mixture. While recording the fluorescence spectra, the suspensions were kept silent being still covered by the O_2/N_2 atmosphere. Since prolonged agitation of the aqueous sols leads to coagulation of the colloid (the isopropanolic colloid is found to be more stable), fresh samples were prepared for each measurement. In order to determine the dependency of the fluorescence yield on the H_2O_2 concentration for oxygen free suspensions, 3-mL aliquots containing calibrated amounts of H_2O_2 were subjected to at least three freeze–pump–thaw cycles ($p \leq 10^{-5}$ Torr) before the measurement.

Fluorescence decay times were measured in collaboration with Douglas Magde at the University of California, San Diego. Details of the experimental setup have been described elsewhere.[54] Colloidal suspensions of ZnO in 2-propanol or in water were excited with short laser pulses (≤10 ps) at 330 nm and the fluorescence decays were followed at 365 nm and at 520 nm. It was ascertained by the use of small pulse energies (with $\simeq 10^6$ photons/pulse absorbed in a volume $\geq 10^{-5}$ cm^3) that the absorbed photon number per pulse did not exceed a thousandth of the ZnO particle concentration; 4×10^9 pulses were averaged in each experiment.

Various compounds, i.e., organic or inorganic anions or cations, were examined as quenchers of the emission. Stern–Volmer-type plots were used to analyze data relating the fluorescence intensity of a sol containing a known concentration of quenching agent to the intensity of a pure colloidal sol. The excitation wavelength was 330 nm.

Preparation of Colloidal ZnO in 2-Propanol, Water, and Acetonitrile. For a typical preparation 1 mmol of $Zn(OAc)_2$ (zinc acetate) was dissolved in 80–90 mL of 2-propanol under vigorous stirring at ≃50 °C and subsequently diluted to a total volume of 920 mL. 80 mL of a 2×10^{-2} M NaOH solution in 2-propanol (pellets of sodium hydroxide dissolved in 2-propanol at ≃50 °C) was then added at 0 °C within 1 min under continuous stirring. The mixture was then immersed for 2 h into a water bath preheated to 65 °C. After 3 days of further aging at room temperature the solvent was removed by rotary evaporation (conditions: 30 °C, 1 Torr) of 10–50-mL aliquots of the isopropanolic ZnO colloid. The remaining hygroscopic white film was immediately resuspended in water to yield a transparent aqueous colloid (pH 7.7). Acetonitrile also dissolved the film yielding colloidal ZnO in an organic solvent.

A flow system consisting of a 250-mL thermostated reactor connected through short silicon and Tygon tubes with a Masterflex peristaltic pump (flow rate ca. 100 mL/min) and a flow cell (Hellma No. 176.50, light path 10 mm, height 11 mm, width 4 mm) was used for investigations of the time evolution of the absorption spectra. Mixtures of the zinc salt and the NaOH solutions in 2-propanol were prepared at the desired temperature and immediately introduced into the flow system. Spectra were recorded for 1 s at regular intervals with the HP 8451A diode array spectrophotometer and stored for further treatment. UV cutoff filters were used when appropriate.

Characterization of the Surface of the Colloidal Particles. Titrations of 40-mL samples of 1×10^{-3} M aqueous colloidal ZnO, thermostated to 25 °C, were carried out with a Radiometer autotitration system consisting of a pHM84 pH meter, a TTT80 titrator, and a ABU80 autoburet. A vigorously stirred suspension of ZnO colloid was titrated with freshly prepared 1×10^{-2} M stock solutions of NaOH (N_2 bubbled) or HCl at a rate of 10 μmol min^{-1}.

Coagulation studies were performed using the above-described flow system at 25 °C and monitoring the absorption changes in the visible (λ_{obsd} = 500 nm). The lack of any absorption of zinc oxide at this wavelength due to electronic transitions allows the observation of particle coagulation that results in an increase in light scattering of the solution (i.e., an increase of the apparent absorption due to forward scattering). In typical experiments, 40 mL of 1×10^{-3} M aqueous colloidal ZnO solutions was titrated at a rate of 5×10^{-7} mol min^{-1} starting at pH 7.6 with a 1×10^{-2} M solution of NaOH, while the absorbance was recorded. The first derivative of the absorption vs. time profile yielded the coagulation rate as a function of pH.

Results

The UV/vis absorption spectra recorded at various times during the preparation of a stable transparent suspension of ZnO colloid in 2-propanol are shown in Figure 1a. Thirteen seconds after mixing the zinc acetate with the base solution at 0 °C an onset of absorption (determined by the linear extrapolation of the steep part of the UV absorption toward the base line) λ_{os} = 306 nm is observed. The absence of any detectable particles in the electron

(35) Bahnemann, D.; Henglein, A.; Spanhel, L. *Faraday Discuss. Chem. Soc.* **1984**, *78*, 151.
(36) Weast, R. C., Astle, M. J., Beyer, W. H., Eds. *CRC Handbook of Chemistry and Physics*; CRC: Boca Raton, FL, 1985-86; Vol. 66, p D-92.
(37) Schindler, P.; Althaus, H.; Feitknecht, W. *Gazz. Chim. Ital.* **1963**, *93*, 168.
(38) Schindler, P.; Althaus, H.; Feitknecht, W. *Helv. Chim. Acta* **1964**, *47*, 982.
(39) Schindler, P.; Althaus, H.; Hofer, F.; Minder, W. *Helv. Chim. Acta* **1965**, *48*, 1204.
(40) Beutel, E.; Kutzelnigg, A. *Monatsh. Chem.* **1930**, *55*, 158.
(41) Bancroft, W. D.; Gurchot, C. *J. Phys. Chem.* **1932**, *36*, 2575.
(42) Nicoll, F. H. *J. Opt. Soc. Am.* **1948**, *38*, 817.
(43) Mollwo, E. *Z. Phys.* **1954**, *138*, 478.
(44) Hecht, H.; Mollwo, E. *Solid State Commun.* **1971**, *9*, 2167.
(45) Mollwo, E.; Zwingel, D. *J. Lumin.* **1976**, *12/13*, 441.
(46) Heiland, G.; Mollwo, E.; Stöckmann, F. *Solid State Physics*; Academic: London, 1959; Vol. 9, p 191.
(47) Riehl, N.; Ortmann, H. *Ber. Bunsen-Ges. Phys. Chem.* **1956**, *60*, 149.
(48) Dingle, R. *Phys. Rev. Lett.* **1969**, *23*, 579.
(49) Bhushan, S.; Pandey, A. N.; Kaza, B. R. *J. Lumin.* **1979**, *20*, 29.
(50) Takata, S.; Minami, T.; Nanto, H.; Kawamura, T. *Phys. Status Solids A* **1981**, *65*, K83.
(51) Minami, T.; Nanto, H.; Takata, S. *Thin Solid Films* **1983**, *109*, 379.
(52) Demas, J. N.; Crosby, G. A. *J. Phys. Chem.* **1971**, *75*, 991.
(53) Heller, H. G.; Langan, J. R. *J. Chem. Soc., Perkin Trans. 2* **1981**, 341.
(54) Skibfted, L. H.; Hancock, M. P.; Magde, D.; Sexton, D. A. *Inorg. Chem.*, submitted for publication.

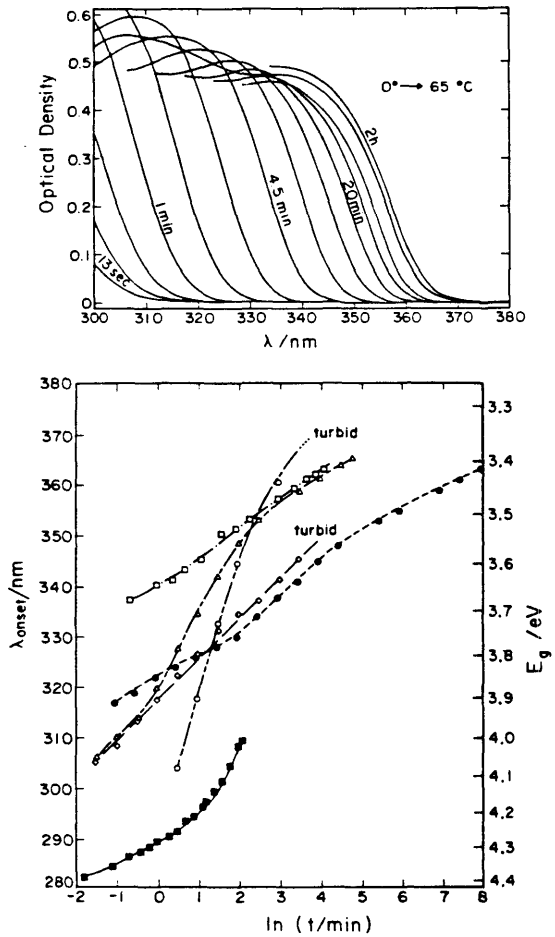

Figure 1. (a, upper) Absorption spectra taken at various times (logarithmic time scale) after mixing 1.0×10^{-3} M $Zn(OAc)_2$ with 1.6×10^{-3} M NaOH in 2-propanol at 0 °C for 1 min. Thereafter the solution is immersed into a preheated water bath at 65 °C. (b, lower) Onset of absorption as a function of time for various preparations of ZnO in 2-propanol: (□) 50 °C, (●) 25 °C, (■) 8 °C, with 3.3×10^{-3} M $Zn(OAc)_2$ and 3.3×10^{-3} M NaOH; (△) 0 °C → 65 °C, with 1.0×10^{-3} M $Zn(OAc)_2$ and 1.6×10^{-3} M NaOH; (◇) 25 °C, (○) −10 °C → 65 °C, with 1.0×10^{-3} M $Zn(ClO_4)_2$ and 1.6×10^{-3} M NaOH.

micrographs taken with a freshly prepared sample indicates that only extremely small ZnO particles are present at this stage (species with diameters $d \leq 5$ Å fall below the detection limit of the TEM). Upon continuous heating for 2 h at 65 °C λ_{os} steadily shifts toward 365 nm. Electron microscopy reveals that the reaction mixture now contains almost spherical particles with a mean diameter of 50 Å and a relatively narrow size distribution (±5 Å) as shown in Figure 2a. Plots of λ_{os} vs. the logarithm of the reaction time are given in Figure 1b for the results shown in Figure 1a as well as for various isothermal preparations. Data of analogous experiments using zinc perchlorate instead of zinc acetate are also presented in this diagram. Despite a rather similar dynamic behavior the formation of turbid suspensions is indicated with perchlorate as the anion; i.e., coagulation of the particles takes place. The linearity of this semilogarithmic presentation in the case of isothermal syntheses at 25 and 50 °C reveals that the spectral shift is strongly retarded toward the end of the preparation.

Some other features should be noted from the growth curves shown in Figure 1b:

The pronounced temperature dependence of the particle growth suggests that activation and not diffusion-controlled processes occur. A reaction mixture of acetate and base kept at 25 °C, for instance, needs 50 h to reach the same onset of absorption (363 nm) as an identical mixture at 50 °C after 1 h.

The choice of the anion is critical for the preparation of transparent, stable ZnO colloids. It has already been mentioned that the use of zinc perchlorate instead of zinc acetate yields a turbid suspension. λ_{os} initially changes more slowly in the case of zinc perchlorate. However, after a few minutes at 65 °C, when $\lambda_{os} = 360$ nm is reached, the colloid coagulates. A preparation made up of zinc acetate and base remains transparent for more than 2 h at 65 °C before precipitation. Experiments with $ZnCl_2$ or $Zn(NO_3)_2$ and otherwise similar reaction conditions reveal an even faster coagulation than in the case of $Zn(ClO_4)_2$ following the initial formation of a clear colloidal suspension.

A strong visible fluorescence is noted for all colloidal suspensions of ZnO. Figure 3 shows absorption and fluorescence spectra of isopropanolic suspensions of ZnO colloid at various growth stages. Excitation wavelengths for the fluorescence spectra were chosen to ensure identical absorbancies of the suspensions. As illustrated in Figure 3, the absorption spectra of freshly prepared colloidal suspensions of ZnO are characterized by blue-shifted onsets of absorption. Furthermore, pronounced absorption maxima ≈25 nm below λ_{os} are noted for the young preparations. Their fluorescence spectra (shown on the right-hand side of Figure 3) exhibit a single broad fluorescence band with an initial maximum around 460 nm. Concomitant to the changes of λ_{os} a bathochromic shift of this visible emission is perceived upon aging of the colloid. In fact the visible fluorescence appears to be consistently red-shifted by 155 ± 5 nm compared to λ_{os}. While the former peak changes from 460 to 516 nm, its intensity passes through a maximum with the highest fluorescence quantum yield of $\phi = 0.16$ measured for a sample that had been reacting at 25 °C for 2 min. After the colloidal suspension has been aged either by heat treatment or long reaction times (i.e., the ZnO colloids have reached their final growth stage as defined by a value of 365 nm for λ_{os}), a second fluorescence is encountered at 365 nm coinciding with the onset of the absorption spectrum. However, young ZnO colloids do not exhibit this fluorescence band.

Absorption and fluorescence spectra of an aqueous colloidal suspension containing 1×10^{-3} M zinc oxide at pH 7.7 are shown in Figure 4. The absence of absorption above 370 nm indicates that this suspension does not scatter light to any appreciable extent in the visible part of the spectrum. This is consistent with the observation (see TEM in Figure 2b) that particle sizes and size distribution have not changed during the preparation of the aqueous sample. However, upon comparison of parts a and b of Figure 2, the formation of chains of ZnO particles is obvious in the latter. Similar observations have been made before during the electron microscopy of aqueous TiO_2 colloids.[55] It is not yet clear whether these chains were already present in solution or were formed upon preparation of the samples for TEM. Recent investigations in this laboratory show the absence of comparable aggregation effects during the electron microscopy of aqueous α-Fe_2O_3 colloids.[56]

The onset of the absorption spectrum for the aqueous suspension, which is shown in Figure 4 is located also at 365 nm. Two maxima are again observed in the fluorescence spectrum, one coinciding with λ_{os} and a green emission at 520 nm. Fast titration to pH 12 likewise yields a transparent sol with similar spectral features.

The reflection and fluorescence spectra of zinc oxide powder (Baker, U.S.P.) are given in parts a and b of Figure 5, respectively. The white powder absorbs practically all UV light below 370 nm (i.e., with energies greater than 3.35 eV). Two fluorescence maxima are noted in the emission spectrum when the powder sample is irradiated with UV light ($\lambda_{ex} \leq 370$ nm). A first sharp fluorescence peak (fwhm ≈ 15 nm) appears at 380 nm, coinciding with the onset of the reflectance drop (Figure 5a). The second

(55) Spanhel, L. Diplomarbeit, Technische Universität Berlin, FRG, FB 6, 1985.

(56) Bahnemann, D. W.; Hoffmann, M. R., unpublished results.

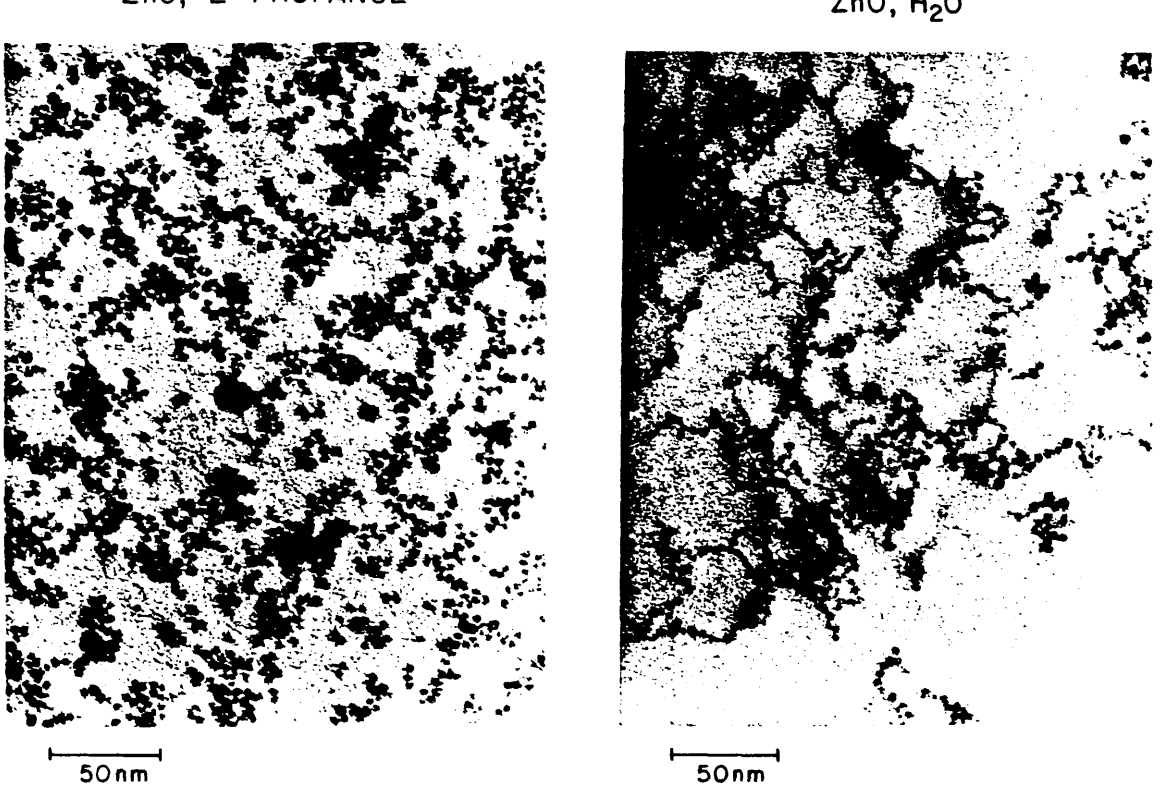

Figure 2. Transmission electron micrographs of ZnO colloid in (a, left) 2-propanol and (b, right) water.

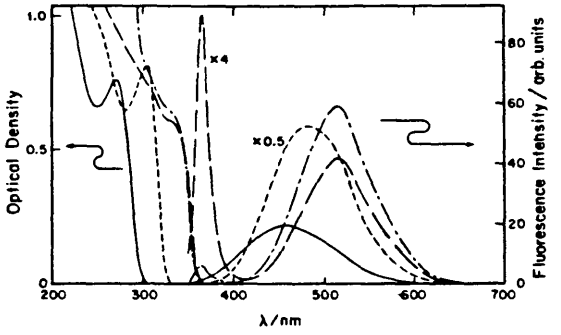

Figure 3. Superposition of absorption and fluorescence spectra measured in 2-propanol at various times after mixing 1.0×10^{-3} M $Zn(OAc)_2$ with 1.6×10^{-3} M NaOH: —, 30 s at 25 °C, after mixing at 0 °C ($\lambda_{ex}^{n} = 280$ nm); ---, 15 min at 25 °C ($\lambda_{ex}^{n} = 310$ nm); – – –, 2 h at 50 °C, 15 h at 25 °C ($\lambda_{ex}^{n} = 340$ nm); – – –, 2 h at 65 °C, 70 h at 25 °C ($\lambda_{ex}^{n} = 340$ nm).

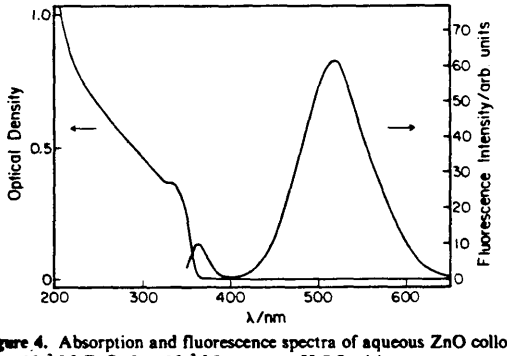

Figure 4. Absorption and fluorescence spectra of aqueous ZnO colloid (1×10^{-3} M ZnO, 2×10^{-3} M acetate, pH 7.7, air).

rather wide (fwhm ≈ 90 nm) green fluorescence band has its maximum around 510 nm.

Titration experiments have been conducted to determine the acid–base properties of colloidal ZnO. The initial pH of a 1×10^{-3} M aqueous suspension of ZnO colloid containing 2×10^{-3} M acetate (this anion is inherently present in all samples from their preparation) is 7.7 as shown in Figure 6. Titration with base promotes coagulation, while titration with acid leads to the dissolution of the colloid below pH 7.4. Figure 6 clearly shows that the pH increases upon addition of aqueous NaOH and eventually passes through an inflection point at pH 9.3 (after 45 μmol of base, i.e., 4.5 mL of a 1×10^{-2} M NaOH solution, have been added to 40 mL of 1×10^{-3} M ZnO). On the other hand, 100 μmol of HCl can be added with no pronounced change in pH, indicating a significant buffering capacity of the oxide system. Another inflection point is noted at pH 6.4. The slow drop of pH below pH 5.5 is well explained by the buffering capacity of the acetate.

Plots of the intensities of the UV ($\lambda_{em} = 365$ nm) and the green ($\lambda_{em} = 516$ or 520 nm) fluorescence as a function of the O_2 partial pressure are shown in parts a and b of Figure 7 for 3.3×10^{-4} M colloidal suspensions of ZnO in 2-propanol and water, respectively. While a similar qualitative behavior is observed in both cases, the fluorescence intensities of the isopropanolic are almost 1 order of magnitude larger than those of the aqueous colloid. Only 20% of this difference is due to the higher extinction coefficient of the isopropanolic sol at the excitation wavelength.

Both fluorescence peaks are initially present in carefully evacuated samples of ZnO. Upon exposure to the weak monochromatic light of the spectrofluorometer ($\lambda_{ex} = 330$ nm) a noticeable dynamic behavior is observed. The green emission is

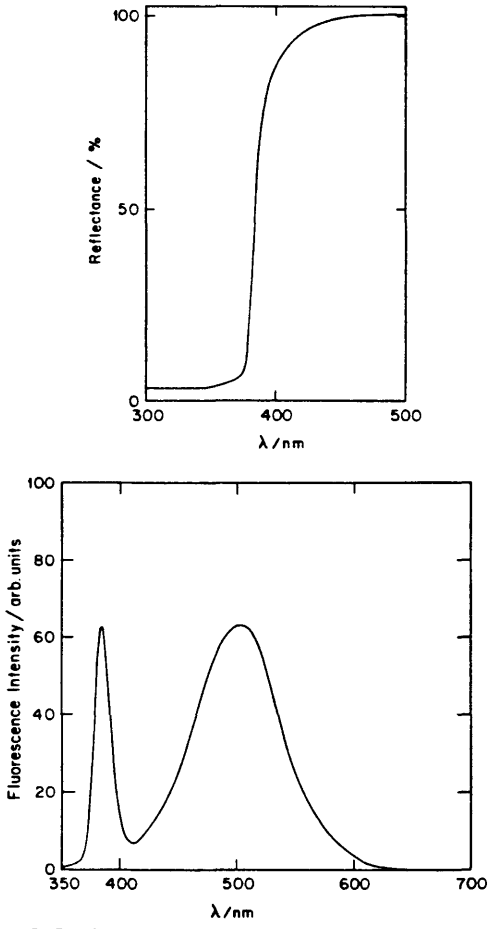

Figure 5. Powder spectra of ZnO crystals: (a, upper) reflectance and (b, lower) fluorescence, λ_{ex} = 320 nm.

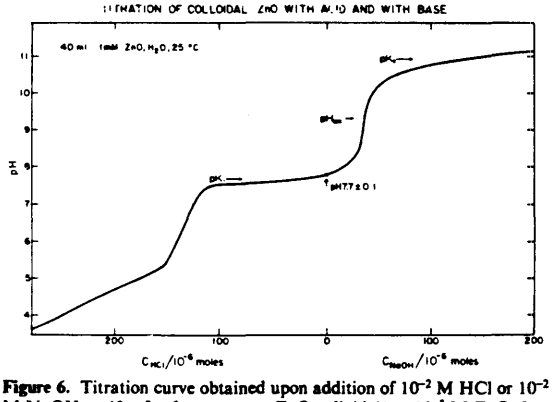

Figure 6. Titration curve obtained upon addition of 10^{-2} M HCl or 10^{-2} M NaOH to 40 mL of an aqueous ZnO colloid (1×10^{-3} M ZnO, 2×10^{-3} M acetate, 25 °C, air).

diminished by more than 1 order of magnitude within 5 s of illumination ($\leq$10 μM photons have been absorbed by the sol during this period), while a considerable increase of the UV band occurs concurrently. No further changes of both fluorescence intensities are observed when the sol is exposed to the spectrofluorometer light for an additional period of 3 min (the time usually necessary to measure a complete emission spectrum). It should also be noted that the absorption spectrum of the colloidal

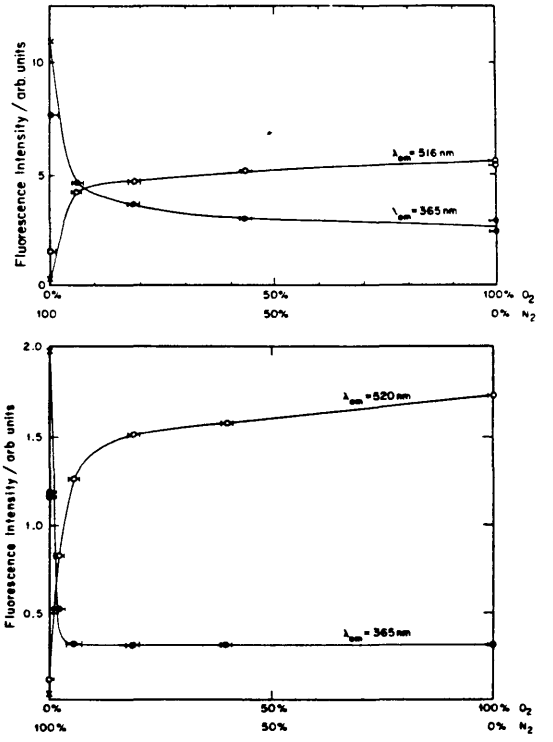

Figure 7. Fluorescence intensity (at equilibrium, see Results section) as a function of O_2 content: —○—/—●—, O_2/N_2 gas mixtures; ×, evacuated samples. (a, upper) 3.3×10^{-4} M ZnO in 2-propanol and (b, lower) 3.3×10^{-4} M ZnO in water.

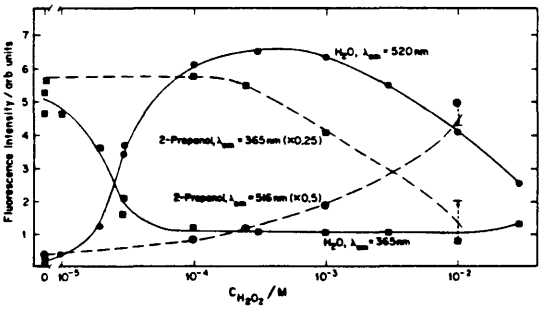

Figure 8. Fluorescence intensity as a function of the H_2O_2 concentration (3.3×10^{-4} M ZnO, evacuated samples).

suspension remained virtually unchanged during all the experiment described in Figures 7 and 8. Even though only an estimate of the initial magnitude of the two luminescence peaks can be given due to the instrument's limited time resolution ($\simeq$1 s), we are confident that they do not differ by more than 20% from the values measured in aerated samples.

Following this short preirradiation period evacuated suspensions of ZnO fluoresce predominantly at 365 nm (cf. Figure 7, ×) with the intensity of this emission a factor of 3 or 7 higher than in oxygenated isopropanolic or aqueous colloids, respectively. All points given in Figure 7 represent equilibrium values measured subsequent to the initial dynamic behavior. Apparent differences between the results obtained for samples under vacuum and under N_2 can thus be explained by traces of O_2 still present in the nitrogen stream. The magnitude of the green fluorescence peak increases significantly with increasing content of molecular oxygen. In both suspensions, an O_2 concentration of 2.5% by volume is sufficient to promote 50% of the maximum intensity of the visible

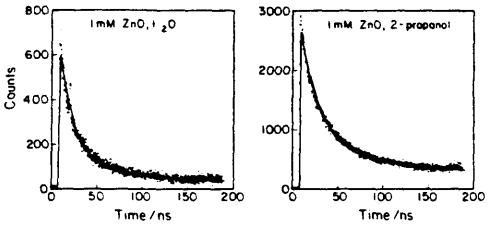

Figure 9. Fluorescence decay curves of ZnO colloid; solid lines represent a biexponential mathematical fit (see text).

emission, while at the same time the UV fluorescence intensity decreases (cf. Figure 7). In isopropanolic suspensions this decay closely matches the observed increase at λ_{em} = 516 nm. Air-saturated sols of ZnO in water exhibit a very weak UV emission but their 365-nm fluorescence in 2-propanol is more than 1 order of magnitude higher. Minor changes in the emission intensities are encountered between aerated and 100% oxygenated colloids of ZnO.

Addition of hydrogen peroxide also results in a green fluorescence and a lower UV emission as shown in Figure 8. However, a substantial difference in the response of the aqueous and the isopropanolic sols in the presence of H_2O_2 is apparent. In the former case, addition of 5×10^{-5} M H_2O_2 yields 50% of the maximum intensity of the visible and suppresses half of the initial UV emission. For H_2O_2 concentrations above 10^{-3} M the green fluorescence is depressed. In the case of the isopropanolic colloids, higher concentrations of H_2O_2 (100-fold) are required to suppress 50% of the UV fluorescence, whereas the green emission increases slightly without reaching a limiting value.

Figure 9 shows the time-resolved decay curves of the visible emission of colloidal suspensions of ZnO where the solid lines represent a double-exponential decay according to the following formula:

$$I(t) = I_1(0)e^{-t/\tau_1} + I_2(0)e^{-t/\tau_2}$$

This fit accounts for the fate of ≃90% of the observed emission. For a 10^{-3} M suspension of ZnO colloid in 2-propanol, 80% of the intensity decays with a characteristic time (τ) of 17 ns, while the remainder decays with τ = 190 ns. The aqueous suspension shows that 84% of the intensity decays with a characteristic time of 14 ns and the remainder with τ = 140 ns. The data for the decay of the UV emission suggest, on the other hand, that its lifetime is less than 100 ps and probably even less than 50 ps (rise time of the photomultipier employed in this study) in both sols. Experiments with a higher time resolution are thus required to resolve differences between the two colloidal preparations.

Table I summarizes rate constants obtained from the Stern–Volmer analysis of fluorescence quenching studies at λ_{em} = 520 nm using aqueous colloidal suspensions of ZnO. Plotting ϕ_0/ϕ vs. the concentration of the quencher (Q) yields straight lines with slopes denoted conventionally as $k_q\tau$ (see second column of Table I):

$$\phi_0/\phi = 1 + k_q\tau[Q]$$

Taking a lifetime τ of the visible fluorescent center of 14 ns, as obtained by the kinetic decay measurements, the bimolecular quenching constant k_q can be calculated (third column). Values between 10^{13} and 10^{15} M^{-1} s^{-1} indicate that at pH 7.7 oxidizing molecules like MnO_4^- or $Cr_2O_7^{2-}$ but also nonoxidizing cations, e.g., Fe^{2+}, are extremely efficient quenchers. Other cations such as Ni^{2+} or Co^{2+} also quench the green fluorescence yielding straight Stern–Volmer plots with lower bimolecular rate constants. Methylviologen (1,1′-dimethyl-4,4′-bipyridinium chloride, MV^{2+}) and Ag^+ are inefficient quenchers at pH 7.7. At pH 12, quenchers which are ineffective at pH 7.7 such as MV^{2+} and Ag^+ are more efficient by a factor of about 10^2. Anions such as $Cr_2O_7^{2-}$ and MnO_4^- which are most effective at pH 7.7 are less effective at pH 12.

TABLE I: Quenching of the Visible Emission of Aqueous ZnO Sols

quencher	$k_q\tau/M^{-1}$	k_q[a]$/M^{-1}$ s^{-1}
	At pH 7.7	
MnO_4^-	8×10^6	6×10^{14}
$Cr_2O_7^{2-}$	3×10^6	2×10^{14}
Fe^{2+}	2.0×10^6	1.4×10^{14}
Cu^{2+}	6.4×10^5	4.6×10^{13}
Fe^{3+}	3.5×10^5	2.5×10^{13}
Cr^{3+}	1.6×10^5	1.1×10^{13}
Zn^{2+}	1.6×10^4	1.1×10^{12}
Co^{2+}	5.9×10^3	4.2×10^{11}
Ni^{2+}	1.7×10^3	1.2×10^{11}
Mn^{2+}	1×10^3	7×10^{10}
MV^{2+}	$\approx 8 \times 10^2$	$\approx 6 \times 10^{10}$
Ag^+	$\approx 5 \times 10^2$	$\approx 4 \times 10^{10}$
	At pH 12	
MnO_4^-	3.7×10^5	2.6×10^{13}
Ag^+	3×10^5	2×10^{13}
MV^{2+}	1.2×10^5	8.6×10^{12}
Mn^{2+}	3.7×10^4	2.6×10^{12}
Co^{2+}	3.2×10^4	2.3×10^{12}
$Cr_2O_7^{2-}$	7×10^3	5×10^{11}
Li^+	$<10^2$	$<7 \times 10^9$

[a] Assuming $\tau = 14 \times 10^{-9}$ s from the fluorescence decay time measurement.

When permanganate or dichromate is used as quencher a time-dependent relationship is noted. For example, 1×10^{-6} M MnO_4^- is sufficient to reduce the emission intensity at 520 nm by a factor of 9 (1×10^{-3} M ZnO, pH 7.7, air, λ_{ex} = 330 nm). Continuous illumination with a weak light source (e.g., 8×10^{-8} M photons absorbed per second by the colloidal suspensions) results in a subsequent increase of the fluorescence intensity over a period of 1 min until it reaches about 75% of the intensity value it had without adsorbates. Similar phenomena are observed at pH 12 or when $Cr_2O_7^{2-}$ is employed instead of MnO_4^-. All values reported in Table I refer to the initial emission intensities.

The optical properties of an evacuated sample of ZnO colloid are changed upon prolonged ultrabandgap illumination as shown in Figure 10. The absorption and fluorescence spectra of an aerated solution of 1×10^{-3} M ZnO in 2-propanol containing 2×10^{-3} M acetate and 6×10^{-6} M methylviologen are given as a reference (full line). The absorption spectrum of an evacuated solution which has been irradiated with 60 μM photons (λ_{ex} = 330 nm) shows the characteristic pattern of reduced methylviologen, $MV^{\bullet+}$,[57] at 396 nm. However, no change is noted in the UV portion of the absorption spectrum which is characteristic for ZnO. Concurrently, the UV emission increases in intensity while the green fluorescence decreases by about 1 order of magnitude. This effect has already been described when the O_2 dependence of the fluorescence was studied (Figure 7a). Further irradiation with 10 mM photons results in a shift in the absorption spectrum of λ_{ox} from 365 to 345 nm. In addition, the blue color of $MV^{\bullet+}$ disappears. The new absorption pattern near 396 nm is characteristic of doubly reduced methylviologen, MV^0.[57] The fluorescence spectrum of this extensively irradiated solution features only the UV emission redshifted to 368 nm. When the colloidal suspension is exposed to air the blue color of $MV^{\bullet+}$ reappears. After 30 s of exposure, the absorption and fluorescence spectra return to the original reference spectra with slight variations in the intensities.

Discussion

Synthesis. The results clearly show that we have been able to synthesize stable transparent solutions of colloidal ZnO suspended in either water, 2-propanol, or acetonitrile. Since the formation of zinc oxide in water is not favorable compared to the formation of $Zn(OH)_2$[36-39] (vide supra) synthesis in a nonaqueous solvent was found to be necessary. Zinc acetate in the presence of 80% of the stoichiometric amount of NaOH yields the most stable

(57) Watanabe, T.; Honda, K. *J. Phys. Chem.* **1982**, *86*, 2617.

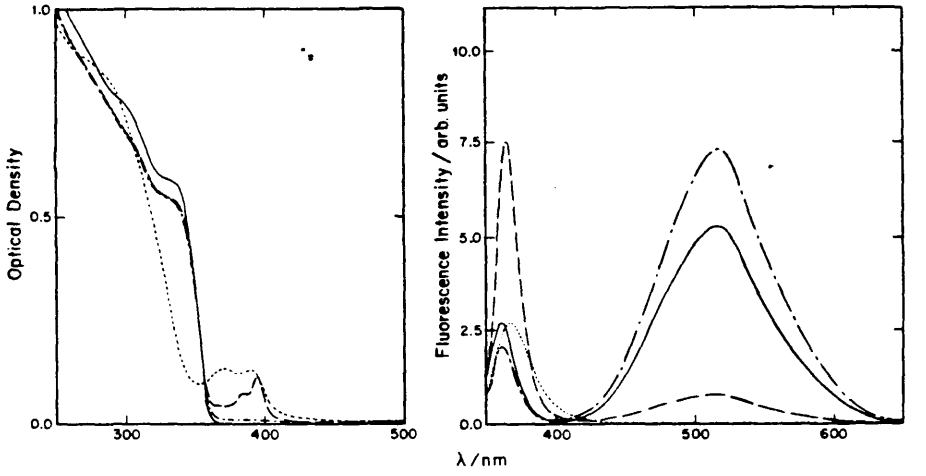

Figure 10. Effect of illumination on the spectroscopic properties of colloidal ZnO, 1×10^{-3} M ZnO, 2×10^{-3} M acetate, 6×10^{-6} M methylviologen, in 2-propanol, $\lambda_{ex} = 330$ nm; —, aerated, no $h\nu$; – –, evacuated, 6×10^{-5} M $h\nu_{abs}$; - - -, evacuated, 1×10^{-2} M $h\nu_{abs}$; – · –, evacuated, 1×10^{-2} M $h\nu_{abs}$, 30 s air.

colloids when 2-propanol is the solvent. Comparison of the spectroscopic properties of ZnO powder (Figure 5) with those of the colloidal preparations in 2-propanol (Figure 3) or water (Figure 4) reveals that this synthesis resulted in the desired product. The formation of zinc hydroxide, which would not result in spectral changes above 220 nm, is not indicated. Moreover, the X-ray diffraction patterns of crystalline ZnO and a powder prepared from the sol qualitatively show similar features, but the quantitative comparison reveals the presence of amorphous material in the colloidal preparation. Even though colloid stabilizers were intentionally not used in this study, the pronounced dependence of the kinetics of synthesis on the type of anion (Figure 1b) and the subsequent stabilization of the final suspension suggests that acetate does stabilize the sol. However, the nature of this effect is not consistent with simple double layer theory in that the acetate anion should destabilize the positively charged ZnO surface. It is also unlikely that the stabilizing activity of a small molecule like acetate could stem from a steric hindrance of the coagulation that occurs with some polymeric stabilizers.

UV/Vis Spectra. During the course of the synthesis of ZnO suspensions in 2-propanol significant spectroscopic changes were observed (Figures 1 and 3); similar observations have been made by others during the preparation of ultrasmall particles of ZnS, CdS, PbS, Zn_3P_2, Cd_3P_2, Cd_3As_2, CuCl, AgCl, AgBr, AgI, and PbI_2.[7-28] These changes have been explained by the "quantum (Q)-size effect" and can be attributed to the gradual transition from ZnO clusters, $(ZnO)_n$ with n starting perhaps as low as 8 or 16[16] to $(ZnO)_n$ particles with $n \approx 3000$ (assuming spherical geometry of the colloidal particles this value of n was estimated from the mean diameter as observed by TEM (Figure 2)). The latter particles exhibit photophysical and photochemical[58] properties of the bulk semiconductor material. Quantum mechanical calculations have been described by Brus[4-6] to account for these shifts of the electronic levels in the Q-state. For a sphere with a radius R and a dielectric coefficient ϵ he derived the following formula to calculate the energy E^* of the lowest excited state of the exciton

$$E^* \simeq E_g + 0.5\hbar^2\pi^2R^{-2}(m_e^{-1} + m_h^{-1}) - 1.8e^2\epsilon^{-1}R^{-1}$$

where E_g is the bulk bandgap energy and m_e and m_h are the effective masses of the electron and hole, respectively. This equation predicts that the energy level of the first excited state increases as the cluster size (R) decreases. Henglein and coworkers, on the other hand, have used a semiclassical treatment[16] and subsequently various quantum-mechanical approaches[22,59] to predict the dependence of the onset of absorption upon particle size. They observed good qualitative agreement with experimental data in the case of CdS.[22]

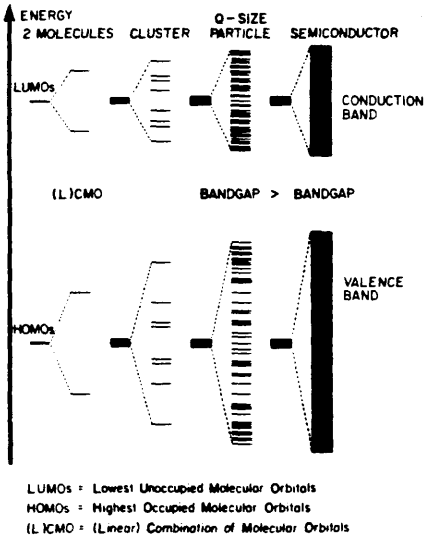

Figure 11. MO model for the particle growth.

Throughout the following discussion we shall use an alternative qualitative molecular orbital (MO) picture[60] to account for the bathochromic spectroscopic shift observed during the early growth stages of ZnO (Figure 11). It is obvious from this figure how the splitting of energetic levels into a filled and an empty region proceeds as the number of contributing MO's increases. In large particles the ensemble of energetic levels becomes dense yielding the valence and the conduction band, respectively. Since electronic transitions from the highest occupied molecular orbitals (HOMO's) to the lowest unoccupied molecular orbitals (LUMO's) yield the observed absorption spectrum the blue-shifted λ_{os} is readily explained for the Q-size particles.

It is interesting to note that ZnO particles must be smaller than 50 Å before a bandgap shift becomes obvious. In a recent in-

(58) Kormann, C.; Bahnemann, D. W.; Hoffmann, M. R., to be published.

(59) Schmidt, H. M.; Weller, H. *Chem. Phys. Lett.* **1986**, *129*, 615.

(60) Atkins, P. W. *Physical Chemistry*; Oxford University Press: Oxford, U.K., 1978; p 484.

vestigation Spanhel[55] showed that TiO_2 crystallites of only 36 Å diameter still show the same λ_{ss} as the bulk material. On the other hand, CdS particles exhibit Q-size effects until particle sizes with diameters around 80 Å are reached.[22] Properties of the respective anions such as size and polarizability seem to be important factors determining the quantum size regime of a material.

Transition probabilities between the MO's are also governed by symmetry selection rules, which become more important as the total number of orbitals decreases. This might explain the pronounced maximum structure observed in the absorption spectra of very small ZnO clusters, indicating that transitions of narrow energy distribution and high probability occur (cf. Figure 3).

Surface Properties. A more detailed description of the surface structure of metal oxides is useful for the better understanding of surface phenomena and for the discussion of the fluorescence behavior of our colloidal particles. In water, metal oxide surface chemistry is controlled by surface hydroxyl groups.[61] The following equilibria must be considered:

$$\equiv MOH_2^+ \rightleftharpoons \equiv MOH + H^+ \qquad pK_1 \qquad (2)$$

$$\equiv MOH \rightleftharpoons \equiv MO^- + H^+ \qquad pK_2 \qquad (3)$$

In some cases pK_1 and pK_2 values may be determined by titration.[61] The surface chemical properties of an oxide surface are sensitive to the composition of the aqueous phase because specific adsorption or binding of solutes to the surface can occur. The surface charge together with the pH of zero point of charge ($pH_{zpc} = {}^1/_2(pK_1 + pK_2)$) are important properties of oxide particles. Besides the above-mentioned charges due to ionizable hydroxo groups, lattice imperfections and the adsorption of surfactant ions are responsible for surface charges. Titration studies as well as experiments aimed at determining the rate of coagulation of the colloidal particles allow the determination of pH_{zpc}.

The acid titration of aqueous colloidal ZnO (Figure 6) results in an estimated value for pK_1 of 7.6 ± 0.1 (flat part of the curve, reflecting the buffering capacity of the surface with similar concentrations of protonated and neutral surface groups). Under the assumption that the surface charge is due only to ionized hydroxo groups (equilibria 2 and 3) a pH_{zpc} of 9.3 ± 0.2 can be derived from the inflection point in Figure 6. Since specific adsorption of carbonate or acetate could have lowered the pH_{zpc}—in fact, specific adsorption of impurities such as fatty acids can provoke a shift in the pH_{zpc} of more than two pH units[62]—additional titration–coagulation experiments were performed. The coagulation rate (as determined by the rate of the sol's turbidity increase) is expected to be a maximum at the pH_{zpc} due to surface electroneutrality. Titration studies with our aqueous ZnO sols showed that starting at pH 7.6 and titrating toward pH 11 the coagulation rate peaked at pH 9.2. These results for pH_{zpc} can be favorably compared with literature values for macrocrystalline ZnO that give a mean pH_{zpc} of 9.0 ± 0.3.[62]

Fluorescence Spectra. The luminescence maximum at 365 nm which closely coincides with the onset of absorption can be assigned as "bandgap" fluorescence caused by a transition from the lower edge of the conduction to the upper edge of the valence band. Temperature studies with bulk crystals are consistent with this interpretation.[44] The name "exciton" emission has been alternatively used[16,21] to describe the UV band of the luminescence spectrum in terms of a quantum-mechanical picture. Similar to earlier observations for CdS[16] small $(ZnO)_n$ clusters prepared in the presence of air do not exhibit this UV fluorescence, but particle growth to a size range $2000 \leq n \leq 3000$ is required for its occurrence (cf. Figure 3). Thus the lifetimes of electrons and holes in the conduction and valence band seem to increase with increasing particle size. However, for smaller clusters (i.e., $n \ll 3000$) relaxation into more favorable energy levels may result in an emission at longer wavelengths. This scheme is consistent with the observation that the yield of the visible emission goes through a maximum during the early stages of growth.

The nature of the visible fluorescence is more difficult to assign.[40-51] The concept of anion vacancies has been discussed by Henglein and co-workers for various n-type semiconductor materials.[15-21] They describe the fluorescence centers as a cation-rich structure ("anion vacancies") on the surface of a crystallite which can attract photogenerated electrons from the conduction band of particles such as ZnS[15] and ZnO.[21] The electronically excited crystallites can vibrationally relax to states of lower energy, which are geometrically different from the ground state. This interpretation explains why these levels are not accessible from the ground state, i.e., do not appear in the absorption spectrum (Franck–Condon principle), and why a radiative transition toward the ground state or to a trapped hole is characterized by a long lifetime. However, our findings are not consistent with this theory. While Koch et al.[21] observed that surface-bound excess zinc ions (i.e., anion vacancies) increased the 540-nm emission of their colloidal ZnO preparations in 2-propanol at pH 12, addition of Zn^{2+} to an aqueous colloid at pH 7.7 quenches this fluorescence in our system (see Table I). Moreover, alkaline colloids at pH 10.4, which should be characterized by cation vacancies due to a negatively charged surface, have almost the same fluorescence intensity as positively charged sols at pH 7.7.

Therefore, we envisage the physical nature of the fluorescence centers in ZnO to be like that proposed by Chestnoy et al.[14] In their study of the luminescence behavior of small CdS particles (22–38 Å in diameter) they attribute the visible fluorescence to photogenerated, trapped electrons tunneling to preexisting, trapped holes. Their model differs from the one previously proposed in that it does not require the presence of surface anion vacancies as a prerequisite for the occurrence of emissions with energies lower than the bandgap energy of the semiconductor. Multiexponential decay kinetics of the visible emission (cf. Figure 9) have also been observed by these authors who explained these results by a high probability of radiationless relaxation.[14]

As shown in Figure 7, the presence of molecular oxygen is essential for conversion of the UV emission into the visible fluorescence band. In an oxygen-free environment, relatively high concentrations of methylviologen (i.e., 10^{-4} M), which has a redox potential similar to O_2,[57] also enhance the 520-nm emission relative to the 365-nm band. Koch et al. recently reported similar observations when they described the disappearance of the visible emission of an evacuated aqueous suspension of colloidal zinc oxide upon UV irradiation.[21] A concurrent blue shift of the absorption spectrum of their sample was originally attributed to a physical shrinkage of the particles[21] but has since been reinterpreted in terms of excess electrons on the colloidal particles, influencing the energy of the exciton state.[23] Both effects were reversible in the presence of O_2. In their discussion, these authors explained the observed quenching of the visible fluorescence by the presence of excess electrons[23] or Zn^+ centers[21] reacting with photogenerated holes. The role of molecular oxygen was then proposed to be that of an e^- acceptor which restores the original conditions. Even though great similarities seem to exist between those results and our findings, substantial differences need to be pointed out:

No shift in the absorption spectra is observed in our ZnO sols while the fluorescence changes occur, suggesting that the presence of excess electrons and/or Zn^+ centers on the particles should be minimal. Several millimoles of photons are in fact necessary to provoke such spectral shifts (cf. later part of Discussion and Figure 10).

The intensity of the UV emission increases by a factor of 3 or 7 in the absence of molecular oxygen with 2-propanol or water being the solvent, respectively. This observation cannot be explained by the proposed mechanism which would most probably invoke the quenching of both fluorescence bands by the excess e^- but should at least not result in an increase of the UV emission.

While a possible explanation for the influence of molecular oxygen and methylviologen on the relative fluorescence intensities could be their electron-accepting ability, this simple picture cannot be applied to explain the marked differences in sensitivity toward H_2O_2 which are observed when either water or 2-propanol is the

(61) Stumm, W.; Morgan, J. J. *Aquatic Chemistry*, 2nd ed.; Wiley-Interscience: New York, 1981.
(62) Parks, G. A. *Chem. Rev.* **1965**, *65*, 177.

solvent (cf. Figure 8). A polar molecule such as hydrogen peroxide should rather be more strongly adsorbed to the hydrophilic ZnO surface in 2-propanol (dielectric constant $\epsilon_{25°C} = 18.3$) than in H_2O ($\epsilon_{25°C} = 78.5$) where it nevertheless exhibits a much higher activity in promoting the visible fluorescence.

In the following we propose a mechanism to explain our observations. The main pathway of energy dissipation is a radiationless relaxation as deduced from the overall low fluorescence yield for fully developed ZnO colloids ($\phi = 0.03$). In the absence of electron acceptors, part of the photogenerated conduction band electrons (e_{CB}^-) can also radiatively combine with valence band holes (h_{VB}^+) giving rise to the bandgap fluorescence. However, following the careful evacuation of our samples both fluorescence bands are initially still apparent with their relative intensities being similar to those observed in the presence of air. Absorption of a few micromoles of photons ($\lambda_{ex} \leq 365$ nm) results in the effective bleaching of the visible emission while there is a significant simultaneous increase of the UV emission (cf. Figure 7, ×). This observation can be explained by a photodesorption of trace amounts of molecular oxygen (reaction 4). O_2 is known to be

$$ZnO/O_2^{\bullet-} + e_{CB}^- + 2H_{aq}^+ \rightarrow ZnO + H_2O_2 \qquad (4)$$

strongly chemisorbed to the surface of zinc oxide (probably in the form of superoxide, $O_2^{\bullet-}$, since an electronegative molecule such as O_2 readily accepts an excess electron from ZnO which is a typical n-type semiconductor) and thus cannot be removed under reduced pressure at room temperature.[63] The concentrations of hydrogen peroxide resulting from this reaction are too small (≤ 1 μM assuming the adsorption of one molecule of O_2 per ZnO particle) to have a noticeable influence on the fluorescence yields (cf. Figure 8).

The significant influence of adsorbed molecular oxygen and methylviologen can then be explained by a relay action of these compounds resulting in the formation of the respective radical ions via reactions 5 and 6. The intermediacy of these semireduced

$$e_{CB}^- + O_2(ads) \rightarrow O_2^{\bullet-}(ads) \qquad (5a)$$

$$e_{CB}^- + MV^{2+}(ads) \rightarrow MV^{\bullet+}(ads) \qquad (5b)$$

$$O_2^{\bullet-}(ads) + Tr \rightarrow Tr^- + O_2(ads) \qquad (6a)$$

$$MV^{\bullet+}(ads) + Tr \rightarrow Tr^- + MV^{2+}(ads) \qquad (6b)$$

species seems necessary for the conduction band electrons to find their way to the appropriate electron traps (Tr). The visible fluorescence then results from the tunneling of these trapped electrons to preexisting, trapped holes.[14]

The influence of hydrogen peroxide on the 520-nm emission band (cf. Figure 8) cannot be understood by a simple electron transfer in accordance with reactions 5 and 6 since the one-electron reduction of H_2O_2 is an irreversible process leading to the formation of hydroxyl radicals. It is therefore suggested that the valence band holes react with H_2O_2 via the overall reaction

$$2h_{VB}^+ + H_2O_2 \rightarrow O_2 + 2H_{aq}^+ \qquad (7)$$

resulting in the generation of molecular oxygen which in turn acts as an electron relay (reactions 5a and 6a). The different sensitivity of the aqueous and the isopropanolic colloid toward hydrogen peroxide (cf. Figure 8) is then explained by a competition of the solvent for the photogenerated holes. 2-Propanol can act as a reductant and is thus able to accept h_{VB}^+; therefore a much higher H_2O_2 concentration is required to intercept the bandgap fluorescence than in the case of water as solvent. The decreasing effect of high concentrations (i.e., $>10^{-3}$ M) of hydrogen peroxide upon the intensity of the visible emission of ZnO in water is a quenching action which will be discussed in detail below. While the $O_2^{\bullet-}/O_2$ and the $MV^{\bullet+}/MV^{2+}$ redox couples serve as electron relays, the fluorescent center must be an *intrinsic* entity of the crystal because the nature of the electron relay does not affect the energy of the long-lived emission.

The fact that small ZnO clusters exhibit a much higher intensity of the green fluorescence than larger zinc oxide particles can be explained by the high specific surface area of the former leading to shorter distances to a surface-bound electron acceptor (e.g., O_2). In addition, due to a smaller number of crystal molecules, the phonon state density responsible for radiationless relaxation should be lower; i.e., there will be less channels for radiationless recombination.

Additional proof for the proposed electron-shuttle mechanism comes from results of an anoxic synthesis of ZnO in 2-propanol. Fluorescence measurements during the course of this synthesis revealed the occurrence of a UV emission at the early stages of the particle growth (i.e., where the solution contained only clusters consisting of a few zinc oxide molecules which are not detectable by TEM) matching the respective onset of the absorption spectrum. A bandgap fluorescence around 320 nm has, for example, been measured 1 min after mixing $Zn(OAc)_2$ with NaOH at 0 °C in a N_2-flushed glovebox in excellent agreement with the absorption onset observed at the same time (cf. Figure 1a). This luminescence subsequently shifted to longer wavelengths as the aging process occurred. The concurrent observation of a very small visible luminescence is explained by traces of O_2 still present in the reaction mixture. Upon exposure to air the UV emission immediately disappeared giving rise to the broad visible fluorescence that had been observed during the original preparations (cf. Figure 3). These results clearly support the proposed electron relay mechanism. This is, to the best of our knowledge, the first time that a blue-shifted bandgap fluorescence has been observed at these very early growth stages during the preparation of Q-size particles. Fojtik et al. also observed a UV emission shifted to shorter wavelengths as compared with the absorption onset of bulk crystals when they prepared small CdS particles.[16] However, this band only appeared with an onset of the concurrent absorption spectrum of $\lambda_{ex} \geq 430$ nm; i.e., particle diameters above 25 Å had been reached.[22] While this value corresponds to almost 200 molecules of CdS per particle, an upper limit of $d = 10$ Å (estimated from the absence of any image in the TEM) suggests that each zinc oxide cluster contains only about 20 ZnO molecules as the UV fluorescence is observed.

Many of the bimolecular fluorescence quenching constants k_q (listed in Table I) exceed the limit of diffusion-controlled reactions. We conclude that the quenching molecules are adsorbed onto the surface of the colloidal particles at the moment of excitation. This is clearly indicated by the different behavior noted at pH 7.7 and pH 12. At pH 7.7 the cations Ag^+, Mn^{2+}, and MV^{2+} are poor quenchers (i.e., the ZnO surface is positively charged) whereas at pH 12 very steep Stern–Volmer plots are obtained. Anions such as MnO_4^- and $Cr_2O_7^{2-}$ are not accommodated readily on negatively charged surfaces but exhibit the highest quenching constants when positive sites are available at pH 7.7. We have in fact used this behavior as a third alternative to estimate the pH_{zpc} of our aqueous colloids by performing titrations in the presence of minute amounts of the appropriate quenchers and measuring the variations in the emission intensity at 520 nm. This method yields pH_{zpc} values in agreement with the results presented above. Some cations are very efficient quenchers even at pH 7.7, e.g., Cr^{3+}, Cu^{2+}, Fe^{3+}, and Fe^{2+}, suggesting that the electrostatic interaction is not the only force governing surface adsorption. We propose an electron-transfer mechanism to account for the fluorescence quenching. Strongly oxidizing adsorbates such as MnO_4^-, $Cr_2O_7^{2-}$, Fe^{3+}, and Ag^+ irreversibly accept photogenerated electrons without back donation to electron traps, whereas Fe^{2+} appears to act as a hole scavenger.

A limited number of quenching experiments have also been performed with 2-propanol as the solvent resulting in k_q values for the suppression of the visible emission similar to those given in Table I for the aqueous sol. However, since an aerated isopropanolic suspension of ZnO still exhibits a considerable bandgap fluorescence (cf. Figure 7a) its quenching was also studied. We noted a complete quenching of the UV emission with $k_q \geq 4 \times 10^{15}$ M^{-1} s^{-1} (e.g., Cu^{2+}) before the visible fluorescence appeared

(63) Many, A. *CRC Critical Reviews in Solid State Sciences*; CRC: Boca Raton, FL, 1974; p 515.

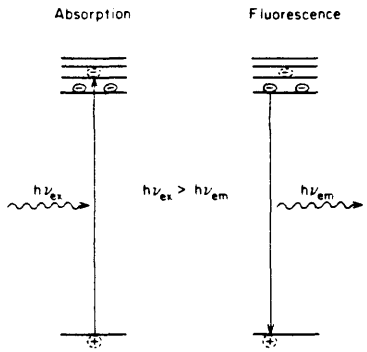

Figure 12. Spectroscopic properties of preirradiated ZnO.

to be affected. This observation is in good agreement with the above mechanism where an electron transfer from the conduction band should be more efficient than from a lower energy trap.

The dynamic behavior that has been observed when compounds such as MnO_4^- or $Cr_2O_7^{2-}$ were employed as fluorescence quenchers is explained by an efficient conversion of a strong oxidant, i.e., a good quencher, to a less effective species following the irreversible uptake of electrons.

Reversible Spectral Shifts. As shown in Figure 10 the absorption spectrum of an oxygen-free isopropanolic suspension of the colloidal particles can be shifted by 20 nm toward shorter wavelengths upon prolonged illumination ($\simeq$10 mM $h\nu$ with λ_{ex} = 330 nm were absorbed during the experiment). This spectral change which corresponds to a shift of 190 mV in the bandgap energy is found to be reversible once molecular oxygen is added to the system. Similar effects have been reported by Albery et al.[64] and Henglein and co-workers[23] for small CdS particles using flash and pulse radiolysis techniques, respectively. The latter attributed their observations to nonlinear optical effects and suggested that electrooptical applications of this phenomenon are indicated. A blue shift of the absorption spectrum that was observed by Koch et al. when they illuminated colloidal ZnO in the absence of oxygen was originally explained on the basis of a decrease in the size of the small ZnO particles[21] but subsequently also interpreted as a nonlinear effect.[23] These authors suggested that the presence of a single excess electron on a small semiconductor particle suffices to create a polarizing field which increases the energy of the excitonic state thus leading to a blue-shifted absorption spectrum.

However, our observations cannot readily be explained by this electrostatic model. While it describes the pronounced UV shift in the absorption spectrum very well, this theory is unable to account for the finding that the bandgap emission of the illuminated solution is *not* blue-shifted but rather slightly red-shifted (cf. Figure 10). Furthermore, a large number of photons have to be absorbed by the sol before a shift in the absorption spectrum is observed suggesting that a considerable number of electrons, rather than only one, have to be stored per particle to yield this effect. Finally, no spectral change is observed in alkaline suspensions where a negatively charged surface should result in overall negatively charged particles, evincing that the mechanism proposed in the case of CdS cannot simply be applied to ZnO. We prefer to use the MO picture introduced above to explain the data shown in Figure 10 (analogous results were also obtained in the absence of MV^{2+}). Illumination of the ZnO particles results in the oxidation of acetate and/or 2-propanol. Concurrently, the e_{CB}^- reduce all available electron acceptors such as chemisorbed dioxygen and methylviologen. Only a few micromoles of photons are necessary to deplete all relay compounds which originally promoted the visible emission, while the absorption band due to ZnO remained unchanged (curve -- in Figure 10). Subsequently, i.e., after the sol had been illuminated with 10 mM $h\nu$ (curve --- in Figure 10), excess electrons start to fill the lower MO's of the conduction band as indicated schematically in Figure 12. Hence, succeeding photogenerated electrons have to reach molecular orbitals of higher energy. Since in these small colloidal particles the density of MO's in the conduction band is relatively low, a net blue shift of the absorption spectrum is the expected result. The emission, on the other hand, occurs through transitions from the lower edge of the conduction band to the upper edge of the valence band in agreement with the absence of any blue shift of the UV fluorescence. Eventually, MV^{2+} is reduced to MV^0 via an intermediate $MV^{\cdot+}$ as indicated by the changes in the absorption spectra. However, it is not possible to decide whether the e_{CB}^- from the ZnO or the α-hydroxyalkyl radicals formed during the one-electron oxidation of 2-propanol lead to the observed formation of doubly reduced methylviologen.

Once O_2 is admitted to the system it reacts with the stored electrons and thereby restores the original spectral characteristics. Chemical reactions such as the oxidation of acetate and 2-propanol and the reduction of molecular oxygen resulted in a net chemical change in the colloidal suspension. We envisage that no spectral change would be observable under the given experimental conditions if we were able to produce zinc oxide colloids in the absence of electron donors since e^-/h^+ recombination should then be the main reaction pathway.

Even though the phrase "nonlinear optical effects" has been used to describe similar phenomena[23] a word of caution should be added at this point. Solid-state physics employs this term for completely reversible transient effects which, for example, occur in semiconductors that are irradiated with short light pulses of high intensity (e.g., laser pulses) the energy of which exceeds the bandgap energy. Hence a large number of e^-/h^+ pairs are generated which during their lifetime alter the optical absorption characteristics of the material in a nonlinear fashion.[65] However, as pointed out above, the observed spectral changes are, at least in our case, accompanied by permanent chemical changes within the illuminated system and can therefore not strictly be described by such a reversible model.

Acknowledgment. We gratefully acknowledge the financial support by the U.S. EPA (CR812356-01-0) and in particular we want to thank Dr. Marcia Dodge for her support. We appreciate extensive scientific discussions with Prof. Arnim Henglein (Hahn-Meitner Institute Berlin) who also supplied a preprint of his recent work[23] thereby stimulating our ideas concerning the nonlinear optical effects. We enjoyed a very pleasant collaboration with Prof. Douglas Magde (University of California, San Diego) during the fluorescence decay studies and like to thank him and Ms. Gale Rojas for their help. D.W.B. thanks the Hahn-Meitner Institut for granting him a leave of absence.

Registry No. MV^{2+}, 4685-14-7; MnO_4^-, 14333-13-2; $Cr_2O_7^{2-}$, 13907-47-6; Fe^{2+}, 15438-31-0; Cu^{2+}, 15158-11-9; Fe^{3+}, 20074-52-6; Cr^{3+}, 16065-83-1; Zn^{2+}, 23713-49-7; Co^{2+}, 22541-53-3; Ni^{2+}, 14701-22-5; Mn^{2+}, 16397-91-4; Ag^+, 14701-21-4; Li^+, 17341-24-1; ZnO, 1314-13-2.

(64) Albery, W. J.; Brown, G. T.; Darwent, J. R.; Saievar-Iranizad, E. *J. Chem. Soc., Faraday Trans. 1* **1985**, *81*, 1999.

(65) Chemla, D. S. *Nonlinear Optics: Materials and Devices; Proceedings in Physics*; Flytzanis, C., Oudar, J. L., Eds.; Springer Verlag: Berlin, 1986; Vol. 7, p 65.

Chapter 3

PREPARATION AND CHARACTERIZATION OF QUANTUM SIZE TITANIUM DIOXIDE

[The text of this chapter appeared in: Claudius Kormann, Detlef W. Bahnemann, and Michael R. Hoffmann, J. Phys. Chem., 1988, **92**, 5196.]

Reprinted from The Journal of Physical Chemistry, 1988, 92, 5196.
Copyright © 1988 by the American Chemical Society and reprinted by permission of the copyright owner.

Preparation and Characterization of Quantum-Size Titanium Dioxide

Claudius Kormann, Detlef W. Bahnemann,† and Michael R. Hoffmann*

W. M. Keck Laboratories, California Institute of Technology, Pasadena, California 91125
(Received: December 15, 1987; In Final Form: February 25, 1988)

The syntheses of transparent colloidal solutions of extremely small titanium dioxide particles ($d < 3$ nm) in water, ethanol, 2-propanol, and acetonitrile are presented. Quantum-size effects are observed during particle growth and at the final stages of synthesis. They are quantitatively interpreted by using a quantum mechanical model developed by Brus. The particles prepared in aqueous solution possess the anatase structure and consist of about 200 TiO_2 molecules at their final growth stage. The colloidal particles can be isolated from solution as white powders that are soluble in water and ethanol with no apparent change in their properties. In organic solvents the quantum-size TiO_2 particles appear to form with rutile structure. Excess negative charge on the particles resulting either from deprotonated surface hydroxyl groups or from photogenerated or externally injected charge carriers causes a blue shift in the electronic absorption spectrum, which is explained by an electrostatic model. Electrons can be trapped in the solid as a Ti^{3+} species, which has a characteristic visible absorption spectrum. As much as 10% of the available Ti^{4+} ions can be reduced photochemically in the solid with a quantum yield of 3%. Molecular oxygen reoxidizes the Ti^{3+} centers, leading to detectable amounts of surface-bound peroxides. The pH of zero point of charge (pH_{zpc}) of the aqueous colloidal suspension has been determined to be 5.1 ± 0.2. The acid-catalyzed dissolution of the aqueous colloid yielding Ti(IV) oligomers has been studied, and an activation energy $E_a = 58 \pm 4$ kJ/mol has been measured for this reaction. The photocatalytic activity of the small TiO_2 particles is demonstrated.

Introduction

Following the observations by Papavassiliou[1] and Ekimov et al.,[2] research in the area of quantum-size semiconductor particles has intensified.[3-13] Most of the quantum-size semiconductors are chalcogenides. However, zinc oxide (ZnO) has been synthesized recently in the quantum-size domain (i.e., particle diameters, d, ≤ 5 nm).[4a,d,13] On the other hand, preparation of colloidal TiO_2 normally results in particles exhibiting bandgap properties of the bulk solid (5 nm ≤ d ≤ 20 nm),[14-19] although Anpo et al. have prepared TiO_2 powders with particle diameters as small as 3.8 nm that have shown quantum-size effects.[20]

This paper describes the synthesis of titanium dioxide colloids with particle diameters $d < 3$ nm that exhibit typical quantum-size properties such as increasing bandgap energies with decreasing particle size and blue-shifts in the UV–vis spectrum upon charge injection. The photophysical, photochemical, and surficial properties of these TiO_2 quantum-size particles have been investigated and are reported herein.

Experimental Procedures

Chemicals and solvents were of reagent grade and used without further purification. The water content of the organic solvents was as follows: 2-propanol (Merck, 0.05%); acetonitrile (Merck, 0.3%); ethanol (USI Chemicals, ≃0.1%). The water employed in all preparations was purified by a Milli-Q/RO system (Millipore) resulting in a resistivity >18 MΩ cm. $TiCl_4$ (Merck) was freshly distilled prior use. P25 TiO_2 powder was a generous gift by the Degussa Corp.

UV–vis absorption spectra were recorded on a HP8451A diode array spectrometer and on a Shimadzu MPS-2000 instrument. Particle sizes were determined by transmission electron microscopy (TEM).[13] The time evolution of the absorption spectra was

† Bereich Strahlenchemie, Hahn–Meitner Institut GmbH, Glienickerstrasse 100, D1000 Berlin 39, West Germany.

(1) Papavassiliou, G. C. *J. Solid State Chem.* **1981**, *40*, 330.

(2) (a) Ekimov, A. I.; Onushchenko, A. A. *Pis'ma Zh. Eksp. Teor. Fiz.* **1981**, *34*, 363. (b) Ekimov, A. I.; Onushchenko, A. A. *Pis'ma Zh. Eksp. Teor. Fiz.* **1984**, *40*, 337. (c) Ekimov, A. I.; Efros, A. L.; Onushchenko, A. A. *Solid State Commun.* **1985**, *56*, 921.

(3) (a) Rossetti, R.; Nakahara, S.; Brus, L. E. *J. Chem. Phys.* **1983**, *79*, 1086. (b) Brus, L. E. *Ibid.* **1983**, *79*, 5566. (c) Brus, L. E. *Ibid.* **1984**, *80*, 4403. (d) Rossetti, R.; Ellison, J. L.; Gibson, J. M.; Brus, L. E. *Ibid.* **1984**, *80*, 4464. (e) Rossetti, R.; Hull, R.; Gibson, J. M.; Brus, L. E. *Ibid.* **1985**, *82*, 552. (f) Rossetti, R.; Hull, R.; Gibson, J. M.; Brus, L. E. *Ibid.* **1985**, *83*, 1406. (g) Chestnoy, N.; Hull, R.; Brus, L. E. *Ibid.* **1986**, *85*, 2237. (h) Brus, L. E. *J. Phys. Chem.* **1986**, *90*, 2555. (i) Chestnoy, N.; Harris, T. D.; Hull, R.; Brus, L. E. *Ibid.* **1986**, *90*, 3393. (j) Brus, L. E. *Nouv. J. Chim.* **1987**, *11*, 123.

(4) (a) Weller, H.; Koch, U.; Gutierrez, M.; Henglein, A. *Ber. Bunsen-Ges. Phys. Chem.* **1984**, *88*, 649. (b) Fojtik, A.; Weller, H.; Koch, U.; Henglein, A. *Ibid.* **1984**, *88*, 969. (c) Weller, H.; Fojtik, A.; Henglein, A. *Chem. Phys. Lett.* **1985**, *117*, 485. (d) Fischer, Ch.-H.; Weller, H.; Fojtik, A.; Lume-Pereira, C.; Janata, E.; Henglein, A. *Ber. Bunsen-Ges. Phys. Chem.* **1986**, *90*, 46. (e) Fojtik, A.; Weller, H.; Henglein, A. *Chem. Phys. Lett.* **1985**, *120*, 552. (f) Baral, S.; Fojtik, A.; Weller, H.; Henglein, A. *J. Am. Chem. Soc.* **1986**, *108*, 375. (g) Koch, U.; Fojtik, A.; Weller, H.; Henglein, A. *Chem. Phys. Lett.* **1985**, *122*, 507. (h) Weller, H.; Schmidt, H. M.; Koch, U.; Fojtik, A.; Baral, S.; Henglein, A.; Kunath, W.; Weiss, K.; Diemann, E. *Ibid.* **1986**, *124*, 557. (i) Schmidt, H. M.; Weller, H. *Ibid.* **1986**, *129*, 615. (j) Henglein, A.; Kumar, A.; Janata, E.; Weller, H. *Ibid.* **1986**, *132*, 133. (k) Spanhel, L.; Weller, H.; Fojtik, A.; Henglein, A. *Ber. Bunsen-Ges. Phys. Chem.* **1987**, *91*, 88. (l) Fojtik, A.; Weller, H.; Fiechter, S.; Henglein, A. *Chem. Phys. Lett.* **1987**, *134*, 477. (m) Henglein, A.; Fojtik, A.; Weller, H. *Ber. Bunsen-Ges. Phys. Chem.* **1987**, *91*, 441. (n) Spanhel, L.; Haase, M.; Weller, H.; Henglein, A. *J. Am. Chem. Soc.* **1987**, *109*, 5649. (o) Fojtik, A.; Henglein, A.; Katsikas, L.; Weller, H. *Chem. Phys. Lett.* **1987**, *138*, 535. (p) Spanhel, L.; Weller, H.; Henglein, A. *J. Am. Chem. Soc.* **1987**, *109*, 6632. (q) Haase, M.; Weller, H.; Henglein, A. *J. Phys. Chem.* **1988**, *92*, 482. (r) Spanhel, L.; Henglein, A.; Weller, H. *Ber. Bunsen-Ges. Phys. Chem.* **1987**, *91*, 1359. (s) Henglein, A. *Top. Curr. Chem.* **1988**, *143*, 113.

0022-3654/88/2092-5196$01.50/0 © 1988 American Chemical Society

measured as described previously.[13]

The photocatalytic oxidation of iodide was studied by using a 450-W Xe illumination system that has been described elsewhere,[13] while some experiments were performed with a 500-W Xe lamp. The output of this lamp was guided through a water-cooled (Pyrex windows) UG 11 band-pass filter onto 3-mL aliquots of colloid. Excitation thus occurred with light between 300 and 400 nm without heating the sample.

For the photocatalytic oxidation of iodide 2-mL samples of 5 mM TiO_2 colloid containing 1 mM iodide were illuminated with 5 mM $h\nu$ at 330 nm. Iodine was determined spectrometrically as I_3^- by using $\epsilon(352\,nm) = 26\,400\ M^{-1}\ cm^{-1}$.[21] The formation of I_3^- was promoted by adding 10 mM I^- and by maintaining the solution at pH 1–3 for the absorption measurement.

Titrations of aqueous colloidal TiO_2 thermostated to 25 °C were carried out with a Radiometer autotitration system consisting of a pHM84 pH meter, a TTT80 titrator, and a ABU80 autoburet. A vigorously stirred N_2-bubbled suspension of TiO_2 colloid was titrated with freshly prepared stock solutions of NaOH (N_2 bubbled) or HCl. pH readings were taken after thermodynamic equilibration of between 10 min and up to 1 h (at high pH).

The acid-catalyzed dissolution of TiO_2 colloid was studied by using the flow system. At $t = 0$ a small amount of concentrated HCl was added to the thermostated colloid, and the decay of the absorption spectrum was recorded.

Preparation of Colloidal TiO_2 in Water, 2-Propanol, Ethanol, and Acetonitrile. In a typical preparation, 1 mmol (0.11 mL) of $TiCl_4$ (titanium tetrachloride), cooled to −20 °C, was slowly added to 200 mL of solvent (1 °C) under vigorous stirring and then kept at this temperature for 3 h. This colloidal preparation was stable for days at room temperature. Powders of TiO_2 colloid, which are soluble in water or ethanol, were obtained by adding 32 mmol (3.5 mL) of $TiCl_4$ slowly to 900 mL of cold (1 °C) water under vigorous stirring. The resulting colloidal suspension was stable for several hours at 5 °C; however, at room temperature, precipitation of TiO_2 occurred within a few hours due to high concentration and ionic strength. To increase the stability of the colloid and to facilitate powder formation during evaporation of the solvent, we reduced the ionic strength by dialyzing twice (Spectrapor membrane) against water (4 L, at room temperature) for a total of about 2 h; the final pH was 2.5. After being stored overnight at 5 °C, 200-mL aliquots were dried with the aid of a rotary evaporator (ca. 25 mbar, 30 °C). The residue was further dried by applying a vacuum of ca. 1 mbar for 30 s, which led to the formation of a white shiny powder (P1). Evaporation and drying also removed HCl, which could be found in a cooling trap.

A transparent suspension of 0.5 g/L of this powder in water resulted in a solution with a pH of 3.1; the transparent colloid was stable for several days at room temperature. Rapid titration with base yielded transparent TiO_2 colloids at pH 9.5–12 without any added stabilizers. TiO_2 colloids at pH 7 required the addition of 2 mM phosphate for stability. Throughout this study colloids obtained by controlled hydrolysis of $TiCl_4$ (5 mM concentration) and from dissolution of P1 powder behaved analogously.

γ-irradiations were carried out with a ^{60}Co source at the Hahn-Meitner Institut.

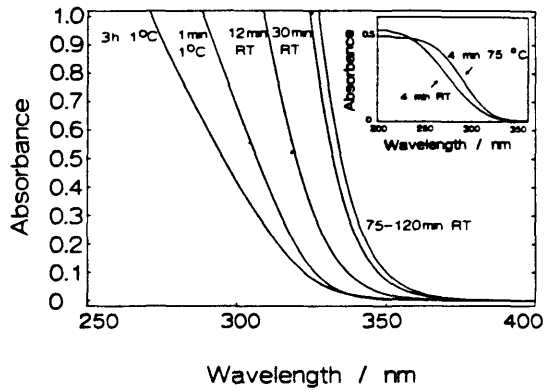

Figure 1. Absorption spectra of TiO_2 colloids at various growth stages. Obtained by hydrolysis of 5 mM $TiCl_4$. Inset: hydrolysis of 10^{-4} M $TiCl_4$.

Results and Discussion

Synthesis and Spectral Properties. Figure 1 shows the UV–vis spectra obtained during the controlled hydrolysis of titanium tetrachloride. Immediately after $TiCl_4$ was mixed with water at 1 °C the onset of absorption appears at $\lambda_{ab} \approx 340$ nm. Upon being aged at 1 °C for 3 h the absorption profile flattens slightly. No change in the spectral response of the solution was noted upon storage at 1 °C for several days. Warming the suspension to 25 °C results in a pronounced steepening of the absorption spectrum and a concomitant red-shift of its onset to approximately 370 nm (Figure 1). No further spectral changes are observed after 75 min at room temperature or 2 min at 75 °C. Similar observations have been made during the growth of zinc oxide particles in colloidal solution and were interpreted in terms of the quantum-size effect.[4a,9,13] Bahnemann et al.[13] used a molecular orbital (MO) description to explain the optical properties of semiconductor particles during their growth from molecular to bulk sizes. In essence, as more MOs of an increasing number of TiO_2 molecules in the polymer overlap, the energy gap between the highest occupied (HOMO) and the lowest unoccupied (LUMO) MO decreases; these changes result in a red-shift of the accompanying optical transition. Simultaneous pH measurements show that hydrolysis of $TiCl_4$ is completed within the first 2 min of reaction at 1 °C. The pH (1.8) of the product suspension does not change during subsequent periods of aging. This pH value corresponds to the formation of 16 mM free H_{aq}^+ during hydrolysis of 5 mM $TiCl_4$; from the stoichiometry of eq 1 we expected 20 mM of H_{aq}^+

$$TiCl_4 + 2H_2O \rightarrow TiO_2 + 4H_{aq}^+ + 4Cl^- \qquad (1)$$

to be produced. Similar deviations from the predicted stoichiometry were observed in the synthesis of α-Fe_2O_3 colloids; these differences were attributed to the buffering capacity of the oxide surface that resulted from surficial acid–base chemistry.[22] As

(5) (a) Williams, F.; Nozik, A. J. *Nature (London)* **1984**, *312*, 21. (b) Nozik, A. J.; Williams, F.; Nenadovic, M. T.; Rajh, T.; Micic, O. I. *J. Phys. Chem.* **1985**, *89*, 397. (c) Nedeljkovic, J. M.; Nenadovic, M. T.; Micic, O. I.; Nozik, A. J. *Ibid.* **1986**, *90*, 12. (d) Micic, O. I.; Nenadovic, M. T.; Peterson, M. W.; Nozik, A. J. *Ibid.* **1987**, *91*, 1295. (e) Rajh, T.; Vucemilovic, M. I.; Dimetrijevic, N. M.; Micic, O. I.; Nozik, A. J. *Chem. Phys. Lett.* **1988**, *143*, 305.

(6) (a) Sandroff, C. J.; Hwang, D. M.; Chung, W. M. *Phys. Rev. B: Condens. Matter* **1986**, *33*, 5953. (b) Sandroff, C. J.; Kelty, S. P.; Hwang, D. M. *J. Chem. Phys.* **1986**, *85*, 5337. (c) Sandroff, C. J.; Farrow, L. A. *Chem. Phys. Lett.* **1986**, *130*, 458.

(7) (a) Tricot, Y.-M.; Fendler, J. H. *J. Phys. Chem.* **1986**, *90*, 3369. (b) Youn, H.-C.; Tricot, Y.-M.; Fendler, J. H. *Ibid.* **1987**, *91*, 581. (c) Watzke, H. J.; Fendler, J. H. *Ibid.* **1987**, *91*, 854.

(8) Dannhauser, T.; O'Neil, M.; Johansson, K.; Whitten, D.; McLendon, G. *J. Phys. Chem.* **1986**, *90*, 6074.

(9) Stramel, R. D.; Nakamura, T.; Thomas, J. K. *Chem. Phys. Lett.* **1986**, *130*, 423.

(10) (a) Wang, Y.; Herron, N. *J. Phys. Chem.* **1987**, *91*, 257. (b) Wang, Y.; Herron, N. *Ibid.* **1987**, *91*, 5005.

(11) Micic, O. I.; Zongguan, L.; Mills, G.; Sullivan, J. C.; Meisel, D. *J. Phys. Chem.* **1987**, *91*, 6221.

(12) Hodes, G.; Albu-Yaron, A.; Decker, F.; Motisuke, P. *Phys. Rev. B: Condens. Matter* **1987**, *36*, 4215.

(13) Bahnemann, D. W.; Kormann, C.; Hoffmann, M. R. *J. Phys. Chem.* **1987**, *91*, 3789.

(14) Fox, M. A. *Top. Curr. Chem.* **1987**, *142*, 71.

(15) Matthews, R. W. *Solar Energy* **1987**, *38*, 405.

(16) Ollis, D. F. *Environ. Sci. Technol.* **1985**, *19*, 480.

(17) Nishimoto, S.-I.; Ohtani, B.; Shirai, H.; Adzuma, S.; Kagiya, T. *Polymn. Commun.* **1985**, *26*, 292.

(18) Duonghong, D.; Ramsden, J.; Grätzel, M. *J. Am. Chem. Soc.* **1982**, *104*, 2977.

(19) Moser, J.; Grätzel, M. *J. Am. Chem. Soc.* **1983**, *105*, 6547.

(20) Anpo, M.; Shima, T.; Kodama, S.; Kubokawa, Y. *J. Phys. Chem.* **1987**, *91*, 4305.

(21) Meyerstein, D.; Treinin, A. *Trans. Faraday Soc.* **1963**, *59*, 1114.

(22) Bahnemann, D. W.; Hoffmann, M. R, to be submitted for publication in *Langmuir*.

will be shown in detail, titanium dioxide surfaces exhibit analogous properties.

Further evidence that the spectral changes occurring during the aging of an aqueous $TiCl_4$ solution are indeed due to particle growth rather than to concentration effects stems from detailed spectral studies of dilute preparations. As shown in the inset in Figure 1, the absorption spectrum of an aqueous solution containing 10^{-4} M $TiCl_4$ does not exhibit Lambert–Beer behavior during the aging process as would be expected for a concentration increase of the absorbing species. In this case the absorption increases considerably at longer wavelengths, while it simultaneously decreases at wavelengths below 240 nm. Thus, the resulting red-shifted spectrum suggests particle growth in the colloidal solution. Absolute particle sizes of the TiO_2 colloids have been determined at various stages of growth by using TEM. The mean diameter of the fully grown colloid (right curve of Figure 1) was found to be 2.4 nm, while the particles aged for 12 min at 25 °C were 2.0 nm in diameter. This change in size corresponds to agglomeration numbers (n) of 210 or 120, respectively, that were determined by assuming spherical geometry and a density corresponding to that of anatase (ρ = 3.9 g cm^{-3}). Experimental limitations (i.e., the resolution of the electron microscope and the rather low contrast of TiO_2) did not allow the unambiguous determination of particle sizes from samples exhibiting even larger spectral blue-shifts. The $\Delta\lambda_{os}$ of approximately 30 nm corresponds to a bandgap shift of 250 meV. Under the experimental conditions of this study TiO_2 particle growth stops with cluster sizes of close to 200 molecules, whereas bandgap shifts to 1 eV and quantum-size effects up to agglomeration numbers of ≈3000 have recently been observed for ZnO colloids.[4a,13] This pronounced difference in the behavior of TiO_2 and ZnO colloids is in agreement with theoretical predictions by Brus and can be explained by the higher effective electron mass, m^*, in TiO_2.[3j] A mathematical treatment using a quantum mechanical rather than the above described MO approach yielded the following formula for the calculation of the bandgap shift (ΔE_g) in quantum-size materials:[3h]

$$\Delta E_g \simeq \left(\frac{\hbar^2\pi^2}{2R^2}\frac{1}{\mu}\right) - \frac{1.8e^2}{\epsilon R} \qquad (2)$$

(R, radius of the particle; μ, reduced mass of the exciton, i.e., $\mu^{-1} = m^*_e{}^{-1} + m^*_h{}^{-1}$ where m^*_e is the effective mass of the electron and m^*_h is the effective mass of the hole; ϵ; dielectric constant of the material.)

Taking R = 1.2 nm (as measured by TEM for the "grown-up" particles), ϵ = 184,[23] and ΔE_g = 150 meV (cf. the discussion of Figure 2 below), one calculates $\mu = 1.63m_e$ (m_e is the electron rest mass). The effective mass of the electron, m^*_e, of TiO_2 has been determined by several authors, who report values between 5 and 13 m_e.[24-26] Assuming a mean value of $m^*_e = 9m_e$, $m^*_h = 2m_e$ is readily computed. It is obvious that the above type of calculation can be considered only as a first approximation. With TiO_2, it appears reasonable that the effective mass of the hole is smaller than that of the electron. Although, to the best of our knowledge, exact values for m^*_h have not been reported, it is believed to be less than $1m_e$ because the valence band should be characterized by conventional transport mechanisms and hole delocalization. The large values for m^*_e are explained by the d-band character of the conduction band involving polaron transport.[27]

According to Brus the radius α of an exciton can be calculated in terms of[3h]

$$\alpha = \frac{\epsilon}{m^*_e/m_e}a_0 \qquad (3)$$

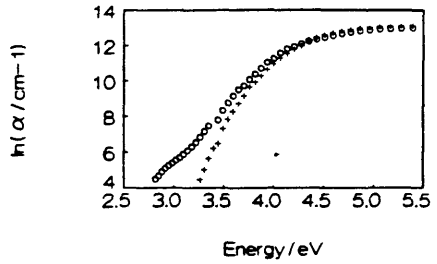

Figure 2. Absorption spectra of TiO_2 colloids: (+) P1, obtained by controlled hydrolysis of $TiCl_4$; (○) P2, obtained by hydrolysis of $Ti(O\text{-}CH(CH_3)_2)_4$.[25]

with a_0 = 0.53 Å being the hydrogen Bohr radius. Exciton radii between 7.5 and 19 Å are thus computed for TiO_2 by using the various literature values for m^*_e.[24-26] Hence, it is apparent that titanium dioxide particles consisting of a few hundred TiO_2 molecules should exhibit quantum-size effects.

It has recently been shown that lattice planes in small semiconductor particles can be visualized when electron microscopy is coupled with an opadization technique.[4b] Indeed, we observe well-resolved lattice planes in TEM pictures even when particle diameters of only 2 nm are measured. Lattice plane distances of 3.7 ± 0.4 Å show that our synthesis has resulted in the formation of anatase titanium dioxide.[28]

Water-soluble shiny white powders, P1, can be obtained from those TiO_2 preparations with a fully developed spectrum, i.e., maximum particle size under the conditions of hydrolysis as described in the Experimental Section. TEM data show that dialyzing the colloid does not change the particle diameters appreciably. Figure 2 shows a plot of ln α versus the photon energy, $E = hc\lambda^{-1}$, for a colloidal solution of P1 in comparison with a solution of the powder (P2) obtained by hydrolysis of titanium tetraisopropoxide.[29] The absorption coefficient α has been calculated from the measured absorbance (A) via

$$\alpha = \frac{2.303\rho 10^3}{lcM}A \qquad (4)$$

where ρ = 3.9 g cm^{-3} is the density,[28] M = 79.9 g mol^{-1} is the molecular weight, c is the molar concentration of TiO_2, and l is the optical path length.

Taking the linear portion of both curves between ln α = 7 and ln α = 10 and assuming that P2 possesses the bandgap of bulk anatase (E_g = 3.2 eV at ln α = 6.5),[28] a 150-meV shift of the bandgap of P1 to E_g = 3.35 eV is evident. Urbach's rule suggests using values between ln α = 6 and 10 for the determination of semiconductor bandgaps.[30] While this method of data analysis is common practice in solid-state sciences,[30] bandgap positions of colloidal semiconductors have mostly been determined from UV–vis spectra at arbitrarily chosen concentrations. Taking the spectrum of the aged colloid at 5 mM concentration (Figure 1, 75–120 min), an absorption onset of 370 nm or 3.35 eV is noted, in good agreement with P1 in Figure 2. However, if the spectrum of the diluted colloid (10^{-4} M, inset of Figure 1, 4 min, 75 °C) were inspected accordingly, λ_{os} = 350 nm or E_g = 3.5 eV would follow. Neither variation of the concentration nor replacement of P1 by the aged nondialyzed colloid has any effect on the curve shown in Figure 2 for P1. Therefore, we can conclude that the described synthesis yields a TiO_2 colloid with particle sizes small enough to result in a bandgap shift of 0.15 eV relative to bulk anatase TiO_2.

Reversible Spectral Shifts. It has recently been observed that the absorption spectrum of quantum-size semiconductor particles,

(23) Parker, R. A. *Phys. Rev.* **1961**, *124*, 1719.
(24) Acket, G. A.; Volger, J. *Physica (Amsterdam)* **1966**, *32*, 1680.
(25) Pascual, J.; Camassel, J.; Mathieu, H. *Phys. Rev. B: Condens. Matter* **1978**, *18*, 5606.
(26) Agekyan, V. T.; Berezhnaya, A. A.; Lutsenko, V. V.; Stepanov. Y. A. *Sov. Phys. Solid State* **1980**, *22*, 6.
(27) We are grateful to one of the reviewers for drawing our attention to this point.
(28) Landolt-Börnstein. *Zahlenwerte und Funktionen aus Naturwissenschaft und Technik*, Springer-Verlag: Berlin, 1982; Vol. III-17g, Section 9.15.2.1.1.
(29) Bahnemann, D. W.; Mönig, J.; Chapman, R. *J. Phys. Chem.* **1987**, *91*, 3782.
(30) Mott, N. F.; Davis, E. A. *Electronic Processes in Non-Crystalline Materials*, Clarendon: Oxford, 1979; pp 273–284.

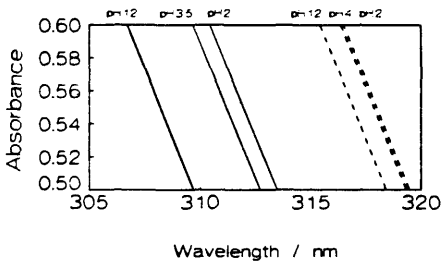

Figure 3. pH-dependent reversible shifts of absorption spectra of TiO_2 colloids: (—) P1; (---) P2.

e.g., ZnO and CdS, can be shifted toward shorter wavelengths by the injection of excess negative charges.[4g,j,q,13] Electrostatic[4j] and molecular orbital[13] models have been proposed to explain this so-called nonlinear optical behavior. Since the overall charge of an oxide particle in aqueous solution can also be changed by a variation of pH, i.e., a change of the relative amount of protonated and deprotonated surface hydroxyl groups (vide infra), it was interesting to study the effect of pH on the absorption spectra of the TiO_2 solutions. As shown in Figure 3, a reversible blue-shift of the spectrum of P1 by almost 50 meV is observed upon titration from pH 2 to 12. Similar experiments with a solution prepared from P2 (identical concentration: 1 mM) show qualitatively analogous results, but the shift amounts to less than 15 meV (cf. Figure 3). Note again the blue-shifted spectrum of P1. The spectral shifts shown in Figure 3 are explained by using the electrostatic model proposed by Henglein et al.[4j] Excess negative charges introduced by an increasingly higher concentration of surface O^- groups as the pH of the solution changes from 2 to 12 (cf. eq 12 and 13) create a polarizing field within the particle. This in turn results in an energy increase of the excitonic state and thus a blue-shift in the absorption spectrum.

Figure 4 shows the spectral response of two different titanium dioxide colloids in ethanolic solution upon bandgap illumination. It is obvious from Figure 4a that an intense blue color develops when a 10 mM solution of P1 is illuminated in the absence of oxygen. Simultaneously, a blue-shift of the electronic spectrum of the semiconductor is noted. Both effects are completely reversible when air is admitted into the sample. No change in the absorption spectrum is noted when anoxic solutions of P1 are illuminated in the absence of added hole scavengers. The formation of blue color in TiO_2 colloids has already been reported in photochemical and radiation chemical studies,[18,31,32] while no spectral blue-shifts were observed. The former was attributed to the generation of Ti^{3+} species within the colloidal particle via

$$TiO_2 \xrightarrow[\lambda_{ex} < 380\ nm]{h\nu} TiO_2(h_{vb}^+, e_{cb}^-) \quad (5)$$

$$C_2H_5OH + h_{vb}^+ \rightarrow CH_3\dot{C}HOH + H^+ \quad (6)$$

$$TiO_2(e_{cb}^-) \rightarrow TiO_2(Ti^{3+}) \quad (7)$$

Alternatively, reducing radicals, e.g., α-hydroxyalkyl radicals, generated by γ-radiolysis of the ethanolic solution can also react with the colloid:[31]

$$C_2H_5OH \xrightarrow{\gamma} CH_3\dot{C}HOH \quad (8)$$

$$TiO_2 + CH_3\dot{C}HOH \rightarrow TiO_2(Ti^{3+}) + CH_3CHO + H^+ \quad (9)$$

Reaction 9 can also occur in the photochemical system following (6) and thus leads to a current-doubling effect. We also observe the formation of a blue color and a concomitant blue-shift of the absorption edge in the UV upon γ-radiolysis of ethanolic P1 solutions (10 mM P1 in ethanol, anoxic, 2×10^5 rad). Two different extinction coefficients have been reported for the blue

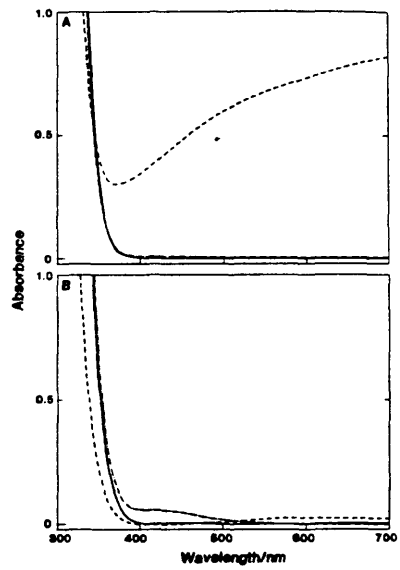

Figure 4. Spectral changes of illuminated TiO_2 colloids. (a) 10 mM P1 in ethanol: (—) before illumination; (---) after illumination with UV light (300–400 nm) for 40 min, $[h\nu_{ill}] \simeq 4 \times 10^{-2}$ M; (---) after admission of air for 30 s. (b) 10 mM $TiCl_4$ added to ethanol (water content ≈0.1%): (—) before illumination; (---) after illumination with UV light (300–400 nm) for 60 min, $[h\nu_{ill}] \simeq 6 \times 10^{-2}$ M; (---) after admission of air for 30 s.

$TiO_2(Ti^{3+})$ species. While colloidal preparations of large particles ($d \simeq 150$ nm) in highly acidic medium led to $\epsilon = 10^4\ M^{-1}\ cm^{-1}$,[31] a value of $\epsilon = 800\ M^{-1}\ cm^{-1}$ has been reported for a preparation of smaller particles ($d \simeq 10$ nm) at moderate pH values.[32] Taking the latter value (which appears appropriate for small particle sizes) a quantum yield of $\phi \simeq 0.03$ is calculated for the formation of Ti^{3+} centers (cf. Figure 4A, absorption increase at 700 nm). Thus 10% of the available Ti^{4+} ions have been photoreduced under the given experimental conditions. Likewise, in the γ-radiolysis experiments, 1.2 color centers per 100 eV of absorbed energy have been formed.

The blue-shift of the absorption spectrum during the anoxic illumination is an intriguing result (cf. Figure 4A). Similar spectral shifts have already been described when quantum-size ZnO or CdS particles contained excess negative charges.[4g,j,k,13] Analogously, we interpret our data in terms of an increased confinement of the exciton within the small TiO_2 particles due to the presence of Ti^{3+} centers, i.e., trapped negative charges. This is, to the best of our knowledge, the first time that this type of effect has been observed in titanium dioxide. Furthermore, we consider this observation as additional proof that our preparation resulted in the formation of quantum-size TiO_2. Finally, it should be noted that bandgap illumination of anoxic colloidal suspensions made from P2 powder in the presence of ethanol did not result in a blue-shifted absorption edge in the UV while, at the same time, the formation of a blue color was observed. This behavior was expected since the P2 particles are reported to be much larger ($d \simeq 40$ nm)[18] than the size limit for quantum-size behavior of TiO_2 (vide supra).

A substantial blue-shift of the absorption spectrum was observed upon illumination of a TiO_2 colloid that had been prepared by hydrolysis of $TiCl_4$ in ethanol (water content ca. 0.1%; Figure 4B). A concomitant formation of a blue color was evident with a quantum yield ($\phi \simeq 6 \times 10^{-4}$) that was less than in the case of the P1 powders. While these spectral changes were reversible upon exposure to oxygen, a transient yellow color ($\lambda_{max} \approx 420$ nm) was formed (cf. Figure 4B), which subsequently faded to yield the original colloid spectrum after several hours. Similar spectral changes have been observed in the γ-radiolysis of the ethanolic oxygen-free colloid. The yellow intermediate may form from the

(31) Henglein, A. *Ber. Bunsen-Ges. Phys. Chem.* **1982**, *86*, 241.
(32) Kölle, U.; Moser, J.; Grätzel, M. *Inorg. Chem.* **1985**, *24*, 2253.

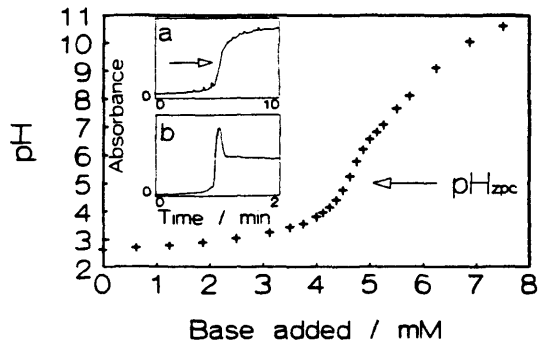

Figure 5. Titration curve of 20 mM TiO_2 colloid (P1) yielding the pH of zero point of charge (arrow), ionic strength = 10 mM. Insets: absorption changes at λ = 600 nm during the course of a titration. (a) Slow titration of 100 mL of 0.5 mM P1 with 1 mM NaOH (0.5 mL min^{-1}). The arrow indicates the point where the coagulation rate is highest. (b) Fast titration of 100 mL of 1 mM P1 with 10 mM NaOH (1 mL min^{-1}).

reactions of the blue Ti^{3+} centers or the trapped conduction band electrons, e_{cb}^-, with oxygen as follows:

$$TiO_2(Ti^{3+}) + O_2 \rightarrow TiO_2\text{–}O_2^{\bullet-} \quad (10)$$

$$TiO_2(e_{cb}^-) + O_2 \rightarrow TiO_2\text{–}O_2^{\bullet-} \quad (11)$$

In the case of P1 particles, the superoxide radicals subsequently undergo rapid decay reactions, while the yellow color of the illuminated P2 particles is indicative of surface-adsorbed peroxide species on the colloid made in ethanol. The titanyl–peroxide reaction yielding a yellow complex is a well-established method for the quantitative analysis of H_2O_2,[33] and it has been shown that μ-peroxo complexes on TiO_2 surfaces are formed upon light adsorption of O_2.[34] In our case, reducing equivalents are stored on the semiconductor particles and enable a subsequent thermal reaction to form such peroxo complexes.

The colloid resulting from hydrolyzing $TiCl_4$ in ethanol is characterized by an absorption edge in the UV that starts already at 400 nm (cf. Figure 4B); on TEM images no particles could be detected. The hydrolysis of $TiCl_4$ in other organic solvents such as 2-propanol or acetonitrile that have not been thoroughly dried yields colloids with similar red-shifted absorption spectra. For comparison, the onset of absorption of P1 and P2 anatase TiO_2 colloid occurs at 370 and 385 nm, respectively. Therefore, we suggest that the hydrolysis of $TiCl_4$ in these organic solvents resulted in the formation of rutile TiO_2 as this material has a smaller bandgap: E_g = 3.0 eV,[28] corresponding to an onset of absorption at λ_{os} = 415 nm. From the actual observed spectrum, which is blue-shifted by 100 meV, a particle size of $\simeq$2.5 nm is calculated, by using the material constants cited above (vide supra).

Surface Properties. Acid-base titrations as well as coagulation studies were carried out to characterize the surface properties of the oxide particles. An oxide surface is described by acid–base equilibria involving surface hydroxyl groups:[35]

$$\equiv MOH_2^+ \rightleftharpoons \equiv MOH + H^+ \quad pK_1 \quad (12)$$

$$\equiv MOH \rightleftharpoons \equiv MO^- + H^+ \quad pK_2 \quad (13)$$

The pH of zero point of charge is given by

$$pH_{zpc} = \tfrac{1}{2}(pK_1 + pK_2) \quad (14)$$

Literature values for the pH$_{zpc}$ for bulk TiO_2 powder[36] and colloid[19] range between 3.5 and 6.7.

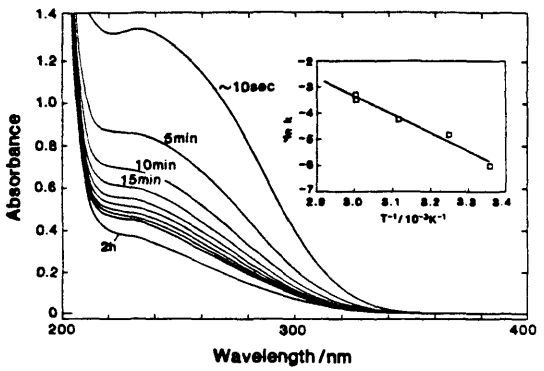

Figure 6. Acid-catalyzed dissolution of TiO_2 colloid. The dissolution of a preparation of 4 × 10^{-4} M TiO_2 colloid is started by rapidly changing the pH to 1 at t = 0 min. Inset: Arrhenius plot of rate constants obtained from first-order decay of A (235 nm); [P1] = 2.5 × 10^{-4} M, pH 1, E_a = 58 ± 4 kJ mol^{-1}, R^2 = 0.98.

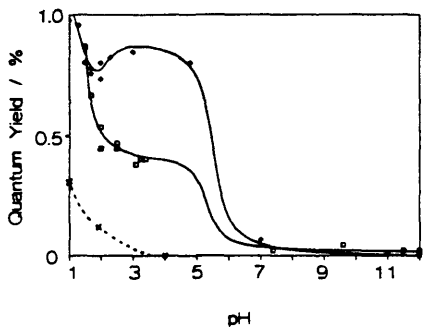

Figure 7. Photocatalytic oxidation of iodide on TiO_2 colloids, [TiO_2] = 5 mM, [I^-] = 1 mM, air, [$h\nu_{330\,nm}$] = 5 mM: (□) P1; (◇) P2; (×) without colloid.

Two approaches were chosen to determine the pH$_{zpc}$ of TiO_2 colloid (P1). From the inflection point of a titration curve (Figure 5, arrow), obtained by titrating a concentrated suspension of colloid, a value of pH$_{zpc}$ 5.0 is inferred.

In addition titration–coagulation studies were carried out. The coagulation rate—as derived from absorption changes at 600 nm (see insets of Figure 5)—passes through a maximum as the pH$_{zpc}$ is reached. At 600 nm an increasing absorption stems only from back scattering of light from larger particles while there is no interference due to electronic transitions. The pH values at which the coagulation rate is a maximum (inset a of Figure 5, arrow) differ slightly when an acid colloid is slowly titrated with base or when an alkaline colloid is titrated with acid. This is expected since coagulation of the particles starts before the pH$_{zpc}$ is attained. The average value of both titrations yields pH$_{zpc}$ 5.1.

The effect of a fast titration is shown in inset b of Figure 5. Again, the maximum coagulation rate is observed at pH 5.0. In this case the surface charge is reversed so rapidly that some of the loosely agglomerated particles are redispersed above pH 5.7 and an absorbance decrease is noted. Thus, very fast titration is a method to prepare transparent colloids on both sides of the pH$_{zpc}$.

TiO_2 colloids can be dissolved readily at low pH. Figure 6 shows how the absorption spectrum of a suspension of 4 × 10^{-4} M TiO_2 colloid decays when 0.1 M of HCl is added rapidly. The residual (stable) spectrum observed after long reaction times is ascribed to Ti(IV) oligomers that have been previously found under similar pH conditions.[37] The absorption decay at 235 nm has been analyzed in terms of first-order kinetics, i.e., ln ($A_t - A_\infty$) = $-kt$, and good fits ($R^2 \geq 0.99$) are obtained over at least 2 half-lives.

(33) Henglein, A.; Schnabel, W.; Wendenburg, J. *Einführung in die Strahlenchemie*; Verlag Chemie: Weinheim, Federal Republic of Germany, 1969; p 168.
(34) Kiwi, J.; Grätzel, M. *J. Mol. Catal.* **1987**, *39*, 63.
(35) Stumm, W.; Morgan, J. J. *Aquatic Chemistry*, 2nd ed.; Wiley-Interscience: New York, 1981; pp 625–640.
(36) Parks, G. A. *Chem. Rev.* **1965**, *65*, 177.
(37) Comba, P.; Merbach, A. *Inorg. Chem.* **1987**, *26*, 1315.

An Arrhenius plot of the rate constants k (inset of Figure 6) yields an activation energy for the dissolution of TiO_2 colloid (P1) of $E_a = 58 \pm 4$ kJ mol^{-1}. From the observation that the spectrum decays but does not blue-shift, we conclude that the rate-determining step of this dissolution is the initial attack of the crystallites by protons. Further degradation of smaller particles appears to proceed quickly. It is interesting to note that TiO_2 powder (P25, 2.5×10^{-4} M) does not dissolve at pH 1, even under drastic conditions (i.e., refluxing for 3 h).

Figure 7 shows the oxidation of iodide by photogenerated holes in air-saturated suspensions of TiO_2 colloids (P1 and P2) that have been illuminated with 5 mM photons at 330 nm. Quantum yields for the oxidation are given as a function of pH. As is obvious from the plot oxidation of I^- (eq 15) occurs only in the acid pH

$$I^- \xrightarrow[\Phi]{h\nu_{vb}^+} I^\cdot \qquad (15)$$

domain. Virtually no iodine or iodate is formed at pH >7. We conclude that I^- has to be adsorbed to the positively charged surface such that efficient hole scavenging can occur. The quantum yields shown in Figure 7 compare with a value of ≈2% reported previously by Herrmann and Pichat,[38] who illuminated a suspension of P25 TiO_2 powder at pH 0 ($[I^-] = 10$ mM) with UV light (300–400 nm); note, however, that at the low pH of their study the rate of the homogeneous oxidation of I^- (i.e., without TiO_2) is considerable (cf. Figure 7).

(38) Herrmann, J.-M.; Pichat, P. *J. Chem. Soc., Faraday Trans. 1* **1980**, *76*, 1138.

Summary

We have shown that controlled hydrolysis of $TiCl_4$ yields extremely small quantum-size TiO_2 particles ($d < 3$ nm, pH_{zpc} 5.1 ± 0.2) that possess anatase structure when prepared in aqueous solution. Excess negative charges created either by charge injection into the conduction band or by deprotonated surface hydroxyl groups lead to a blue-shift in the optical absorption spectrum of the transparent colloidal solution, which is understood in terms of an electrostatic model. Bandgap illumination of the semiconducting material results in the formation of blue Ti^{3+} centers under anoxic conditions with a quantum yield of 3%. The photocatalytic properties of the particles have been further demonstrated by the oxidation of I^-; the marked pH dependence of the quantum yield of this process reveals that surface adsorption of iodide ions is a prerequisite for iodine formation.

Acknowledgment. We are grateful for the assistance of M. Weller (HMI), Carol Garland (CIT), and K. Weiss (Fritz-Haber-Institut, Berlin) during the electron microscopic studies. D.W.B. thanks Prof. A. Henglein (HMI) and the Hahn-Meitner Institut for granting him a leave of absence. We extend our appreciation to G. Mills for helpful discussions and useful criticism. Financial support was provided by the U.S. EPA (R81162-01-0).

Registry No. TiO_2, 13463-67-7; HCl, 7647-01-0; I^-, 20461-54-5; $TiCl_4$, 7550-45-0; Ti, 7440-32-6.

Chapter 4

PHOTOCATALYTIC PRODUCTION OF H_2O_2 AND ORGANIC PEROXIDES IN AQUEOUS SUSPENSIONS OF TIO_2, ZnO, AND DESERT SAND

[The text of this chapter appeared in: Claudius Kormann, Detlef W. Bahnemann, and Michael R. Hoffmann, Environ. Sci. Technol. 1988, **22**, 798.]

Reprinted from ENVIRONMENTAL SCIENCE & TECHNOLOGY, Vol. 22, Page 798, July 1988
Copyright © 1988 by the American Chemical Society and reprinted by permission of the copyright owner.

Photocatalytic Production of H_2O_2 and Organic Peroxides in Aqueous Suspensions of TiO_2, ZnO, and Desert Sand

Claudius Kormann, Detlef W. Bahnemann,† and Michael R. Hoffmann*

Environmental Engineering Science, W. M. Keck Laboratories, California Institute of Technology, Pasadena, California 91125

■ The formation of H_2O_2 and organic peroxides in illuminated aqueous suspensions of ZnO, TiO_2, and desert sand in the presence of O_2 and organic electron donors has been studied. The photocatalytic rate of formation of H_2O_2 on ZnO was shown to depend on the O_2 partial pressure, on the concentration of organic electron donors, and on the concentration of H_2O_2. During the initial phase of irradiation the rate production of H_2O_2 is given by

$$\frac{d[H_2O_2]}{dt} = (\Phi_0 - \Phi_1[H_2O_2])\frac{d[h\nu]_{abs}}{dt}$$

where Φ_0 is the quantum yield for H_2O_2 formation, Φ_1 is the quantum yield for H_2O_2 degradation, and $d[h\nu]_{abs}/dt$ is the photon flux. The steady-state concentration of H_2O_2 was shown to be independent of the absorbed photon flux as predicted by the above equation; $[H_2O_2]_{ss} = \Phi_0/\Phi_1$. Steady-state concentrations of H_2O_2 in excess of 100 μM were obtained in illuminated suspensions of ZnO. In the case of ZnO, the quantum yield for H_2O_2 formation, Φ_0, approached 15% at 330 nm, whereas the photodegradation reactions were relatively inefficient. On the other hand, Φ_0 for TiO_2 (1% at 350 nm) was found to be an order of magnitude less than the value for ZnO. Φ_0 for a sample of desert sand (Death Valley, CA) was found to be 10^{-4}. Photooxidation of acetate and other organic electron donors on colloidal ZnO has been shown to produce substantial concentrations of organic peroxides, ROOH. Illumination of ZnO suspensions containing acetate produced greater than 40% of the measured total peroxide (H_2O_2 and ROOH) as ROOH.

Introduction

Overview. Hydrogen peroxide, H_2O_2, is the most effective oxidant of S(IV) in haze aerosols, clouds, and hydrometeors at low pH (*1*). Oxidation of S(IV) by H_2O_2 appears to be the major pathway for the formation of sulfuric acid in humid atmospheres (*2–4*).

In 1874, Schöne reported that H_2O_2 was present in rainwater (*5*). Since then, hydrogen peroxide concentrations as high as 60 μM for rainwater and 250 μM for cloudwater samples have been reported (*6–8*). Gas-phase concentrations in the range of 1–30 ppb have been predicted (*9, 10*), while concentrations in the range of 0.2–4.1 ppb have been measured by Heikes et al. (*11*) in the lower troposphere over the eastern United States. Measurements of H_2O_2 in polar ice samples clearly show that H_2O_2 was abundant in the atmosphere for more than 1000 years (*12*). Hydrogen peroxide can be generated in the gas phase due to the combination of hydroperoxyl radicals, $HO_2^{\cdot}$ (*13*), at the air–water interface due to photoinduced redox processes (*8*) and in the aqueous phase via photocatalyzed reactions with humic/fulvic acid and green algae as mediators (*14–16*). Furthermore, $HO_2^{\cdot}$ radicals that are produced in the gas phase can be scavenged by the water droplets where they then form H_2O_2. In situ generation of hydrogen peroxide together with H_2O_2 scavenged from the gas phase is thought to be the main source for the H_2O_2 accumulated in cloudwater droplets (*13, 17, 18*).

In addition to these pathways for H_2O_2 formation several other mechanisms are possible. For example, many metal oxides, some of which are abundant in the environment, have been shown to act as photocatalysts for a wide variety of reactions (*19*) such as the photoassisted reduction of N_2 to NH_3 (*20*). Atmospheric particulate matter originates mainly from natural sources (720–1850 Tg yr^{-1} in 1979 globally) but also from man-made emissions (125–385 Tg yr^{-1} in 1982 in the U.S.) with iron, titanium, and zinc being some of the most abundant transition metals detected in ambient samples (*21*).

Organic peroxides constitute another very important group of potential environmental oxidants. They have been detected in surface waters (*22*), on pine needles (*23*), and in rainwater and cloudwater (*7*). While their formation in the atmosphere has been established (*9, 24*), there are few reports in the literature of their formation in the aqueous phase (*14*). Recent review articles clearly indicate that mechanistic and quantitative aspects of the appropriate photochemical processes occurring in natural waters are still far from being understood (*25–28*).

Background. Many metal chalcogenides and oxides are known to be semiconductors. These materials can act as sensitizers for light-induced redox processes due to their electronic structure consisting of a valence band with filled molecular orbitals (MO's) and a conduction band with empty MO's. Absorption of a photon with an energy above the bandgap energy E_g generally leads to the formation of an electron/hole pair in the semiconductor particle (*29*) (eq 1).

$$\text{semiconductor} \xrightarrow{h\nu} e_{cb}^- + h_{vb}^+ \quad (1)$$

In the absence of suitable scavengers, recombination occurs within a few nanoseconds (*30*). Valence band holes (h_{vb}^+) have been shown to be powerful oxidants (*31–34*), whereas conduction band electrons (e_{cb}^-) can act as reductants (*35–37*). For a broad range of semiconductors and pH, the redox potential of the e_{cb}^- varies from +0.5 to −1.5 V [vs normal hydrogen electrode (NHE)] and that of the h_{vb}^+ from 1.0 to >3.5 V. This wide range of redox potentials fully covers the redox chemistry of the H_2O/O_2 systems (*38*).

H_2O_2 can be formed either by the reduction of O_2 by e_{cb}^- or by the oxidation of H_2O by h_{vb}^+:

$$O_2 + 2e_{cb}^- + 2H_{aq}^+ \rightarrow H_2O_2 \quad (2)$$

$$2H_2O + 2h_{vb}^+ \rightarrow H_2O + 2H_{aq}^+ \quad (3)$$

Photoassisted dioxygen reduction has been studied in great detail (*39–48*) since Baur and Neuweiler (*39*) in 1927 observed the formation of H_2O_2 when they illuminated aqueous zinc oxide suspensions in the presence of glycerin and glucose. Appreciable yields of hydrogen peroxide are detected only when appropriate electron donors D are added prior to illumination. The electron donor D, which must be adsorbed on the particle surface, reacts with the a valence band hole:

†Present address: Institut für Solarenergieforschung, Sokelandstrasse 5, D3000 Hannover, West Germany.

0013-936X/88/0922-0798$01.50/0 © 1988 American Chemical Society

$$D + h_{vb}^{+} \rightarrow D^{\bullet+} \quad (4)$$

Electron donors bound to the surface of the semiconductor particles interfere with e^-/h^+ recombination allowing e_{cb}^- (conduction band electrons) to react with molecular oxygen via reaction 2. Calvert et al. (*42*) have shown that H_2O_2 formed in irradiated suspensions of ZnO contained oxygen atoms derived exclusively from O_2. Cadmium sulfide, CdSe, and ZnO showed the highest catalytic activity for dioxygen reduction (*43*, *44*), while TiO_2 has been reported to have negligible activity with respect to H_2O_2 production (*43*, *45–47*). The oxidation of water via eq 3, however, has not yet been demonstrated unambiguously. For example, Rao et al. (*49*) reported on the formation of H_2O_2 during photolysis of aqueous suspension of ZnO and TiO_2, while Salvador and Decker (*50*) were unable to verify this observation. The intermediate production of H_2O_2 as the first molecular step of the four-hole oxidation of water to dioxygen has been predicted (*50*, *51*), and a variety of free radical intermediates has been detected (*52–54*). However, when the oxidation of H_2O proceeds with high yields, there is little evidence of hydrogen peroxide formation (*55–58*).

In addition to photocatalytic formation of hydrogen peroxide, stable hydroperoxides may form as a byproduct of the photooxidation of organic electron donors or by the nucleophilic addition of H_2O_2 to RCHO to yield alkyl hydroperoxides (*59*).

The above discussion indicates that a detailed study of the mechanism of the light-induced hydrogen peroxide production on various oxide surfaces is warranted in order to determine the viability of these pathways in environmental systems. Hence, our research has been focused on the kinetics and mechanisms of the formation of H_2O_2 and organic peroxides in irradiated suspensions of metal oxides and naturally occurring aluminum silicate mineral matrices such as desert sands.

Experimental Section

Materials. Titanium dioxide was obtained from Degussa (P25); it had a Brunauer–Emmett–Teller (BET) surface area of 50 ± 15 $m^2\ g^{-1}$ and an average particle diameter of 30 nm (*60*). Suspensions of 0.5 g L^{-1} (pH 4) were freshly prepared by sonication. This concentration resulted in an absorption of more than 95% of the incident photons at 330 nm. Transparent ZnO colloids with an average particle diameter of 5 nm were prepared as described previously (*61*). Suspensions of desert sand (Death Valley, dunes near Stovepipe Wells) were purified by a sequence of acidic leachings and centrifugations (4 × 0.1 N H_2SO_4, 1 × 0.05 M HF, 1 × 0.1 M HNO_3, and at least 3 × H_2O) in order to remove (photoinactive) carbonates, to oxidize trace organic materials, and to leach the more soluble cations that may be active in degrading H_2O_2 (such as traces of Fe^{II} ions). In fact, a considerable amount of magnetite (Fe_3O_4, black dust) could be retrieved with the aid of a stirring bar from the suspension prior to this procedure. *p*-Hydroxyphenylacetic acid (POPHA) (Kodak) was recrystallized twice from water. All other chemicals were of reagent grade and used without further purification. The water employed in all preparations was purified by a Milli-Q/RO system with an attached ORGANEX-Q unit; the resulting water had a resistivity of >18 MΩ cm.

Apparatus. The irradiation apparatus consisted of an Osram XBO 450W xenon lamp in a Müller LX 1450-2 lamp housing and a GM 252 (Kratos) monochromator. An additional 300-nm UV cutoff filter was placed at the monochromator outlet. The collimated beam of 1–1.6 cm^2 cross section was focused onto quartz irradiation vessels (3–16 mL) that were equipped with a small Teflon stirring bar and were bubbled with air (TiO_2) or calibrated O_2/N_2 mixtures (ZnO) to ensure constant O_2 content and to keep particles in suspension. In general, samples were bubbled at least 10 min before illumination. Actinometry was performed with (*E*)-2-[1-(2,5-dimethyl-3-furyl)-ethylidene]-3-isopropylidenesuccinic anhydride in toluene according to the method of Heller (*62*) yielding I = (50–1200) × 10^{-6} M $h\nu$ min^{-1}, depending on the reaction volume and the monochromator exit slit. Reaction temperatures were 24 ± 1 °C. TiO_2 suspensions were irradiated at 350 nm, which corresponds to an energy that is above the bandgap of TiO_2 (3 eV) (*63*). ZnO colloids were illuminated at 320 and 330 nm, i.e., energies that lie above the bandgap energy for the material (3.4 eV) (*61*). For colloidal suspensions the amount of photons absorbed could be calculated accurately from the absorption spectrum of the colloid and the actinometry.

Fluorescence spectra were measured on a Shimadzu RF-540, whereas absorption spectra were measured on a HP8451A instrument. UV filters were used when appropriate.

Analysis. Hydrogen peroxide concentrations were determined by three different methods. A polarographic technique allowed the in situ measurement of H_2O_2 with a sensitivity of 10^{-7} M and a time constant of 1 s (YSI-Clark 2510 oxidase probe connected to a YSI Model 25 oxidase meter). The electrode was calibrated following each kinetic experiment by standard additions of H_2O_2. The second method, sensitive to $\simeq 2 \times 10^{-8}$ M H_2O_2, involved dimerization of *p*-hydroxyphenylacetic acid (POPHA) in the presence of H_2O_2 and horseradish peroxidase to yield a detectable fluorescent product (λ_{ex} = 315 nm, λ_{em} = 406 nm) (*64*). Aliquots (2 mL) of the irradiated P25 suspensions were rapidly filtered through 0.2-μm HPLC filters (Gelman Sciences) to 0.1–0.5 mL amounts of POPHA reagent (8.0 ± 0.1 mg of POPHA, 2.0 ± 0.1 mg of peroxidase, and 50 mL 0.1 M pH 8.8 Tris buffer). Calibration was performed again by standard additions of H_2O_2 to the mixture and was found to be linear in the concentration ranges of interest. A reproducible background fluorescence, which we attribute to reagent impurities, amounted to $\approx 10^{-8}$ M H_2O_2.

Stock solutions of H_2O_2 were calibrated iodometrically by $\epsilon_{I_3^-}$ (352 nm) = 26 400 $M^{-1}\ cm^{-1}$ (*65*, *66*). The iodide method (detection limit of $\approx 10^{-6}$ M) allows one to distinguish between H_2O_2 and organic peroxides since the latter react more slowly with the molybdenum–iodide system. Aliquots (1.5 mL) of P25 suspensions were filtered, and then 0.75 mL of 0.1 M potassium biphthalate was added. At t = 0 min, 0.75 mL of iodide reagent (0.4 M potassium iodide, 0.06 M NaOH, $\approx 10^{-4}$ M ammonium molybdate) was added, and the absorbance vs time profile was recorded. Addition of the biphthalate buffer to ZnO colloids led to the dissolution of the colloid; this result was desirable in that it eliminated the absorption interference of colloid. No interference due to the presence of 10^{-3} M zinc ions were observed.

Results

Before the actual experimental results are presented, we wish to compare the different analytical techniques that were employed for the determination of inorganic and organic peroxides. The POPHA fluorescence technique responds to both H_2O_2 and organic peroxides, whereas the polarographic method only detects H_2O_2. A typical result for the iodide method is given in Figure 1, which shows an absorbance (λ = 352 nm) vs time profile for an aerated suspension of TiO_2 following the absorption of 2.8 × 10^{-3}

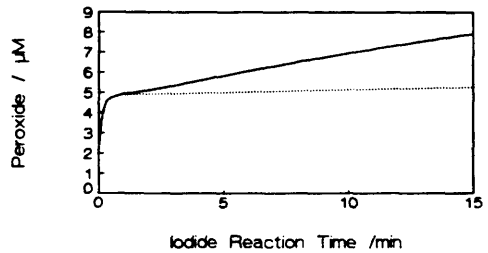

Figure 1. Detection of peroxides by the iodide method ($RO_2H + 2I^- \xrightarrow{I^-} ROH + I_3^-$). (—) Suspension of TiO_2 (0.5 g/L), 30 mM acetate, air, illuminated with 2.8 mM photons (λ_{ex} = 350 nm). (···) 5 μM standard addition of H_2O_2 to a suspension of TiO_2 of identical composition kept in the dark.

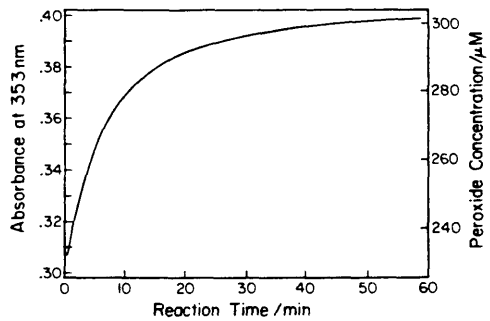

Figure 2. Detection of organic peroxides (iodide method) in a suspension of ZnO colloid (1 mM) that has been illuminated with 5.5 mM photons (330 nm); [acetate] = 2 mM, pH 7.7, O_2 bubbled.

M photons (λ_{ex} = 350 nm) in the presence of 3×10^{-2} M acetate. A fast formation of I_3^- is noted within 30 s, followed by a further slow increase that eventually levels off at long (≈1 h) reaction times. Hydrogen peroxide reacts substantially faster than I^- than does ROOH (*59*). These results show that more than 40% of the total peroxide formed during acetate oxidation is ROOH. The evolution of the absorbance at 352 nm, which is due to the faster reacting H_2O_2, is complete within 30 s. A slight reproducible color increase due to autoxidation (i.e., reaction with O_2) of I^- is noted over prolonged reaction time (≈1 h). Suspensions of TiO_2 with 3×10^{-2} M acetate in dark controls result in a very low absorption increase due to the nonphotolytic autoxidation of I^-.

Figure 2 illustrates the formation of organic peroxides on ZnO colloids. It shows the "slow" part of color evolution of the I_3^- ion that is observed when I^- is oxidized by organic peroxides. This plot is corrected for the absorption increase due to the autoxidation of I^- (e.g., less than 10% of the total absorption after 1 h). The amount of H_2O_2 formed is calculated from the I_3^- formed within the first 2 min of reaction, while the concentration of total peroxide is derived from the absorbance after 2 h when the absorption increases are due solely to the autoxidation of I^-.

Figure 3 shows the H_2O_2 concentration vs illumination time profile for an aerated suspension of TiO_2 particles irradiated with UV light (350 nm) in the presence of acetate. From the initial slope of this plot a quantum yield of 1% is calculated for the formation of H_2O_2. When a H_2O_2 concentration of ≈1 μM is reached, the increase levels off. The solid line represents a fit according to a simple rate expression (eq 9) that will be discussed below.

Figure 4 shows an analogous profile for an irradiated (320 nm) suspension of ZnO colloid. The quantum yield determined from the initial slope is 10%. The production

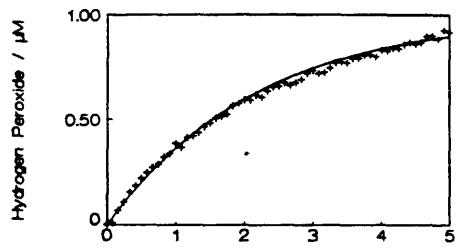

Figure 3. Hydrogen peroxide formation as function of illumination time in a suspension of 0.5 g/L TiO_2 (P25); [acetate] = 10 mM, air, λ_{ex} = 350 nm, $I = 4.7 \times 10^{-6}$ M photons per min. (+) Polarographic detection; (—) mathematical fit obtained by integration of eq 9 with the data of Table I.

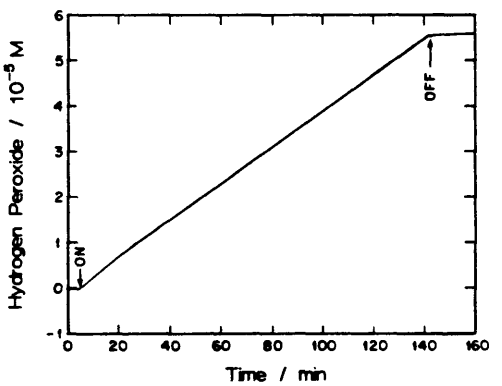

Figure 4. Hydrogen peroxide formation on colloidal ZnO (1 mM); [acetate] = 2 mM, pH 7.7, O_2 bubbled, λ_{ex} = 320 nm, quantum yield = 10% (polarographic detection).

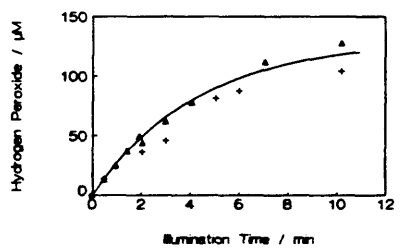

Figure 5. Hydrogen peroxide formation as function of illumination time in a suspension of ZnO colloid (1 mM), [acetate] = 2 mM, pH 7.7, air, λ_{ex} = 330 nm, $I_{abs} = 3.4 \times 10^{-6}$ M $h\nu$ min^{-1}. (+, Δ) Two different batches of colloid. Detection by iodide method. (—) Mathematical fit obtained as described for Figure 3.

of H_2O_2 is linear (i.e., zero order) over a wide concentration range (up to 60 μM).

The use of the iodide method is appropriate to probe the higher peroxide concentration range as is shown in Figure 5 for an aerated sample of ZnO (λ_{ex} = 330 nm). At higher H_2O_2 concentrations, the initial slope decreases, and a steady state is attained. The solid line represents a fit according to the mechanism given in the discussion.

Figure 6 shows an increase in the yield of total peroxide with an increase in acetate concentration in a suspension of TiO_2 with a fixed amount of adsorbed photons (i.e., 1.2×10^{-3} M). In the absence of acetate, more than 2×10^{-7} M of peroxide is formed during illumination. Small amounts (3×10^{-4} M) of added acetate strongly enhance the peroxide yield. A kinetic analysis of the H_2O_2 evolution (using the polarographic method) shows that for acetate

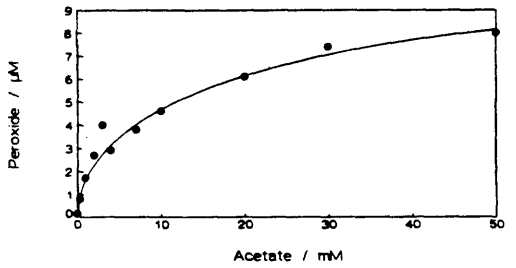

Figure 6. Peroxide formation on TiO_2 (P25) as function of acetate concentration. 0.5 g/L TiO_2, 1.2 mM photons (λ_{ex} = 350 nm), air (fluorescence method).

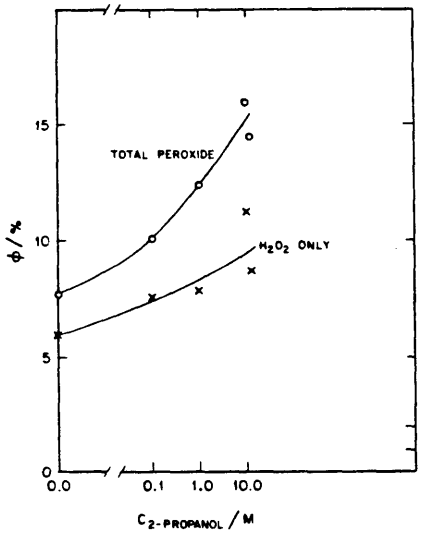

Figure 7. Quantum yield of H_2O_2 and organic peroxide formation on ZnO colloid (1 mM) as function of 2-propanol; [acetate] = 2 mM, 4.8 ± 0.3 mM photons (λ_{ex} = 330 nm), O_2 bubbled. Detection of peroxides with the iodide method (cf. Figure 1). H_2O_2, t_r = 2 min; total peroxide, t_r > 60 min.

concentrations $\leq 3 \times 10^{-3}$ M steady-state concentrations are reached after 1.2×10^{-3} M $h\nu$ have been absorbed. On the other hand, further illumination of samples with [acetate] > 10^{-2} M would produce even higher peroxide concentrations than indicated in Figure 6.

A similar plot is obtained (Figure 7) for the ZnO system [10^{-3} M ZnO, 2×10^{-3} M acetate, $(4.8 \pm 0.3) \times 10^{-3}$ M photons absorbed at 330 nm]. It shows the yield of H_2O_2 and total peroxide (ROOH + H_2O_2) as the concentration of added electron donor (2-propanol) is increased. In this case, the yield of organic peroxides is comparable to the yield of H_2O_2 at higher 2-propanol concentrations. Overall quantum yields of more than 15% are obtained.

The yield of hydrogen peroxide as a function of [O_2] in illuminated suspensions of ZnO colloid is illustrated in Figure 8. At an oxygen concentration that corresponds to the O_2 content in air, a limiting value for the quantum yield of H_2O_2 formation is reached. Minute amounts of H_2O_2 were observed in samples purged with N_2, but the H_2O_2 yield increased sharply upon introduction of O_2.

Steady-state concentrations of hydrogen peroxide in irradiated TiO_2 suspensions are functions of the relative rates of formation and degradation of H_2O_2. Figure 9 illustrates this point for a sample of TiO_2 with 30 mM acetate. From the sharp increase of hydrogen peroxide concentration in the initial phase of irradiation a quantum

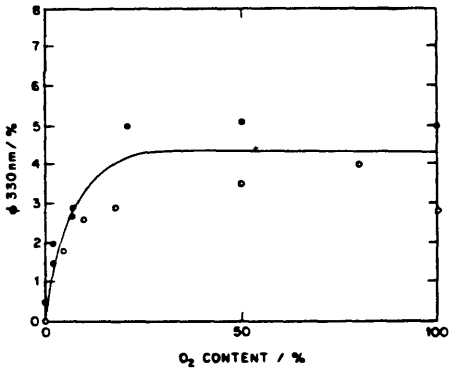

Figure 8. Quantum yield of H_2O_2 formation on ZnO colloid (1 mM) as function of O_2 content; [acetate] = 2 mM, 5.4 ± 0.3 mM photons absorbed (λ_{ex} = 330 nm). Detection of H_2O_2 with the iodide method. (○, ●) Two different batches of colloid.

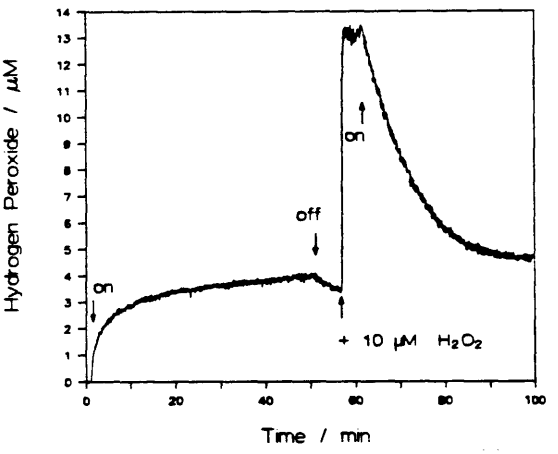

Figure 9. Photocatalytic hydrogen peroxide formation and degradation on TiO_2 (0.5 g/L) (P25); [acetate] = 30 mM, air, I(350 nm) = 4.7 × 10^{-6} M photons per minute. Polarographic detection.

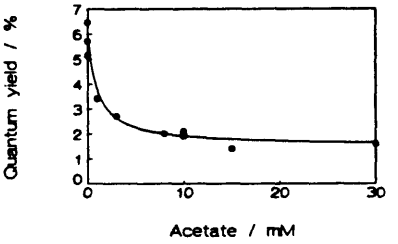

Figure 10. Quantum yield of photodegradation of H_2O_2 on illuminated TiO_2 as function of acetate concentration. Calculated from declining slopes of plots such as Figure 9.

yield of 5% is calculated. In this experiment, for which the concentration of electron donors is relatively high, the steady-state concentration of 5 μM H_2O_2 is reached slowly. After turning off the light source, a slight decrease (≈1 μM) of H_2O_2 is noted over 10 min, possibly due to adsorption of H_2O_2 to the particle surfaces or a slow reaction of Ti^{III} with H_2O_2. A standard addition of 10^{-5} M H_2O_2 establishes the concentration scale of the plot. H_2O_2 is stable on TiO_2 in the dark. However upon turning on the light source, H_2O_2 concentrations that are initially above the steady-state concentrations are rapidly depleted to the level of the steady state.

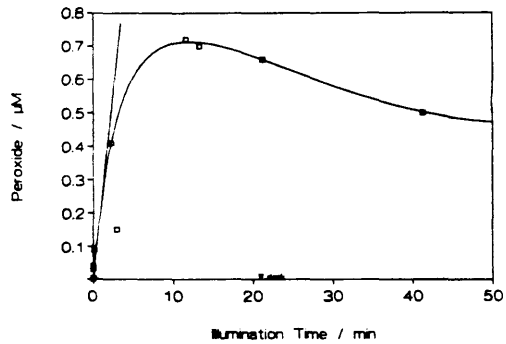

Figure 11. Formation of peroxides on TiO_2 in the absence of added electron donors. Detection with fluorescence technique: 0.5 g/L TiO_2, air, I(350 nm) = 4.7×10^{-6} M photons per minute. Initial quantum yield (straight line): 0.5%.

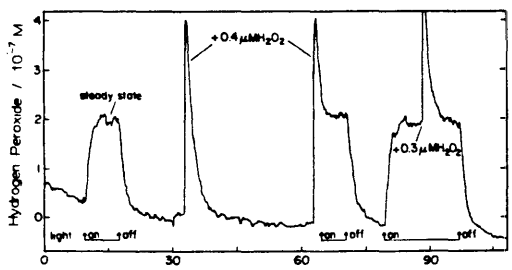

Figure 12. Formation of hydrogen peroxide in an illuminated suspension of Death Valley desert sand (40 g/L); [acetate] = 10 mM, [KCl] = 10 mM, air, I(350 nm) = 1.2×10^{-5} M photons per minute.

Figure 10 illustrates the relative effect of increasing acetate concentrations on the rate of photodegradation of H_2O_2 on P25 particles. In this case an increase in [$CH_3CO_2^-$] results in a decrease in the rate of destruction of H_2O_2.

Figure 11 shows that peroxides are also formed on TiO_2 in the absence of added hole scavengers. The concentration vs irradiation time profile is obtained by the fluorescence method. Peroxide concentrations reached a maximum of 7×10^{-7} M after absorption of ca. 5×10^{-4} M $h\nu$. However, further irradiation resulted in lower peroxide concentrations. Similar behavior was observed in kinetic runs with the polarographic electrode. The initial slope as represented by the straight line represents a quantum yield of 0.5% (which is a conservative value; from other runs with better time resolution we obtained an upper value of 3%). No peroxide formation ($<2 \times 10^{-8}$ M) is observed in suspensions that were stirred/bubbled for 20 min in the dark.

Figure 12 shows the formation of hydrogen peroxide on an O_2 bubbled suspension of 40 g/L desert sand. Acetate (1×10^{-2} M) was present as a hole scavenger. H_2O_2 formation was observed at an initial rate of 1.5×10^{-7} M min^{-1} at a photon flux of 1.2×10^{-3} M $h\nu$ min^{-1}; this gave a quantum yield of $\Phi_0 = 10^{-4}$. A steady-state concentration of 2×10^{-7} M was reached fairly rapidly. In the absence of light, H_2O_2 decayed exponentially. Standard additions of 4×10^{-7} M H_2O_2 establish the scale of the plot shown in Figure 12. After a standard addition of 4×10^{-7} M, the H_2O_2 concentration was degraded to the steady-state concentration of 2×10^{-7} M upon irradiation.

Discussion

Pathways for H_2O_2 Formation. Three qualitatively different pathways for the photocatalytic production of hydrogen peroxide are plausible. (1) H_2O_2 can be produced through reduction of O_2 by conduction band electrons (eq 2). The yield of photogenerated conduction band electrons can be increased by adding electron donors. Higher oxygen concentrations are expected to enhance the removal of the electrons. Both assumptions are consistent with the experiments illustrated in Figures 6–8. (2) H_2O_2 can be produced via the oxidation of water (eq 3). This process most likely occurs in the absence of added electron donors. (3) H_2O_2 can be generated by secondary reactions of oxidized organic molecules such as the dimerization and decomposition of the methylperoxy- (*67*) or the α-peroxyacetic acid radicals (*68*), or by reaction of α-hydroxymethylene radicals with oxygen (*59, 69, 70*). These reactions may be important at high concentrations of organic molecules and/or after long illumination.

In the presence of electron donors, pathway 2 can be neglected. It has been shown by Bahnemann et al. (*71*) that the oxidation of organic molecules by valence band holes is the principal process. The relative importance of pathways 1 and 3 can be evaluated with the aid of a complete product analysis. However, this task is complicated by the multitude of organic molecules that may be formed (vide infra). Nonetheless, an empirical expression for the rate of formation of H_2O_2 can be obtained which shows either that pathway 3 is negligible during the initial phase of illumination or that its contribution to the formation of H_2O_2 is independent of the H_2O_2 concentration.

Given an excess concentration of electron donors to scavenge photogenerated valence band holes and a constant O_2 concentration to accept conduction band electrons, the rate of formation of H_2O_2 will be zero order (eq 5). We have shown in a previous study that a low concentration of O_2 is sufficient to lead to an efficient transfer of conduction band electrons to adsorbed oxygen molecules (*61*). On the other hand, H_2O_2 may also be photodegraded. It can be reduced to water (eq 6) or oxidized to O_2 (eq 7).

$$\frac{d[H_2O_2]}{dt} = f_1([D],[O_2]) = \Phi_0 \frac{d[h\nu]_{abs}}{dt} \quad (5)$$

$$H_2O_2 + 2e_{cb}^- \xrightarrow{H^+} 2H_2O \quad (6)$$

$$H_2O_2 + 2h_{vb}^+ \rightarrow O_2 + 2H^+ \quad (7)$$

Both processes are first order in H_2O_2 for low concentrations of H_2O_2. The combination of these reactions will result in the attainment of a steady-state concentration of hydrogen peroxide during continuous irradiation. The rate of formation can be assumed to be given by eq 5, whereas the rate of degradation of H_2O_2 should follow

$$-\frac{d[H_2O_2]}{dt} = f_2([D],[O_2],[H_2O_2]) = \Phi_1[H_2O] \frac{d[h\nu]_{abs}}{dt} \quad (8)$$

Hence the overall production of H_2O_2 is given by eq 9.

$$\frac{d[H_2O_2]}{dt} = (\Phi_0 - \Phi_1[H_2O_2]) \frac{d[h\nu]_{abs}}{dt} \quad (9)$$

Under these conditions the steady-state concentration of H_2O_2 is independent of the absorbed photon flux during the experiment (eq 10).

$$[H_2O_2]_{ss} = \Phi_0/\Phi_1 \quad (10)$$

The initial phase of H_2O_2 formation on TiO_2 and on ZnO can be described with this simple rate law as shown by the solid lines of Figures 3 and 5. The parameters corresponding to these fits are summarized in Table I.

High concentrations of H_2O_2 are obtained readily in illuminated suspensions of ZnO not only because of the relatively high quantum yield for H_2O_2 formation but also

Table I. Initial Phase of Photocatalytic H_2O_2 Formation

material	Φ_0,[a] %	Φ_1,[b] M^{-1}	$[H_2O_2]_{ss}$,[c] μM
TiO_2, 10 mM acetate	1	1×10^4	1
ZnO, 2 mM acetate	9	7×10^2	130
sand, 10 mM acetate	0.01	5×10^3 [d]	0.2

[a] Φ_0, quantum yield of formation. [b] Φ_1, efficiency of degradation. [c] $[H_2O_2]_{ss} = \Phi_0/\Phi_1$, steady-state concentration. [d] Includes thermal degradation.

because of the relative inefficiency of the photodegradation reactions. On the other hand, only low hydrogen peroxide concentrations are found in illuminated TiO_2 suspensions because H_2O_2 is degraded more efficiently. This finding is not surprising in view of the high stability of Ti–peroxo complexes (*72*). Hydrogen peroxide formed on the TiO_2 surface is not readily released. Modifying the surface properties of TiO_2 particles may thus lead to higher H_2O_2 yields.

Further illumination of ZnO and TiO_2 suspensions leads to higher H_2O_2 concentrations than expected from eq 9 and the parameters of Table I. In fact, H_2O_2 concentrations of more than 5×10^{-6} M (in addition to 5×10^{-6} M organic peroxides) were found on illuminated TiO_2, while concentrations of H_2O_2 produced on ZnO approached millimolar levels upon prolonged illumination. Obviously, eq 9 is applicable only during the initial phase of illumination. During later stages of irradiation, organic peroxides appear to compete effectively with H_2O_2 for the degradation pathways (eq 6 and 7).

Formation of Peroxides from Organic Radicals. In a recent review on the sources of hydrogen peroxide in cloudwater (*73*), reactions of organic radicals were mentioned as a possible source.

Reaction 4 describes the oxidation of organic molecules (i.e., electron donors) by photogenerated valence band holes leading to organic radicals $D^{\bullet+}$ (or $D^{\bullet}$). Carbon-centered radicals add oxygen at diffusion-controlled rates (*74*) (eq 11) to form the corresponding peroxy radical.

$$R^1R^2R^3C^{\bullet} + O_2 \rightarrow R^1R^2R^3C(O_2)^{\bullet} \quad (11)$$

Depending on the nature and concentration of the peroxy radicals, first- or second-order decay kinetics prevail. Under environmental conditions low steady-state concentrations are likely to favor first-order decay processes.

Depending on the other substituents on the carbon atom, two different reaction patterns have been observed by pulse radiolysis and analyzed in terms of reaction kinetics and products (*59*, *67–70*, *75–77*). If one of the substituents is OH, O^-, or NR_2 [e.g., $CH_3\dot{C}HOH$ (*70*), $\dot{C}O_2^-$ (*76*), or $\dot{C}H_2N(CH_3)_2$ (*77*)] (i.e., a heteroatom with a non- or antibonding electron pair), the peroxy radical is unstable and decays within a few milliseconds to yield the corresponding aldehyde, ketone, acid, or imine and a superoxide radical ($O_2^{\bullet-}$):

$$R^1R^2(OH)C(O_2)^{\bullet} \rightarrow R^1R^2CO + O_2^{\bullet-} + H^+ \quad (12)$$

Specific and general base catalysis further accelerates the elimination of $O_2^{\bullet-}$ from α-hydroxyalkylperoxy radicals (*69*). Superoxide ($O_2^{\bullet-}$) ultimately forms hydrogen peroxide in a bimolecular process (eq 13) (*78*). No organic peroxides are formed according to this route.

$$O_2^{\bullet-} + HO_2^{\bullet} \xrightarrow{H^+} H_2O_2 + O_2 \quad (13)$$

If none of the substituents R^1, R^2, or R^3 (eq 11 and 12) provides a nonbonding electron pair to the carbon-centered radical, the corresponding peroxy radical (e.g., $^{\bullet}O_2CH_2CO_2^-$) is stable toward unimolecular or base-catalyzed elimination of $O_2^{\bullet-}$. For example, only trace amounts of H_2O_2 were observed when this radical was generated by the photolysis of NO_3^-–acetate solutions (*79*). The reactivity of such peroxy radicals has been described by Sheldon and Kochi (*80*). Organic hydroperoxides result after abstraction of weakly bound [D(R–H) < 90 kcal/mol] hydrogen atoms from such sources as $HO_2^{\bullet}$, aldehydes, ternary carbon centers, or hydrogen atoms in α-position to a carbon–carbon double bond (e.g., from toluene). These radicals may also add to olefins yielding dialkyl peroxides. Addition and abstraction ratios for various olefins have been tabulated (*80*).

Fraser et al. (*81*) proposed that 2-propanol reacts as a hole scavenger on TiO_2 (eq 14 and 15) to produce only

$$(CH_3)_2CHOH + h_{vb}^+ \rightarrow (CH_3)_2\dot{C}OH + H_{aq}^+ \quad (14)$$

$$(CH_3)_2\dot{C}OH + h_{vb}^+ \rightarrow (CH_3)_2CO + H_{aq}^+ \quad (15)$$

acetone as the final product even in the presence of O_2. However, from Figure 7 we see that higher 2-propanol concentrations do lead to higher concentrations of organic peroxides. Hence, pathways other than eq 14 and 15 must be considered.

$OH^{\bullet}$ radicals are possibly formed by reaction of surficial hydroxide with photogenerated holes (eq 16). From pulse

$$OH_s^- + h_{vb}^+ \rightarrow OH_s^{\bullet} \quad (16)$$

radiolysis it is known that $OH^{\bullet}$ radicals will oxidize 2-propanol to yield 85% $(CH_3)_2\dot{C}OH$ and 11% $(CH_3)(\dot{C}H_2)CHOH$ (i.e., α- and β-carbon-centered radicals), respectively (*82*, *83*). While reactions of the strongly reducing α-isopropyl radical will ultimately yield only acetone and H_2O_2, the reactivity of the β radical is expected to be different. The β radical may add O_2 in a diffusion-controlled reaction (*74*) according to eq 17 in analogy to similar reactions of organic peroxy radicals (*75*). This radical may either be stabilized on the particle surface until a further reduction to an alkylhydroperoxide (eq 18) or it may dimerize and fragment to yield several products among which organic peroxides and H_2O_2 are expected to be found (*67*, *68*, *75*).

$$(CH_3)(\dot{C}H_2)CHOH + O_2 \rightarrow (CH_3)(\dot{O}_2CH_2)CHOH \quad (17)$$

$$(CH3)(\dot{O}_2CH_2)CHOH + e_{cb}^- + H^+ \rightarrow CH_3(HO_2CH_2)CHOH \quad (18)$$

As is obvious from Figure 1 the oxidation of acetate also yields organic peroxides, a finding that can be explained as follows. Kräutler et al. assumed the intermediacy of the methyl radical in their study of the oxidation of acetate of illuminated TiO_2 suspensions (*84*). They observed the formation of methane and ethane. When oxygen was present, their mechanism accounted for only ≈30% of the rate of decomposition of acetic acid, and they did not attempt to analyze the remaining 70%. In the presence of oxygen, methyl radicals may react to yield methylperoxy radicals, which in turn dimerize and decompose to yield an array of products such as CH_3O_2H, CH_3OOCH_3, CH_3OH, HCO_2^-, CH_2O, and H_2O_2 (*67*).

Over the pH domain of this study (TiO_2, pH 4.0–4.7; ZnO, pH 7.7), the particle surfaces are positively charged since the pH of zero point of charge (pH_{zpc}) is 6.0 for TiO_2 (*85*) and 9.3 for ZnO (*61*). Under these conditions anions such as acetate are adsorbed to the oxide surfaces (*86*).

Variation of the acetate concentration was found to have a pronounced effect on the photocatalytic process. In addition to increasing the yield of formation of H_2O_2, an increase in $[CH_3CO_2^-]$ was found to decrease the rate of photodegradation of H_2O_2. This latter effect may be at-

tributed to either a steric effect in which acetate blocks the sites where H_2O_2 is degraded or an efficient competition of acetate with H_2O_2 for valence band holes.

It is noteworthy that neither Figure 6 nor Figure 10 yield linear plots but resemble adsorption isotherms. If Figure 10 were interpreted as an adsorption isotherm, one would conclude that at an acetate concentration of $\approx 2 \times 10^{-3}$ M half of the surface sites were covered. This amount of surface coverage may be considered an upper limit. In fact, the presence of fewer acetate molecules may be sufficient to promote the electronic effects observed, as will be demonstrated for the adsorption of oxygen.

Figure 8 shows again an adsorption isotherm-type behavior of the quantum yield of H_2O_2 formation on the O_2 partial pressure. An increase in the oxygen content from 20% to 100% of saturation did not result in a corresponding increase in the quantum yield for H_2O_2 production. However, even at 100% O_2 (i.e., $p_{O_2} = 1$ atm, hence $c_{O_2} = 1.2 \times 10^{-3}$ M) the reactive sites on the particle surfaces are not expected to be saturated with O_2. Water is likely to form much stronger bonds to reactive sites on the surface under the pH conditions of our experiments (e.g., $\equiv$|-Zn^+ and $\equiv$|-Ti^+) than O_2, thus only a few O_2 molecules appear to be adsorbed on each particle. At an O_2 content of ≈10% where the quantum yield has reached half of its final value (Figure 8), we estimate on a numerical basis that half of the particles interact with only one molecule of O_2 each. Fluorescence spectroscopy of the ZnO colloid supports this interpretation (*61*).

H_2O_2 Formation in the Absence of Sacrificial Electron Donors. Water can be oxidized photochemically on TiO_2 as follows (*51*, *87–89*):

$$2H_2O \xrightarrow[TiO_2]{4h\nu} 2H_2 + O_2 \quad (19)$$

$$2H_2O \xrightarrow[TiO_2]{2h\nu} H_2 + H_2O_2 \quad (20)$$

$$2H_2O + O_2 \xrightarrow[TiO_2]{2h\nu} 2H_2O_2 \quad (21)$$

In the absence of deposited noble metal catalysts, hydrogen fixation on titanium dioxide seems unlikely. Isotopic exchange experiments have shown the absence of D or H exchange between D_2 and surface hydroxyls of TiO_2 both in the dark and under intense bandgap irradiation (*90*). Hence, the reaction given in eq 21 appears to be the most plausible stoichiometry for H_2O_2 production in illuminated suspensions of pure TiO_2.

In the case of a nonstoichiometric TiO_2 such as "blue" TiO_2 (*49*) or an *n*-type TiO_2, oxygen may be reduced by the excess electrons according to eq 22, yielding $O_2^{\cdot-}$ and hence H_2O_2 (eq 23). The release of $O_2^{\cdot-}$ may occur in the dark but may also require activation by light.

$$(TiO_2)_n^{x-} + xO_2 \rightarrow [(TiO_2)_n(O_2)_x]^{x-} \rightarrow (TiO_2)_n + xO_2^{\cdot-} \quad (22)$$

$$xO_2^{\cdot-} + xH^+ \rightarrow (1/2x)H_2O_2 + (1/2x)O_2 \quad (23)$$

We have shown that H_2O_2 is detectable in the homogeneous phase after illumination of an aqueous suspension of TiO_2, although the concentration is low, $\leq 10^{-6}$ M. The initial rate of formation was relatively high, but the maximum steady-state concentration (7×10^{-7} M) was attained after a small number of photons had been absorbed (Figure 11). This initial phase of H_2O_2 production may be due to photoactivated release of $O_2^{\cdot-}$ according to eq 22 or it may result from degradation of trace amounts of organics (eq 4, 11–13) initially present in the system. The steady-state concentration of H_2O_2 production due to water oxidation (2×10^{-7} M) is low because of efficient degradation of the molecule.

Formation of Hydrogen Peroxide on a Suspension of Desert Sand. Illumination of a suspension of desert sand containing acetate as a hole scavenger (Figure 12) resulted in H_2O_2 formation with the attainment of a steady-state concentration of 2×10^{-7} M. Desert sand suspensions show photochemical behavior similar to that of TiO_2 and ZnO. However, H_2O_2 is also degraded in the dark on desert sand. This may be due to a "Fenton-type" reaction between H_2O_2 and Fe^{2+} (*91*). Our sample contained a substantial amount of magnetite ($Fe^{II}Fe^{III}_2O_4$); some of the magnetite may have remained within the sample after the cleanup procedure. Also, the photocatalytic dissolution of Fe_2O_3 yielding ferrous ions when electron-donating molecules are present has been observed and may be of importance in this reaction system (*92*). Further studies are in progress to characterize the photocatalytic activity of desert sands.

Emissions and Transport of TiO_2, ZnO, and Sand in the Atmosphere. Titanium and zinc minerals are found in dust in the atmosphere (*93*). Weathering of crustal rocks of the continents is thought to be the main source of this atmospheric dust. Estimates of the amount of mineral dust capable of long-range transport are on the order of hundreds of million tons annually with the Sahara being a predominant source ($260–400 \times 10^6$ tons per year) (*94*). While dust concentrations over the oceans are diluted to less than a few micrograms per cubic meter, higher concentrations were found over land (≈10 μg m^{-3}) and over the Sahara (≈100 μg m^{-3}) (*94*). Considerable amounts—about 5×10^6 tons originating from the Sahara—of dust particles of the appropriate size range (0.1–1 μm) are transported over several thousand kilometers (*95*). The concentration of Ti in sand was found to range between 4000 and 16 000 ppm (*93*, *96*); zinc is a somewhat less abundant mineral: ≈200 ppm (*93*). Thus about 1 000 000 tons of Ti minerals, mostly oxides (50 000 tons of Zn), are emitted naturally into the atmosphere above the Sahara. Man-made atmospheric emissions in the U.S. were ≈90 000 tons of TiO_2 (1973) (*97*) and 160 000 tons of zinc (1969) (*98*).

In urban areas, typical concentrations of inorganic material are about 5 μg m^{-3} with average Ti contents of 2% and Zn of 1.6% (*99*), while typical concentrations of organic carbon/soot are near 20 μg m^{-3} (*100*). Assuming that this material was incorporated fully into a cloud with a liquid water content (LWC) of 0.1 g m^{-3}, the concentration of zinc oxide would be approximately 8 μM. In our experiments the [ZnO] colloid was 1.0 mM. In haze aerosol, the concentration of ZnO can be as large as 10 mM due to the smaller LWC of these droplets (i.e., LWC $\simeq 10^{-5}$–10^{-4} g m^{-3}). In terms of potential electron donors a large fraction of 20 μg m^{-3} of suspended organic carbon may be suitable as electron donor substrates. Munger et al. (*101*) have found concentrations of acetate in cloud and fogs in Southern California that range from 14 to 581 μM and concentrations of formate that range from 43 μM to 1.5 mM. Both of these anions would be suitable electron donors for the photocatalytic production of peroxide. From our studies we have found that an increase in elecron donor concentration would result in a higher quantum yield for the formation of peroxides, a lower rate of degradation, higher steady-state concentrations under constant illumination, and a higher yield of ROOH relative to H_2O_2.

Acknowledgments

We thank Marcia Dodge for her support of this research

subject. D.W.B. thanks the Hahn-Meitner Institut (Berlin) for granting him a leave of absence.

Registry No. H_2O_2, 7722-84-1; TiO_2, 13463-67-7; ZnO, 1314-13-2.

Literature Cited

(1) Hoffmann, M. R.; Kerr, J. A.; Calvert, J. G. *Chemical Transformation Modules for Eulerian Acid Deposition Models. The Aqueous-Phase Chemistry*; NCAR: Boulder, CO, 1984; Vol. II.
(2) Hoffmann, M. R.; Boyce, S. D. In *Advances in Environmental Science and Technology*; Schwartz, S. E., Ed.; Wiley: New York, 1983; Chapter 12, pp 147–189.
(3) Hoffmann, M. R.; Jacob, D. J. In *SO_2, NO, and NO_2 Oxidation Mechanisms: Atmospheric Considerations*; Calvert, J. G., Ed.; Acid Precipitation Series; Butterworth: Boston, MA, 1984; Vol. III, pp 101–172.
(4) Jacob, D. J.; Hoffmann, M. R. *J. Geophys. Res. C: Oceans Atmos.* **1983**, *88*, 6611–6621.
(5) Schöne, E. *Ber. Dtsch. Chem. Ges.* **1874**, *7*, 1693–1708.
(6) Lazrus, A. L.; Gandrud, B. W.; Gilin, S. N.; Heikes, B. G.; Kok, G. L.; Lind, J. A.; Shetter, R. E.; Walega, J. G.; McLaren, S. E. *J. Geophys. Res.*, in press.
(7) Kelly, T. J.; Daum, P. H.; Schwartz, S. E. *J. Geophys. Res. D: Atmos.* **1985**, *90*, 7861–7871.
(8) Zika, R. G.; Saltzman, E.; Chameides, W. L.; Davis, D. D. *J. Geophys. Res. C: Oceans Atmos.* **1982**, *87*, 5015–5017.
(9) Stockwell, W. R. *Atmos. Environ.* **1986**, *20*, 1615–1632.
(10) Seinfeld, J. H. *Atmospheric Chemistry and Physics of Air Pollution*; Wiley: New York, 1986; pp 235–237.
(11) Heikes, B. G.; Kok, G. L.; Walega, J. G.; Lazrus, A. L. *J. Geophys. Res. D: Atmos.* **1987**, *92*, 915–931.
(12) Neftel, A.; Jacob, P.; Klockow, D. *Nature (London)* **1984**, *311*, 43–45.
(13) Chameides, W. L.; Davis, D. D. *J. Geophys. Res. C: Oceans Atmos.* **1982**, *87*, 4863–4877.
(14) Zika, R. G. *Elsevier Oceanogr. Ser. (Amsterdam)* **1981**, *31*, 299–325.
(15) Cooper, W. J.; Zika, R. G. *Science (Washington, D.C.)* **1983**, *220*, 711–712.
(16) Moffett, J. W.; Zika, R. G. *Mar. Chem.* **1983**, *13*, 39–251.
(17) Graedel, T. E.; Goldberg, K. I. *J. Geophys. Res. C: Oceans Atmos.* **1983**, *88*, 10865–10882.
(18) Chameides, W. L. *J. Geophys. Res. D: Atmos.* **1984**, *89*, 4739–4755.
(19) Fendler, J. H. *J. Phys. Chem.* **1985**, *89*, 2730–2740.
(20) Schrauzer, G. N.; Strampach, N.; Hui, L. N.; Palmer, M. R.; Saleshi, J. *Proc. Natl. Acad. Sci. U.S.A.* **1983**, *80*, 3873–3876.
(21) Seinfeld, J. H. *Atmospheric Chemistry and Physics of Air Pollution*; Wiley: New York, 1986; pp 26–31.
(22) Larson, R. A.; Smykowski, K.; Hunt, L. L. *Chemosphere* **1981**, *10*, 1335–1338.
(23) Stärk, G.; Stauff, J. *Staub—Reinhalt. Luft* **1986**, *46*, 396–400.
(24) Carlier, P.; Hannachi, H.; Mouvier, G. *Atmos. Environ.* **1986**, *20*, 2079–2099.
(25) Zepp, R. G. In *Dynamic Exposure and Hazard Assessment of Toxic Chemicals*; Haque R., Ed.; Ann Arbor Science: Ann Arbor, MI, 1980; pp 69–100.
(26) Zafiriou, O. C. In *Chemical Oceanography*; Riley, J. P., Chester, R., Eds.; 1983; Vol. VIII, pp 339–379.
(27) Zafiriou, O. C.; Joussot-Dubien, J.; Zepp, R. G.; Zika, R. G. *Environ. Sci. Technol.* **1984**, *18*, 358A–371A.
(28) Weiner, E. R.; Goldberg, M. C. *Toxicol. Environ. Chem.* **1985**, *9*, 327–339.
(29) Bard, A. J. *Science (Washington, D.C.)* **1980**, *207*, 139–144.
(30) Rothenburger, G.; Moser, J.; Grätzel, M.; Serpone, N.; Sharma, D. K. *J. Am. Chem. Soc.* **1985**, *107*, 8054–8059.
(31) Izumi, I.; Dunn, W. W.; Wilbourn, K. O.; Fan, F. F.; Bard, A. J. *J. Phys. Chem.* **1980**, *84*, 3207–3210.
(32) Harvey, P. R.; Rudham, R.; Ward, S. *J. Chem. Soc., Faraday Trans. 1* **1983**, *79*, 2975–2981.
(33) Herrmann, M.-M.; Mozzanega, M.-N.; Pichat, P. *J. Photochem.* **1983**, *22*, 333–343.
(34) Fox, M. A.; Chen, C.-C.; Park, H.-H.; Younathan, J. N. *ACS Symp. Ser.* **1985**, *No. 278*, 69–78.
(35) Brown, G. T.; Darwent, J. R. *J. Chem. Soc., Faraday Trans. 1* **1984**, *80*, 1631–1643.
(36) Bahnemann, D.; Henglein, A.; Spanhel, L. *Faraday Discuss. Chem. Soc.* **1984**, *No. 78*, 151–163.
(37) Gerischer, H. *Top. Appl. Phys.* **1979**, *31*, 115–172.
(38) Latimer, W. M. *Oxidation Potentials*, 2nd ed.; Prentice-Hall: New York, 1952; pp 38–50.
(39) Baur, E.; Neuweiler, C. *Helv. Chim. Acta* **1927**, *10*, 901–907.
(40) Markham, M. C.; Laidler, K. J. *J. Phys. Chem.* **1953**, *57*, 363–369.
(41) Rubin, T. R.; Calvert, J. G.; Rankin, G. T.; MacNevin, W. *J. Am. Chem. Soc.* **1953**, *75*, 2850–2853.
(42) Calvert, J. G.; Theurer, K.; Rankin, G. T.; MacNevin, W. M. *J. Am. Chem. Soc.* **1954**, *76*, 2575–2578.
(43) Stephens, R. E.; Ke, B.; Trivich, D. *J. Phys. Chem.* **1955**, *59*, 966–969.
(44) Hair, M. L.; Harbour, J. R. *Adv. Chem. Ser.* **1980**, *No. 184*, 173–183.
(45) Pappas, S. P.; Fischer, R. M. *J. Paint Technol.* **1974**, *46*, 65–72.
(46) Cundall, R. B.; Rudham, R.; Salim, M. S. *J. Chem. Soc., Faraday Trans. 1* **1976**, *72*, 1642–1651.
(47) Harbour, J. R.; Hair, M. L. In *Magnetic Resonance in Colloid and Interface Science*: Fraissard, J. P.; Resing, H. A., Eds.; Riedel: Dordrecht, 1980; pp 431–436.
(48) Harbour, J. R.; Tromp, J.; Hair, M. L. *Can. J. Chem.* **1985**, *63*, 204–208.
(49) Rao, M. V.; Rajeshwar, K.; Pal Verneker, V. R.; DuBow, J. *J. Phys. Chem.* **1980**, *84*, 1987–1991.
(50) Salvador, P.; Decker, F. *J. Phys. Chem.* **1984**, *88*, 6116–6120.
(51) Rives-Arnau, V. *J. Electroanal. Chem. Interfacial Electrochem.* **1985**, *190*, 279–281.
(52) Jaeger, C. D.; Bard, A. J. *J. Phys. Chem.* **1979**, *83*, 3146–3152.
(53) Anpo, M.; Shima, T.; Kubokawa, Y. *Chem. Lett.* **1985**, 1799–1802.
(54) Serwicka, E. *Colloids Surf.* **1985**, *13*, 287–293.
(55) Baur, E.; Perret, A. *Helv. Chim. Acta* **1924**, *7*, 910–915.
(56) Perret, A. *J. Chim. Phys. Phys.-Chim. Biol.* **1926**, *23*, 97–129.
(57) Hada, H.; Yonezawa, Y.; Saakawa, M. *Bull. Chem. Soc. Jpn.* **1982**, *55*, 2010–2014.
(58) Nishimoto, S.-I.; Ohtani, B.; Kajiwara, H.; Kagiya, T. *J. Chem. Soc., Faraday Trans. 1* **1983**, *79*, 2685–2694.
(59) Bothe, E.; Schulte-Frohlinde, D. *Z. Naturforsch. B: Anorg. Chem., Org. Chem.* **1980**, *35B*, 1035–1039.
(60) Degussa, *Technical Bulletin Pigments*, 4th ed.; Degussa: Hanau-Wolfgang, Federal Republic of Germany, 1984; No. 56.
(61) Bahnemann, D. W.; Kormann, C.; Hoffmann, M. R. *J. Phys. Chem.* **1987**, *91*, 3789–3798.
(62) Heller, H. G.; Langan, J. R. *J. Chem. Soc., Perkin Trans. 2* **1981**, 341.
(63) Morrison, S. R. *Electrochemistry at Semiconductor and Oxidized Metal Electrodes*: Plenum: New York, 1980.
(64) Guilbault, G. G.; Brignac, P. J.; Juneau, M. *Anal. Chem.* **1968**, *40*, 1256–1263.
(65) Allen, A. O.; Hochanadel, C. J.; Ghormley, J. A.; Davis, T. W. *J. Phys. Chem.* **1952**, *56*, 575–586.
(66) Mönig, J. Diplomathesis, Technical University of Berlin, Germany, 1980, pp 38–40.
(67) Schuchmann, H.-P.; von Sonntag, C. *Z. Naturforsch. B: Anorg. Chem., Org. Chem.* **1984**, *39B*, 217–221.
(68) Schuchmann, M. N.; Zegota, H.; von Sonntag, C. *Z. Naturforsch. B: Anorg. Chem., Org. Chem.* **1985**, *40B*, 215–221.

(69) Bothe, E.; Schuchmann, M. N.; Schulte-Frohlinde, D.; von Sonntag, C. *Photochem. Photobiol.* **1978**, *28*, 639–644.
(70) Bothe, E.; Schuchmann, M. N.; Schulte-Frohlinde, D.; von Sonntag, C. *Z. Naturforsch. B: Anorg. Chem., Org. Chem.* **1983**, *38B*, 212–219.
(71) Bahnemann, D. W.; Fischer, Ch.-H.; Janata, E.; Henglein, A. *J. Chem. Soc., Faraday Trans. 1* **1987**, *83*, 2559–2571.
(72) Boonstra, A. H.; Mutsaers, C. A. H. A. *J. Phys. Chem.* **1975**, *79*, 1940–1943.
(73) McElroy, W. J. *Atmos. Environ.* **1986**, *20*, 427–438.
(74) Adams, G. E.; Willson, R. L. *Trans. Faraday. Soc.* **1969**, *65*, 2981–2987.
(75) Piesiak, A.; Schuchmann, M. N.; Zegota, H.; von Sonntag, C. *Z. Naturforsch.* **1984**, *39B*, 1262–1267.
(76) Adams, G. E.; Willson, R. L. *Trans. Faraday Soc.* **1969**, *65*, 2981–2987.
(77) Das, S.; Schuchmann, M. N.; Schuchmann, H.-P.; von Sonntag, C. *Chem. Ber.* **1987**, *120*, 319–323.
(78) Bielski, B. H. J.; Cabelli, D. E.; Arudi, R. L.; Ross, A. B. *J. Phys. Chem. Ref. Data* **1985**, *14*, 1046.
(79) Hoigné, J., personal communication, 1987.
(80) Sheldon, R. A.; Kochi, J. K. *Metal-Catalyzed Oxidations of Organic Compounds*; Academic: New York, 1981.
(81) Fraser, I. M.; MacCallum, J. R. *J. Chem. Soc., Faraday Trans. 1* **1986**, *82*, 2747–2754.
(82) Asmus, K.-D.; Möckel, H.; Henglein, A. *J. Phys. Chem.* **1973**, *77*, 1218–1221.
(83) Ilan, Y.; Rabani, J.; Henglein, A. *J. Phys. Chem.* **1976**, *80*, 1558–1562.
(84) Kräutler, B.; Bard, A. J. *J. Am. Chem. Soc.* **1978**, *100*, 5985–5992.
(85) Huang, C.-P.; Stumm, W. *J. Colloid Interface Sci.* **1973**, *43*, 409.
(86) Stumm, W.; Morgan, J. J. *Aquatic Chemistry*; Wiley: New York, 1981.
(87) Muraki, H.; Saji, T.; Fujihira, M.; Aoyagui, S. *J. Electroanal. Chem. Interfacial Electrochem.* **1984**, *169*, 319–323.
(88) Salvador, P.; Gutierrez, C. *J. Phys. Chem.* **1984**, *88*, 3696–3698.
(89) Vanden Kerchove, F.; Praet, A.; Gomes, W. P. *J. Electrochem. Soc.* **1986**, *133*, 1522–1523.
(90) Sato, S. *J. Phys. Chem.* **1987**, *91*, 2895–2897.
(91) Fenton, H. J. H. *J. Chem. Soc.* **1894**, *65*, 899.
(92) Faust, B. C.; Hoffmann, M. R. *Environ. Sci. Technol.* **1986**, *20*, 943–948.
(93) Schütz, L.; Rahn, K. A. *Atmos. Environ.* **1982**, *16*, 171–176.
(94) Junge, C. In *Saharan Dust: Mobilization, Transport, Deposition*; Morales, C. Ed.; Wiley: Chichester, U.K. 1979; SCOPE 14, pp 49–60.
(95) Jaenicke, R. In *Saharan Dust: Mobilization, Transport, Deposition*; Morales, C., Ed.; Wiley: Chichester, U.K., 1979; SCOPE 14, pp 233–242.
(96) Bressan, D. J.; Carr, R. A.; Wilkniss, P. E. *ACS Symp. Ser.* **1973**, *No. 123*, 17–30.
(97) *National Inventory of Sources and Emissions*; NTIS: Springfield, VA, 1972; Section V, NTIS:PB 210680.
(98) *National Inventory of Sources and Emissions of Titanium*; U.S. Environmental Protection Agency; U.S. Government Printing Office: Washington, DC, 1973; EPA-450/3-74-008.
(99) Seinfeld, J. H. *Air Pollution*; Wiley: New York, 1986; pp 29–30.
(100) Gray, H. A.; Cass, G. R.; Huntzicker, J. J.; Heyerdahl, E. K.; Rau, J. A. *Environ. Sci. Technol.* **1986**, *20*, 580.
(101) Munger, J. W.; Collett, J.; Daube, B. C.; Hoffmann, M. R. *Tellus*, in press.

Received for review August 19, 1987. Accepted December 28, 1987. We gratefully acknowledge the financial support of the U.S. EPA (CR812356-01-0).

Chapter 5

PHOTOCATALYTIC PRODUCTION OF HYDROGEN PEROXIDE

[The text of this chapter appeared in: Detlef W. Bahnemann, Michael R. Hoffmann, Andrew P. Hong, and Claudius Kormann, ACS Symposium Series 349, The Chemistry of Acid Rain, American Chemical Society: Washington, 1987, pp 120–132.]

Chapter 10

Photocatalytic Formation of Hydrogen Peroxide

Detlef W. Bahnemann[1], Michael R. Hoffmann, Andrew P. Hong, and Claudius Kormann

W. M. Keck Laboratories, California Institute of Technology, Pasadena, CA 91125

The two-electron reduction of molecular oxygen to hydrogen peroxide can be catalyzed by metal oxide semiconductor particles in the presence of visible and near-UV light. Even though very high quantum yields for this process are observed, rather low steady-state concentrations of H_2O_2 are reached. Detailed mechanisms are presented to explain these experimental findings. Metal oxide particles are found in atmospheric and surface waters. The environmental significance of photocatalytic formation of H_2O_2 on these particles in natural systems is discussed.

Hydrogen peroxide, H_2O_2, is one of the most powerful oxidants in haze aerosols,clouds, and hydrometeors at low pH (1). A major pathway for the formation of sulfuric acid in humid atmospheres below pH 5 seems to be the oxidation of sulfur dioxide by H_2O_2 (2-4). Hydrometeor concentrations of hydrogen peroxide as high as 50 μM have recently been reported by Kok and co-workers (5-7), while typical atmospheric H_2O_2 levels up to 5 ppb have been predicted from Henry's law calculations (8,9). Various sources for the production of H_2O_2 in the atmosphere have been proposed: it can be generated in the gas phase by the combination of hydroperoxyl radicals, $HO_2\cdot$ (10), at the air-water interface due to photoinduced redox processes (11), and in the aqueous phase via photo-catalyzed reactions with humic/fulvic acid and green algae as mediators (Zepp, R. G., EPA Environmental Research Laboratory at Athens, personal communication). Furthermore , $HO_2\cdot$ radicals

[1]Permanent address: Hahn-Meitner Institut, Bereich Strahlenchemie, Glienicker Straße 100, D 1000 Berlin 39, Federal Republic of Germany

0097-6156/87/0349-0120$06.00/0
© 1987 American Chemical Society

which are produced in the gas phase can be scavenged by the water droplets where they then form H_2O_2. This *in situ* generated hydrogen peroxide together with the H_2O_2 scavenged from the gas phase is thought to be the main source for the H_2O_2 accumulated in cloudwater droplets (10,12,13). Another very likely possibility for H_2O_2 production, however, has so far been neglected in the design of models for aerosol-, fog-, and cloudwater chemistry. Various metal oxides, some of which are very abundant in natural environments, have been shown to act as photocatalysts for a large variety of reactions (14), *e.g.*, the photolysis of desert sands resulted in the production of ammonia from dinitrogen (15). Atmospheric particulate matter originates mainly from natural sources (721-1850 Tg yr^{-1} in 1979 globally) but also from man-made emissions (125-385 Tg yr^{-1} in 1982 in the USA) with iron, titanium, and zinc being some of the most abundant transition metals detected in ambient samples (16). These metals are present as hydroxides but also frequently as the respective oxides, depending upon the environmental conditions (17). Hence the present work addresses the question of hydrogen peroxide formation in aqueous solutions as catalyzed by metal oxides upon irradiation with visible and near-UV light.

Photocatalysis with Semiconductors

Many metal chalcogenides and oxides are known to be semiconductors. These materials can act as sensitizers for light-induced redox processes due to their electronic structure consisting of a valence band with filled molecular orbitals (MO's) and a conduction band with empty MO's. Absorption of a photon with an energy above the bandgap energy Eg generally leads to the formation of an electron/hole pair in the semiconductor particle (18):

$$\text{semiconductor} \xrightarrow{h\upsilon} e^-(cb) + h^+(vb) \qquad (1)$$

In the absence of suitable scavengers, recombination occurs within a few nanoseconds (19). Valence band holes ($h^+(vb)$) have been shown to be powerful oxidants (20-23) whereas conduction band electrons ($e^-(cb)$) can act as reductants (24,25). The redox potentials of both, e^- and h^+, are determined by the relative position of the conduction and valence band, respectively. Bandgap positions are material constants which have been determined for a wide variety of semiconductors (26). Most materials show "Nernstian" behavior which results in a shift of the surface potential by 59 mV in the negative direction with a pH increase of $\Delta pH = 1$. Consequently electrons are better reductants in alkaline solutions while holes have a higher oxidation potential in the acid pH-range (26). Thus, with the right choice of semiconductor and pH, the redox potential of the $e^-(cb)$ can be varied from +0.5 to -1.5 V (vs. NHE) and that of the $h^+(vb)$ from +1.0 to more than +3.5 V. This sufficiently covers the full range of redox chemistry of the H_2O/O_2 system (27).

H_2O_2 can therefore be formed via two different pathways in an aerated aqueous solution provided $e^-(cb)$ and $h^+(vb)$ are generated:

$$O_2 + 2e^-(cb) + 2H^+_{aq} \rightarrow H_2O_2 \quad (2)$$

$$2H_2O + 2h^+(vb) \rightarrow H_2O_2 + 2H^+_{aq} \quad (3)$$

Reaction 2 has been studied in great detail (28-44) since Baur and Neuweiler (28) in 1927 observed the formation of H_2O_2 when they illuminated aqueous zinc oxide suspensions in the presence of glycerin and glucose which in turn were oxidized. Appreciable yields of hydrogen peroxide are detected only when appropriate electron donors, D, are added prior to illumination. This strongly indicates that it is the electron donor, D, which is adsorbed on the catalyst's surface and hence sacrificed via Reaction 4.

$$D + h^+(vb) \rightarrow D^+\cdot \quad (4)$$

The presence of surficial D interferes with the e^-/h^+ recombination leaving $e^-(cb)$ (conduction band electrons) behind which then react with dioxygen via Reaction 2. Small quantities of H_2O_2 detected in the absence of added donors contained only oxygen atoms from O_2 as shown by labelling studies (34) which indicates the presence of contaminants in the semiconductor that are able to fill the $h^+(vb)$. Cadmium sulfide, CdSe, and ZnO showed the highest catalytic activity for dioxygen reduction (35,38). Titanium dioxide, on the other hand, which seems to be the material with the greatest potential for water splitting is reported to have negligable activity (35,41-43). The oxidation of water via Reaction 3, however, has not yet been demonstrated unambiguously. While Rao *et al.* (45) reported the formation of H_2O_2 in water splitting experiments on ZnO and TiO_2, Salvador and Decker (46) could not verify this observation. The intermediate production of H_2O_2 as the first molecular step of the four-hole oxidation of water to dioxygen has been predicted (46,47) and a variety of free radical intermediates have already been detected (48-50). Whenever the oxidation of H_2O is found to proceed with high yields there is no indication of hydrogen peroxide formation (51-54), but the dioxygen production seems to proceed via different intermediate peroxides as shown by Baur and Perret (51,52); they studied the photocatalytic formation of O_2 on ZnO in the presence of silver nitrate and observed the intermediate production of silver peroxides. In the case of TiO_2, the absence of detectable amounts of H_2O_2 and O_2 during water photoelectrolysis experiments has been explained with the well-documented adsorption and photo-uptake of these oxo-species by the material (55-71) and their incorporation into the molecular structure as peroxytitanates (68,72,73).

The above discussion indicates that a detailed study of the mechanism of the light-induced hydrogen peroxide production on

various oxide surfaces is warranted in order to judge its potential environmental implications. Using a newly developed polarographic technique for the kinetic analysis of hydrogen peroxide concentrations with a sensitivity of 10^{-7} M, we present further insight into the photocatalytic formation and destruction of H_2O_2.

Experimental Details

Several catalysts were prepared from chemicals of highest available grade. Mechanistic studies were performed using colloidal dispersions of zinc oxide, ZnO, which contained particles with a mean diameter of 5 nm (Bahnemann, D. W.; Kormann, C.; Hoffmann, M. R. J. Phys. Chem. submitted 11/3/86). Suspensions of such small aggregates exhibit negligible light scattering properties and conventional spectroscopic techniques can be used to study ongoing reactions (74). The preparation of titanium dioxide particles, TiO_2, coated with cobalt(II)tetrasulfophthalocyanine, Co(II)TSP, has recently been reported (Hong, A. P.; Bahnemann, D. W.; Hoffmann, M. R. J. Phys. Chem. accepted for publication 12/12/86). These particles have a mean diameter of 30 nm with 30% of the surface area covered with Co(II)TSP. Desert sand obtained from Death Valley has been treated with several acid washing cycles and selected by size and weight (Kormann, C.; Bahnemann, D. W.; Hoffmann, M. R. unpublished data). The H_2O_2 concentration was measured continuously with a YSI-Clark 2510 Oxidase Probe connected to a YSI model 25 oxidase meter. The surface of the electrode was covered with a dialysis membrane (molecular weight cutoff 12,000 - 14,000) to prevent any interference caused by the catalyst particles. Equilibration times between 30 and 60 minutes were allowed to ensure a stable signal once the electrode was immersed into the reaction solution. Following equilibration, changes in H_2O_2 content were monitored at a sensitivity of 10^{-7} M and a time constant of 1 s. The electrode was calibrated following each kinetic experiment using a standard addition method; linear response was obtained between 10^{-7} and $2 \cdot 10^{-5}$ M H_2O_2. Since this polarographic method is sensitive to any species with a redox potential of 700 mV, different methods were used to verify the formation of hydrogen peroxide. Following the illumination an aliquot of the solution was taken and titrated with iodide in the presence of a catalyst (75,76) to form the I_3^- anion which was quantitatively measured by spectrophotometry (ϵ(352nm) = 26400 M^{-1} cm^{-1}) (77). As a second check and when very small concentrations of H_2O_2 were detected with the polarographic method a very sensitive fluorometric determination (detection limit: $1.2 \cdot 10^{-8}$ M H_2O_2) was employed. This latter procedure involves the reaction of H_2O_2 with p-hydroxyphenylacetic acid in the presence of horseradish peroxidase to yield a product which fluoresces at 400 nm (λ(ex) = 320 nm) (78,79). Even though the polarographic method can not differentiate between H_2O_2 and other species with a similar electrochemical half-wave potential, the use of two alternative chemical analysis techniques eliminates such artifacts. Interferences by other chemicals such as ozone

can also be excluded in this study since it is extremely unlikely that they should occur with all three methods to the same extend.

Figure 1 shows the expermental set-up for the photolysis studies. White light of a 450 W Xe lamp (Osram XBO) passes through a water filter, a monochromator (PRA B102) and an appropriate UV-filter before the continuously stirred sample is irradiated. The analog signal of the oxidase meter is amplified to give the right amplitude for the input of the A/D converter (MBC Dash 8) which digitizes the data and feeds them into an IBM PC/AT for kinetic analysis. Aberchrome 540 is used for the determination of the light flux to enable an absolute measurement of the quantum yields (80).

Results and Discussion

The formation of hydrogen peroxide upon the illumination of an air-saturated aqueous colloidal suspension of zinc oxide particles is shown in Figure 2. No H_2O_2 is produced when light energies below the bandgap energy of ZnO where employed (Eg(ZnO)= 3.4 eV or λ(ex) = 365 nm), *e.g.*, λ(ex) = 400 nm. As the irradiation was performed at lower wavelengths, *e.g.*, λ(ex) = 366 and 320 nm, the sudden increase of the signal from the polarographic analyzer indicated H_2O_2 formation with a wavelength-independent quantum yield of 6%. No hydrogen peroxide is formed or depleted in the absence of light. Prolonged illumination leads to the formation of a steady-state in $[H_2O_2]$ of $1.2 \cdot 10^{-4}$ M in irradiated samples. The quantum-yields ϕ determined from the initial slope of the $[H_2O_2]$ vs. time plots depended strongly on the oxygen-content of the solution: ϕ increased to 10% in O_2-saturated samples and decreased sharply below $2 \cdot 10^{-5}$ M O_2. No H_2O_2 is produced when anoxic solutions were irradiated. The following mechanism explains these observations. Electrons and holes are formed in the zinc oxide particles under bandgap irradiation (Reaction 1). Their recombination is prevented by the presence of 2 mM acetate ions which are strongly adsorbed onto the ZnO surface and are oxidized via:

$$CH_3COO^- + h^+(vb) \rightarrow (CH_3COO)^\bullet \qquad (5)$$

$$(CH_3COO)^\bullet \rightarrow {}^\bullet CH_2COO^-/H^+_{aq} \text{ and/or } {}^\bullet CH_3/CO_2 \qquad (6)$$

The fate of the radicals produced via Reaction 6 is currently being investigated. Initial results indicate the formation of organic peroxides and suggest the intermediate formation of peroxy-radicals (Kormann, C.; Bahnemann, D. W.; Hoffmann, M. R. unpublished results). With the inhibition of charge recombination conduction band electrons are now available to reduce molecular oxygen yielding H_2O_2 (Reaction 2). The observed steady-state concentration of hydrogen peroxide can be understood as a competition between Reactions 2 and 7.

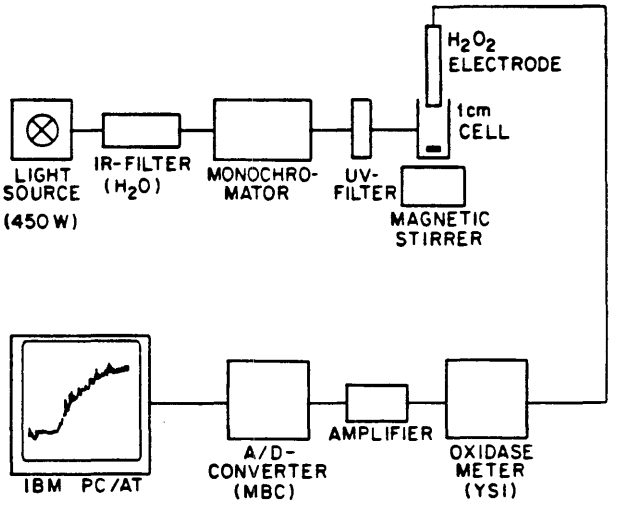

Figure 1. Experimental configuration used for irradiations and hydrogen peroxide detection.

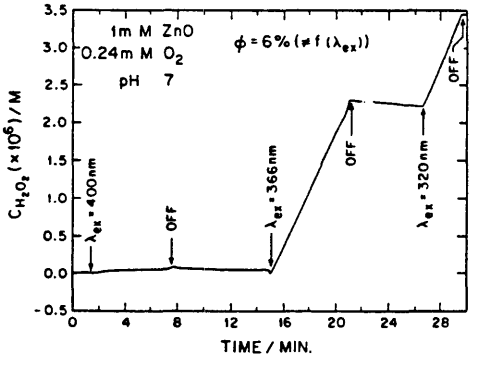

Figure 2. H_2O_2 formation upon illumination of an aqueous colloidal suspension of zinc oxide in the presence of 2 mM acetate (other exp. cond. are given in the figure).

$$H_2O_2 \quad 2e^-(cb) + 2H^+_{aq} \rightarrow 2H_2O \qquad (7)$$

The value $[H_2O_2](ss) = 1.2 \cdot 10^{-4}$ M measured in air-saturated solutions ($[O_2](ss) = 2.4 \cdot 10^{-4}$ M) suggests that Reaction 7 is about twice as efficient as the initial dioxygen reduction.

H_2O_2 is also produced in the absence of hole scavengers provided the right catalyst is used. Figure 3 shows the formation of hydrogen peroxide upon bandgap illumination of an oxygenated aqueous suspension of TiO_2 coated with Co(II)TSP which acts as an electron relay to transfer $e^-(cb)$ onto O_2 (Hong, A. P.; Bahnemann, D. W.; Hoffmann, M. R. J. Phys. Chem. accepted for publication 12/12/86). It is clearly obvious from Figure 3 that the same steady-state concentration of H_2O_2 is reached once the system is perturbed by the addition of H_2O_2 during prolonged irradiation. As in the case of ZnO no formation or depletion of hydrogen peroxide is observed in the absence of light. An octahedrally coordinated surface complex, *e.g.*, $Ti\text{-}O^-\text{-}Co(III)TSP\text{-}O_2^{-}\bullet$, has been identified as the catalytically active species in the TiO_2-Co(II)TSP system. With dioxygen being bound in the form of superoxide, $O_2^{-}\bullet$, this complex proved to be extremely stable but acts as an effective acceptor for conduction band electrons produced upon irradiation of the bulk TiO_2:

$$Ti\text{-}O^-\text{-}Co(III)TSP\text{-}O_2^{-}\bullet + e^-(cb) \rightarrow Ti\text{-}O^-\text{-}Co(III)TSP\text{-}H_2O + H_2O_2 \quad (8)$$
$$+ 2\ H^+_{aq}$$

The aquo complex formed in Reaction 8 readily accepts another $e^-(cb)$ to form a reduced metal center which then quickly reacts with O_2

$$Ti\text{-}O^-\text{-}Co(II)TSP\text{-}H_2O + O_2 \rightarrow Ti\text{-}O^-\text{-}Co(III)TSP\text{-}O_2^{-}\bullet \qquad (9)$$

yielding again the stable $O_2^{-}\bullet$ complex.

H_2O_2 is formed in quantum yields close to 50% by this reaction sequence. The observed net formation of H_2O_2 indicates that the valence band holes, $h^+(vb)$, are able to oxidize water via Reaction 3. The low steady-state concentrations $[H_2O_2](ss)$ which are reached during these experiments (5 - 25 μM depending on the nature of the catalyst) suggest that oxidation of H_2O_2 via

$$H_2O_2 + 2h^+(vb) \rightarrow O_2 + 2H^+_{aq} \qquad (10)$$

efficiently competes with Reaction 3. When present at high concentrations, hydrogen peroxide can also compete with molecular oxygen (Reaction 9) for the open coordination site on Co(II)TSP:

$$Ti\text{-}O^-\text{-}Co(II)TSP\text{-}H_2O + H_2O_2 \rightarrow Ti\text{-}O^-\text{-}Co(III)TSP\text{-}OH + OH^- \qquad (11)$$

Reaction 11 is analogous to Reaction 8 in that it leads to the overall reduction of H_2O_2 by two $e^-(cb)$. The major difference

between the zinc oxide and the TiO_2-Co(II)TSP systems is that the surface complex (Co(II)TSP) acts as an electron relay in one case while sacrificial electron donors such as acetate are a prerequisite for interruption of the e^-/h^+ recombination in the other case.

Following the studies of these rather well-defined model systems aerated aqueous suspensions of desert sand particles were irradiated (λ(ex) = 350 nm) in the presence of sodium acetate. The very rapid formation of a steady-state concentration of 0.2 μM H_2O_2 upon illumination is shown in Figure 4. This, however, decays very quickly when the light is turned off. A similar depletion is apparent when H_2O_2 is added in the dark. If the light is turned on during this decay period a steady-state of 0.2 μM is again established. These cycles can be repeated many times without any apparent loss in activity. It has already been demonstrated (15) that desert sand contains minerals such as hematite, α-Fe_2O_3, and anatase, TiO_2, and can thus be photocatalytically active. We envision a mechanism similar to that proposed for the model systems above to account for the observed formation of H_2O_2 on desert sands. In this case the e^-/h^+ pair (Reaction 1) is intercepted by the donor acetate (Reactions 5 and 6) leaving e^-(cb) behind to reduce O_2 via Reaction 2. The efficient destruction of H_2O_2, on the other hand, might be caused by metal ion contaminants (M^{x+}) adsorbed on the sand particles (81-85). Hydrogen peroxide can thus react with M^{x+} in a Fenton type reaction (86),

$$M^{x+} + H_2O_2 \rightarrow M^{(x+1)+} + OH^- + OH\cdot \qquad (12)$$

followed by the free radical Reactions 13 to 17 (87,88).

$$H_2O_2 + OH\cdot \rightarrow H_2O + HO_2\cdot \qquad (13)$$

$$HO_2\cdot \rightleftharpoons O_2^-\cdot + H^+_{aq} \qquad (14)$$

$$HO_2\cdot + O_2^-\cdot + H^+_{aq} \rightarrow H_2O_2 + O_2 \qquad (15)$$

$$HO_2\cdot + OH\cdot \rightarrow H_2O + O_2 \qquad (16)$$

$$OH\cdot + OH\cdot \rightarrow H_2O_2 \qquad (17)$$

This reaction sequence results in the overall disproportionation of H_2O_2 and thus explains its rapid disappearance in the dark. Finally, a word of caution should be added regarding other possibilities to photogenerate hydrogen peroxide in such an ill-defined natural system. In spite of the rigorous pre-treatment it is possible that trace amounts of organic adsorbates are still present on the desert sand samples employed in this study. On the other hand, it is well documented that naturally occurring humic type materials can also be photochemically active (89). Thus we cannot exclude the possibility that part of the observed rather low steady-state

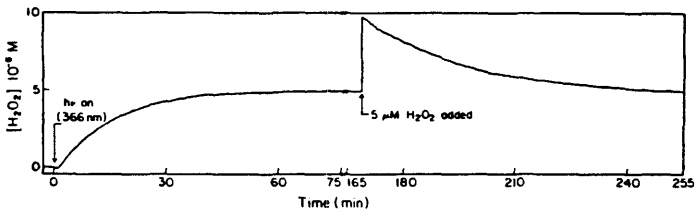

Figure 3. Formation and depletion of H_2O_2 upon irradiation (λ(ex) = 366 nm) of an oxygenated aqueous suspension of 0.3 g TiO_2-Co(II)TSP/l at pH 12.

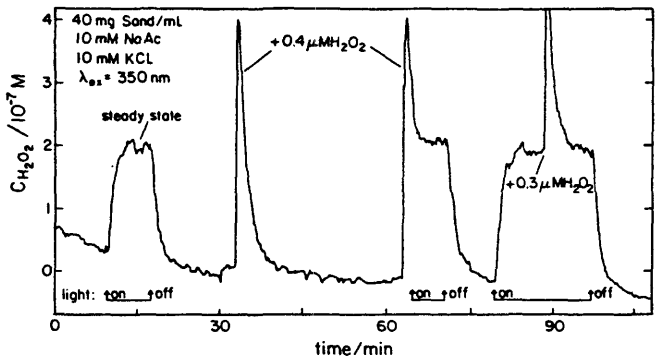

Figure 4. Formation and depletion of H_2O_2 upon illumination and in the dark observed in an aerated aqueous suspension of Death Valley desert sand (other exp. cond. are given in the figure).

concentration of H_2O_2 is formed via the direct excitation of such molecules. Further experiments are currently being performed to differentiate between these pathways.

Concluding Remarks

We have shown that hydrogen peroxide can be produced photocatalytically in the presence of semiconductor particles. Quantum yields up to 50% and steady-state concentrations between 0.2 and 120 μM H_2O_2 have been observed. While the reduction of molecular oxygen by e^-(cb) seems to be the most likely process for H_2O_2-formation, oxidation of water by h^+(vb) should in principle yield the same products.

It is the observation of hydrogen peroxide production upon the illumination of an aerated aqueous suspension of desert sand particles that presents the most intriguing result of this study. Submicron sand particles are very abundant in the atmosphere where they act as condensation nuclei (90). Their involvement as catalysts and/or photocatalysts in chemical transformations occurring in natural environments has so far been neglected even though they are rather persistent in the atmosphere with half-lives of several days before precipitation takes place. We propose the surface reaction of photocatalytically formed H_2O_2 with sulfur dioxide (SO_2) and nitrous oxides (NO_x) as an additional pathway for the formation of acid rain. Even though due to its metal-catalyzed dismutation the steady-state concentration of H_2O_2 observed in the desert sand experiment was rather low, it may nevertheless be high enough to yield reasonable quantities of oxidation products like H_2SO_4 or HNO_3. Further experiments are in progress to study the photocatalytic activity of natural systems.

Acknowledgment

We gratefully acknowledge the financial support of the U.S. EPA (CR812356-01-0 and R811612-01-0) and in particular we want to thank Drs. Donald Carey and Marcia Dodge for their support.

Literature Cited

1. Hoffmann, M. R.; Kerr, J. A.; Calvert, J. G. Chemical Transformation Modules for Eulerian Acid Deposition Models. Vol.II: The Aqueous-Phase Chemistry; NCAR, Boulder, CO, 1984.
2. Hoffmann, M. R.; Boyce, S. D. Advances in Environmental Science and Technology; Schwartz, S. E., Ed.; Wiley, New York, 1983, 12, 147.
3. Hoffmann, M. R.; Jacob, D. J. SO_2, NO, and NO_2 Oxidation Mechanisms: Atmospheric Considerations; Calvert, J. G., Ed.; Acid Precipitation Series - Vol. 3; Teasley, J. I., Series Ed.; Butterworth, Boston, MA, 1984, 101.
4. Jacob, D. J.; Hoffmann, M. R. J. Geophys Res. 1983, 88, 6611.

5. Kok, G. L.; Darnall, K. R.; Winer, A. M., Pitts, J. N., Jr.; Gay, B. W. Environ. Sci. Tech. 1978, 12, 1077.
6. Kok, G. L. Atmos. Environ. 1980, 14, 653.
7. Richards, L. W.; Anderson, J. A.; Blumenthal, D. L.; McDonald, J. A.; Kok, G. L. Atmos. Environ. 1983, 17, 911.
8. Schwartz, S. E. Annals of the New York Academy of Sciences, Section of Environmental Sciences 1985, xx, xxx.
9. Seinfeld, J. H. Atmospheric Chemistry and Physics of Air Pollution; John Wiley & Sons, New York, NY, 1986, 236.
10. Chameides, W. L.; Davis, D. D. J. Geophys Res. 1982, 87, 4863.
11. Zika, R. G.; Saltzman, E.; Chameides, W. L.; Davis, D. D. J. Geophys. Res. 1982, 87, 5015.
12. Graedel, T. E.; Goldberg, K. I. J. Geophys. Res. 1983, 88, 865.
13. Chameides, W. L. J. Geophys. Res. 1984, 88, 4739.
14. Fendler, J. H. J. Phys. Chem. 1985, 89, 2730.
15. Schrauzer, G. N.; Strampach, N.; Hui, L. N.; Palmer, M. R.; Saleshi, J. Proc. Natl. Acad. Sci. USA 1983, 80, 3873.
16. Seinfeld, J. H. Atmospheric Chemistry and Physics of Air Pollution; John Wiley & Sons, New York, NY, 1986, 26.
17. Stumm, W.; Morgan, J. J. Aquatic Chemistry; John Wiley & Sons, New York, NY, 1981, 238.
18. Bard, A. J. Science 1980, 207, 139.
19. Rothenburger, G.; Moser, J.; Grätzel, M.; Serpone, N.; Sharma, D. K. J. Am. Chem. Soc. 1985, 107, 8054.
20. Izumi, I.; Dunn, W. W.; Wilbourn, K. O.; Fan, F. F.; Bard, A. J. J. Phys. Chem. 1980, 84, 3027.
21. Harvey, P. R.; Rudham, R.; Ward, S. J. Chem. Soc. Faraday Trans. 1 1983, 79, 2975.
22. Herrmann, M.-M.; Mozzanega, M.-N.; Pichat, P. J. Photochem. 1983, 22, 333.
23. Fox, M. A.; Chen, C.-C.; Park, H.-H.; Younathan, J. N. ACS Symp. Ser. 1985, 278, 69.
24. Brown, G. T.; Darwent, J. R. J. Chem. Soc. Faraday Trans. 1 1984, 80, 1631.
25. Bahnemann, D.; Henglein, A.; Spanhel, L. Faraday Discuss. Chem. Soc. 1984, 78, 151.
26. Gerischer, H. Topics in Applied Physics 1979, 31, 115.
27. Latimer, W. M. Oxidation Potentials, 2nd Edition; Prentice-Hall, New York, NY, 1952, 38-50.
28. Baur, E.; Neuweiler, C. Helv. Chim. Acta 1927, 10, 901.
29. Böhi, J. Helv. Chim. Acta 1929, 12, 121.
30. Chari, C. N.; Qureshi, M. J. Indian Chem. Soc. 1944, 21, 97.
31. Chari, C. N.; Qureshi, M. J. Indian Chem. Soc. 1944, 21, 297.
32. Markham, M. C.; Laidler, K. J. J. Phys. Chem. 1953, 57, 363.
33. Rubin, T. R.; Calvert, J. G.; Rankin, G. T.; MacNevin, W. M. J. Am. Chem. Soc. 1953, 75, 2850.
34. Calvert, J. G.; Theurer, K.; MacNevin, W. M. J. Am. Chem. Soc. 1954, 76, 2575.
35. Stephens, R. E.; Ke, B.; Trivich, D. J. Phys. Chem. 1955, 59, 966.

36. Kuriacose, J. C.; Markham, M. C. J. Catalysis 1962, 1, 498.
37. Morrison, S. R.; Freund, T. J. Chem. Phys. 1967, 47, 1543.
38. Harbour, J. R.; Hair, M. L. J. Phys. Chem. 1977, 81, 1791.
39. Harbour, J. R.; Hair, M. L. J. Phys. Chem. 1979, 83, 652.
40. Hair, M. L.; Harbour, J. R. Adv. Chem. Ser. 1980, 184, 173.
41. Pappas, S. P.; Fischer, R. M. J. Paint Technology 1974, 46, 65.
42. Cundall, R. B.; Rudham, R.; Salim, M. S. J. Chem. Soc. Faraday Trans. 1 1976, 72, 1642.
43. Harbour, J. R.; Hair, M. L. "Magnetic Resonance in Colloid and Interface Science", Fraissard, J. P.; Resing, H. A., Eds.; Riedel Publ. Co. 1980, 431.
44. Harbour, J. R.; Tromp, J.; Hair, M. L. Can. J. Chem. 1985, 63, 204.
45. Rao, M. V.; Rajeshwar, K.; Pal Verneker, V. R.; DuBow, J. J. Phys. Chem. 1980, 84, 1987.
46. Salvador, P.; Decker, F. J. Phys. Chem. 1984, 88, 6116.
47. Rives-Arnau, V. J. Electroanal. Chem. 1985, 190, 279.
48. Jaeger, C. D.; Bard, A. J. J. Phys. Chem. 1979, 83, 3146.
49. Anpo, M.; Shima, T.; Kubokawa, Y. Chem. Lett. 1985, 1799.
50. Serwicka, E. Colloids and Surfaces 1985, 13, 287.
51. Baur, E.; Perret, A. Helv. Chim. Acta 1924, 7, 910.
52. Perret, A. J. Chim. Phys. 1926, 23, 97.
53. Hada, H.; Yonezawa, Y.; Saikawa, M. Bull. Chem. Soc. Jpn. 1982, 55, 2010.
54. Nishimoto, S.-I.; Ohtani, B.; Kajiwara, H.; Kagiya, T. J. Chem. Soc. Faraday Trans. 1 1983, 79, 2685.
55. Kennedy, D. R.; Ritchie, M.; MacKenzie, J. Trans. Faraday Soc. 1958, 54, 119.
56. McLintock, I. S.; Ritchie, M. Trans. Faraday Soc. 1965, 61, 1007.
57. Stone, F. S. Anal. Real. Soc. Espan. Fis. Quim. 1965. 61, 109.
58. Boonstra, A. H.; Mutsaers, C. A. H. A. J. Phys. Chem. 1975, 79, 1694.
59. Boonstra, A. H.; Mutsaers, C. A. H. A. J. Phys. Chem. 1975, 79, 1940.
60. Boonstra, A. H.; Mutsaers, C. A. H. A. J. Phys. Chem. 1975, 79, 2025.
61. Munuera, G.; Rives-Arnau, V.; Saucedo, A. J. Chem. Soc. Faraday Trans. 1 1979, 75, 736.
62. González-Elipe, A. R.; Munuera, G.; Soria, J. J. Chem. Soc. Faraday Trans. 1 1979, 75, 748.
63. Munuera, G.; González-Elipe, A. R.; Soria, J.; Sanz, J. J. Chem. Soc. Faraday Trans. 1 1980, 76, 1535.
64. Munuera, G.; Navio, A. Stud. Surf. Sci. Catal. Pt. B, New Horiz. Catal. 1981, 7, 1185.
65. Munuera, G.; González-Elipe, A. R.; Rives-Arnau, V.; Navio, A.; Malet, P.; Soria, J.; Conesa, J. C.; Sanz, J. "Adsorption and Catalysis on Oxide Surfaces", Che M.; Bond, G. C., Eds.; Elsevier Sci. Publ. 1985, 113.
66. Tanaka, K.; White, J. M. J. Phys. Chem. 1982, 86, 4708.

67. Tatsumi, K.; Shiotani, M.; Freed, J. H. J. Phys. Chem. 1983, 87, 3425.
68. Yesodharan, E.; Grätzel, M. Helv. Chim. Acta 1983, 66, 2145.
69. Duonghong, D.; Grätzel, M. J. Chem. Soc. Chem. Comm. 1984, 1597.
70. Oosawa, Y.; Grätzel, M. J. Chem. Soc. Chem. Comm. 1984, 1629.
71. Che, M.; Gianello, E.; Tench, A. J. Colloids and Surfaces 1985, 13, 231.
72. Mühlebach, J.; Müller, K.; Schwarzenbach, G. Inorg. Chem. 1970, 9, 2381.
73. Schwarzenbach, D. Inorg. Chem. 1970, 9, 2391.
74. Bahnemann, D.; Henglein, A.; Lilie, J.; Spanhel, L. J. Phys. Chem. 1984, 81, 709.
75. Patrick, W. A.; Wagner, H. B. Anal. Chem. 1949, 21, 1279.
76. Savage, D. J. Analyst (London) 1951, 76, 224.
77. Mönig, J. Diplomathesis, Technical University of Berlin, Germany, 1980, pp. 38–40.
78. Guilbault, G. G.; Brignac, P. J.; Juneau, M. Anal. Chem. 1968, 40, 1256.
79. Lazrus, A. L.; Kok, G. L.; Gitlin, S. N.; Lind, J. A.; McLaren, S. E. Anal. Chem. 1985, 57, 917.
80. Heller, H. G.; Langan, J. R. J. Chem. Soc. Perkin Trans. 2, 1981, 341.
81. James, R. O.; Healy, T. W. J. Coll. Interface Sci. 1972, 40, 42.
82. James, R. O.; Healy, T. W. J. Coll. Interface Sci. 1972, 40, 53.
83. Huang, C.-P.; Stumm, W. J. Coll. Interface Sci. 1973, 43, 409.
84. Davis, J. A.; Leckie, J. O. J. Coll. Interface Sci. 1978, 67, 90.
85. Elliott, H. A.; Huang, C. P. J. Coll. Interface Sci. 1979, 70, 29.
86. Fenton, H. J. H. J. Chem. Soc. 1894, 65, 899.
87. Haber, F.; Weiss, J. Proc. R. Soc. London Ser. A 1934, 147, 332.
88. Weinstein, J.; Bielski, B. H. J. J. Am. Chem. Soc. 1979, 101, 38.
89. Zafiriou, O. C.; Joussot-Dubien, J.; Zepp, R. G.; Zika, R. G. Environ. Sci. Technol. 1984, 18, 359A.
90. Pruppacher, H. R.; Klett, J. D. Microphysics of Clouds and Precipitation; D. Riedel Publ. Co., Dordrecht, Holland, 1978.

RECEIVED March 16, 1987

Reprinted from ACS SYMPOSIUM SERIES No. 349
The Chemistry of Acid Rain: Sources and Atmospheric Processes
Russell W. Johnson and Glen E. Gordon, Editors
Copyright © 1987 by the American Chemical Society
Reprinted by permission of the copyright owner

Chapter 6

ENVIRONMENTAL PHOTOCHEMISTRY: IS IRON OXIDE AN ACTIVE PHOTOCATALYST? A COMPARATIVE STUDY: Fe_2O_3, ZnO, TiO_2.

[The text of this chapter is being submitted to the Journal of Photochemistry.]

INTRODUCTION

The photocatalytic reactions promoted by aqueous suspensions of colloidal metal oxides has been the subject of an abundant number of recent investigations.[1] Iron oxide, an n–type semiconductor with a bandgap of 2.2 eV, has been studied extensively for use in solar photoelectrolysis cells.[2,3] Leland and Bard[4] recently studied the photoelectrochemical properties of colloids and particles of different forms of iron oxide. They found α–Fe_2O_3, the most stable polymorph, to be the most effective catalyst for the photo–oxidation of sulfite. Frank and Bard[5] investigated the photocatalytic oxidation of cyanide and sulfite at several semiconductor powders. They found TiO_2 to be an active photocatalyst for cyanide oxidation, while no oxidation was seen for α–Fe_2O_3. Cunningham et al.[6] obtained evidence for the photocatalytic formation of $OH^{\bullet}$ radicals in illuminated suspensions of α–FeOOH. Pronounced differences in the activities of two Fe_2O_3 samples were found when Pichat and Co–workers examined the photocatalytic behavior of various semiconductor oxide powders dispersed in oxalic acid solutions.[7] The photocatalytic activity of α–Fe_2O_3 (hematite) has also been studied by several authors in the context of the dissolution of solid oxide phases.[8,9] Stramel and Thomas[10] studied the photochemistry of iron oxide colloids but were unsuccessful in promoting chemical reaction by irradiating into the Fe_2O_3 absorption band. Ferric oxides and oxyhydroxides (α–Fe_2O_3, Fe_3O_4, α–FeOOH, γ–FeOOH) are ubiquitous constituents of the aqueous environment and have also been identified as components of airborne particles.[11] Their potential importance in the photocatalytic transformation of sulfur compounds in the aqueous atmospheric environment has been evaluated by Hoffmann and Co–workers.[12]

In the work described below, the photocatalytic activity of α–Fe_2O_3 colloids are compared to the activities of ZnO and TiO_2. The formation of H_2O_2 is investigated and the oxidation of organic molecules is studied with high sensitivity.

EXPERIMENTAL

Materials

Transparent α–Fe_2O_3 colloids were prepared by the controlled hydrolysis of $FeCl_3$ which was followed by membrane dialysis until the residual Cl^- concentration was below 10^{-5} M. Particle diameters were found to be between 3 and 20 nm. Details of the synthesis and characterization of this catalyst have been described elsewhere.[12] Titanium dioxide (bandgap energy: 3 eV)[13] was obtained from Degussa (P25); it had a BET surface area of 50 ±15 $m^2\ g^{-1}$ and an average particle diameter of 30 nm. Zinc oxide (bandgap energy: 3.4 eV)[13] was u.s.p. grade from Baker. Suspensions were freshly prepared by sonication (<60 seconds in Bransonic 5200 cleaning bath). The concentrations employed resulted in an absorption of more than 95% of the incident photons at 330 nm. Chloroacetic acid (MCB) contained ≃2 mol% of Cl^- as detected by HPIC. All chemicals were of reagent grade and used without further purification. The water employed in all preparations was purified by a Milli–Q/RO system with an attached ORGANEX–Q unit (ρ>18 MΩ cm).

Apparatus

Illumination apparatus and actinometry have been described elsewhere.[14] Typically a volume of 2 ml suspension was illuminated with the collimated beam of an Osram XBO 450 W lamp through a 300 nm UV cutoff and an IR filter. The incident photon flux between 300 and 400 nm was $I \simeq 5 \cdot 10^{-3}$ M $h\nu$ min^{-1}. Reaction temperatures were between 25 and 30 ^{0}C.

Hydrogen peroxide concentrations were determined by an enzymatic and a polarographic method. Details have been described elsewhere.[14] Ion Chromatography (HPIC) was performed with a Dionex 2020i instrument (Column: AS4A with AG4 pre–column, eluant: 0.005 M $Na_2B_4O_7$, flow rate: 2.0 ml min^{-1}, detection: suppressed conductivity, sample volume: 50 μl). Chloride concentrations were also determined using a chloride sensitive electrode (Orion 94–17). In a typical illumination experiment 25–50 μl aliquots were taken, diluted in 2500 μl of water (in the case of the Fe_2O_3 colloid, 0.5 mM NaOH was used to precipitate the colloid) and subsequently analyzed by HPIC. The degradation of volatile chlorinated hydrocarbons was monitored by gas chromatography (HP 5880A Level Four instrument, column: 12m HP–1, isothermal at 35 ^{0}C, carrier gas: nitrogen at 1ml min^{-1}, electron capture detector (300 ^{0}C). Typically, 10 μl of the headspace of the aqueous sample solutions were injected.

RESULTS AND DISCUSSION

Metal oxide particles such as Fe_2O_3, ZnO, and TiO_2 behave as short–circuited electrochemical cells where both cathodic and anodic electron transfer occur on the same particle. Excitation of the metal oxide (MO) particle with light ($h\nu > E_{gap}$) leads to the formation of an electron–hole pair:

$$MO + h\nu \longrightarrow MO(e_{cb}^- + h_{vb}^+)$$

While electron donors such as acetate fill the photogenerated valence band holes

$$D + h_{vb}^+ \longrightarrow D^+$$

the remaining conduction band electrons can reduce oxygen to yield hydrogen peroxide

$$e_{cb}^- + \tfrac{1}{2} O_2 + H^+ \longrightarrow \tfrac{1}{2} H_2O_2$$

The formation of H_2O_2 in illuminated aqueous suspensions of ZnO, TiO_2, and desert sand has been studied previously.[14] It has been shown that during the initial phase the rate production of H_2O_2 is given by

$$\frac{d[H_2O_2]}{dt} = (\phi_0 - \phi_1[H_2O_2]) \cdot \frac{d[h\nu]_{abs}}{dt}$$

where ϕ_0 is the quantum yield for H_2O_2 formation, ϕ_1 is the quantum yield for H_2O_2 degradation, and $d[h\nu]_{abs}/dt$ is the photon flux.[14] A steady state

concentration of H_2O_2, $[H_2O_2]_{ss} = \phi_0/\phi_1$, is reached because H_2O_2 itself accepts or donates electrons and is degraded.

No hydrogen peroxide is found when suspensions of α–Fe_2O_3 colloids or powders are illuminated with intense light $\lambda > 300$ nm. The upper limit for the quantum yield for H_2O_2 formation is calculated to be $\phi_0 < 10^{-5}$, considering the amount of photons absorbed and the detection limits of the methods used. The experimental conditions were comparable to the experiments with the other oxides and were varied as follows [α–Fe_2O_3] = $5 \cdot 10^{-4}$–$1 \cdot 10^{-3}$ M, electron donor: [isopropanol] = 1 M or [acetate] = 10 mM, $[O_2] = 2.3 \cdot 10^{-4}$–$1.3 \cdot 10^{-3}$ M, pH 2–5, ionic strength I= 10^{-3}–10^{-2} M (KCl).

The different behavior of the three oxides can be explained if one takes into account the redox potentials of the conduction band electrons and of individual electron transfer reactions. While the redox potentials of the conduction band for bulk ZnO and TiO_2 electrodes have been reported to be $E_{cb} = 0.0$ V and $E_{cb} = +0.05$ V, respectively, the corresponding value for α–Fe_2O_3 is $E_{cb} = +0.3$ V at pH 2.[13] The redox potential of photogenerated conduction band electrons in small particles may be somewhat more negative (by ca. 0.1 V) than the redox potential of the conduction band for bulk electrodes due to characteristic size effects.[15,16]

On the other hand, the reduction of oxygen yielding the hydroperoxy radical is endothermic:

$$e_{cb}^- + O_2 + H^+ \longrightarrow HO_2^\bullet$$

In homogeneous solution a value of E^0 = ca. –0.15 V (at pH 2) has been given.[17] This value may be more positive when dioxygen is bound to the surface. It is obvious that the reduction of O_2 by a conduction band

electron is most endothermic (ΔG^0= –0.45 V or +44 kJ/mol) in the case of α–Fe_2O_3. Hence, it is not surprising that the oxygen molecule is not photo–reduced on α–Fe_2O_3 particles.

Photocatalytic oxidation

Oxidation of organic or inorganic molecules occurs by photogenerated holes or via intermediate $OH^\bullet$ radicals after the photogenerated conduction band electrons have reacted with oxygen (TiO_2, ZnO)[14] or with ferric ions.[8,9] It has been shown that the presence of oxygen is necessary for photocatalytic oxidations to occur [14] or to prevent the reductive dissolution of α–Fe_2O_3 particles via [8,9]

$$D + \{\alpha\text{–}Fe_2O_3\}(Fe^{3+}) + h\nu \longrightarrow \{\alpha\text{–}Fe_2O_3\} + D^+ + Fe^{2+}_{aq}$$

In the present study chloroacetate was chosen as electron donor because its disappearance as well as the formation of its degradation product, chloride, can be detected with accuracy and high sensitivity by HPIC. Over the pH range of this study (pH 5–8) the molecule is negatively charged (pk_a= 2.9) and is adsorbed to the positively charged particle surfaces, since $pH<pH_{zpc}$ (pH of zero point of charge).[18]

Millimolar concentrations of chloroacetate are degraded with the concomitant formation of chloride ions in a 1:1 ratio when aqueous suspensions containing ZnO (Fig.1a) or TiO_2 (Fig.1b) particles are irradiated with UV light. Although the detailed mechanism of such photocatalytic oxidations is still unknown, it has been shown that photocatalytic oxidations of various chlorinated hydrocarbons proceed to complete degradation with quantitative formation of

carbonate, chloride, and protons,[19,20] e. g.

$$CH_2ClCO_2^- + 3/2\ O_2 + H_2O \longrightarrow 2\ HCO_3^- + Cl^- + 2\ H^+$$

From the slope of the plots (Fig.1a–b) and the actinometry of the experiment quantum yields of degradation are calculated to be ca. 3% for TiO_2 and 0.1% for ZnO.

Figure 1c shows that illumination of α–Fe_2O_3 colloid in the presence of chloroacetate and oxygen does not lead to the release of chloride ions or to a degradation of the organic acid. An upper limit for the quantum yield of degradation of $\phi < 10^{-6}$ can be calculated from the amount of light absorbed after 7 hours of illumination ($\lambda > 300$ nm) and the variation of the chloride signal (HPIC).

Figure 2 shows how chloroform is degraded when a suspension of TiO_2 particles is illuminated with UV light. The initial quantum yield is found to be 2% in agreement with similar experiments by Pruden et al.[21] The reaction stoichiometry

$$2\ CHCl_3 + O_2 + H_2O \longrightarrow CO_2 + 6\ H^+ + 6\ Cl^-$$

has been confirmed by measuring the chloride production rate,[21] the formation of carbonate,[21,22] the rate of hydroxide consumption at constant pH,[22] and the depletion of oxygen.[22] Under the same experimental conditions, chloroform is not degraded (quantum yield as determined by GC headspace technique $\phi << 0.1\%$) and no chloride is formed when α–Fe_2O_3 colloids are illuminated in the presence of oxygen. Chloral ($CCl_3CH(OH)_2$) is a molecule carrying a hydrophilic group which facilitates adsorption to the particle surfaces, however

no photodegradation ($\phi << 0.1\%$) of this molecule is found when α–Fe_2O_3 colloids are illuminated with UV light at pH 2.6 ($[CCl_3CH(OH)_2] = 10^{-4}$ M).

The absence of photocatalytic activity of α–Fe_2O_3 in the oxidation of such molecules as chloroform, chloroacetic acid, and chloral cannot be explained in terms of the redox potential of the valence band. This oxidation potential is sufficiently positive, i.e. $E_{vb} = + 2.5$ V, to oxidize water yielding $OH^\bullet$ radicals. The $OH^\bullet$ radicals in turn are known to oxidize all of the above organic molecules. It must be concluded that neither the oxidizing power of a valence band hole nor the intermediate $OH^\bullet$ radical are available at the surface of a α–Fe_2O_3 particle after light excitation. Kennedy and Frese proposed that two optical absorption processes occur in ferric oxide, one of which leads to a second type of hole, similar to a Fe^{4+} species, of relatively low oxidizing power.[2] It appears that the presence of the crystal lattice of Fe_2O_3 provides effective relaxation channels for the excited state.

Our experimental observation that organic molecules such as acetate, chloral or $CHCl_3$ are not oxidized on α–Fe_2O_3 particles does not contradict other reports on the photocatalytic activity of this material.[5,7–9,23,24] Thus, there are reports on the photocatalytic oxidation of sulfite,[9] thiols,[23] and iodide.[24] Note, however that these molecules are much better reducing agents that react easily with ferric ions in the dark.[25–27] Light excitation in these cases helps to overcome relatively small activation energies. In fact, Waite et al.[23] preferred to term the reaction with thiols "photoassisted", as they observed substantial dark reaction rates.

Other "photocatalytic" reactions involve such electron donors as oxalate or citrate that are also strong complexing agents, i. e. they form inner sphere complexes with ferric ions. Pichat and co–workers studied the oxidation of oxalate on (uncharacterized) Fe_2O_3 specimens.[7] Oxalate is known to be an

excellent complexing agent which may dissolve iron oxide under formation of the ferritrioxalate complex.[28,29]

It is conceivable that the photoactive species is a monomolecular iron complex rather than a α–Fe_2O_3 particle. Faust and Hoffmann[9] showed that while the quantum efficiency of the surface complexes between Fe(III) and S(IV) is high, light absorption is dominated by the α–Fe_2O_3 particles, which are less active. Baxendale and Bridge[30] found that the quantum yield for the photo–oxidation of formate in the presence of Fe^{3+} decreases as the Fe^{3+} concentration is increased. They concluded that polymolecular species were formed which were less reactive.

Is iron oxide an active photocatalyst?

Clearly, the answer will depend on the system studied. While TiO_2 and ZnO appear to be active photo–oxidation catalysts with virtually any electron donor,[1,14,19–21] α–Fe_2O_3 particles appear to react only with a select set of molecules (i. e., with strong reducing agents, that already react in the dark, and with multidentate ligands). Table 1 summarizes quantum yields for photocatalytic reactions of iron oxide particles obtained from the literature and from this work. In the majority of the studies strongly binding and reducing agents were used as electron donors. While sulfite or oxalate were found to be effectively oxidized, other electron donors such as citrate, benzoate or cyanide did show only little or no activity.

Except for sulfite, oxalate and iodide (cf., however, footnote [b], Table 1), very low quantum yields ($3 \cdot 10^{-8}$–$5 \cdot 10^{-5}$) were reported for the other molecules. It appears questionable whether such low quantum yields are relevant to environmental processes involving the oxidation of organic molecules since the rate of reaction is proportional to the product of ϕ times the concentration of the

semiconductor which is also low. The present study did not detect any photocatalytic activity of α–Fe_2O_3 particles $\phi << 10^{-5}...10^{-3}$ (experimental resolution) in the oxidation of "normal" organic molecules (i.e. molecules, that are not particularly strong reducing or complexing agents).

Table 1: Photocatalytic activity of iron oxide particles

Material	Quantum yield	System studied	Ref.
α–Fe_2O_3	0.027	Fe(II) production in the	
	at 350 nm	presence of sulfite	9
α–Fe_2O_3	*100*[a]	sulfite oxidation	4
γ–Fe_2O_3	*60*[a]	" "	4
δ–FeOOH	*14*[a]	" "	4
β–FeOOH	*11*[a]	" "	4
γ–FeOOH	*124*[a]	" "	4
α–FeOOH	*6*[a]	" "	4
α–Fe_2O_3	*3*[a]	oxidation of oxalate	4
γ–Fe_2O_3	*41*[a]	" "	4
δ–FeOOH	*11*[a]	" "	4
β–FeOOH	*10*[a]	" "	4
γ–FeOOH	*29*[a]	" "	4
α–FeOOH	*6*[a]	" "	4
Fe_2O_3	active	oxidation of oxalate	7
α–FeOOH	0.8[b]	oxidation of iodide by laser photolysis	24
α–FeOOH	$3 \cdot 10^{-8}$–$2 \cdot 10^{-5}$	formation of salicylate by	
		oxidation of benzoate	6
α–Fe_2O_3	enhanced dissolution of α–Fe_2O_3		
	in the presence of thiols		23
γ–Fe_2O_3	$3 \cdot 10^{-5}$	dissolution with citrate	8
α–Fe_2O_3	no activity	oxidation of polyacrylic acid,	
		formation of CO_2	10
α–Fe_2O_3	no activity	oxidation of cyanide	5
α–Fe_2O_3	no activity	oxidation of chloroacetate,	
		chloroform and chloral	this work
α–Fe_2O_3	no activity	formation of H_2O_2	this work

[a] *Relative* quantum yields calculated from pseudo–first–order rate constants given in Table 1 of ref. 4

[b] The authors of ref. 4, however, find equal yields of iodide oxidation in presence and absence of α–Fe_2O_3.

FIGURE CAPTIONS

Figure 1: Photocatalytic degradation of chloroacetate with concomitant formation of chloride in aqueous suspensions of metal oxides.

a) $2 \cdot 10^{-2}$ M ZnO powder, pH 8, air, UV light (300–400 nm) with I≃ $5 \cdot 10^{-3}$ M $h\nu$ min^{-1}; b) $6.3 \cdot 10^{-3}$ M TiO_2 (P25) powder, pH 5, air, UV light; c) $1 \cdot 10^{-3}$ M α–Fe_2O_3 colloid, pH 5, air, full lamp spectrum.

Figure 2: Photocatalytic degradation of chloroform in the presence of aqueous TiO_2 powder (P25, $6.3 \cdot 10^{-3}$ M , pH 5, air).

REFERENCES

[1] a) Fendler, J. H. *J. Phys. Chem.* 1985, **89**, 2730.

b) Harriman, A. in *Photochemistry*, Bryce–Smith, D.; Gilbert, A.; Eds. Royal Society of Chemistry, London: 1988, Vol. 19, pp 509–542. Since it is not the purpose of this paper to review this abundant literature, only two references are proposed.

[2] Kennedy, J. H.; Frese, K. W. *J. Electrochem. Soc.* 1978, **128**, 709.

[3] Iwanski, P.; Curran, J. S.; Gissler, W.; Memming, R. *J. Electrochem. Soc.* 1981, **128**, 2128.

[4] Leland, J. K.; Bard, A. J. *J. Phys. Chem.* 1987, **91**, 5076. This article extensively reviews further publications on the photoelectrochemical properties of iron oxide.

[5] Frank, S. N.; Bard, A. J. *J. Phys. Chem.* 1977, **81**, 1484.

[6] Cunningham, K. M.; Goldberg, M. C.; Weiner, E. R. *Environ. Sci. Technol.* 1988, **22**, 1090.

[7] Herrmann, J.–M.; Mozzanega, M.–N.; Pichat, P. *J. Photochem.* 1983, **22**, 333.

[8] Waite, T. D.; Morel, F. M. *J. Colloid Interface Sci.* 1984, **102**, 121.

[9] Faust, B. C.; Hoffmann, M. R. *Environ. Sci. Technol.* 1986, **20**, 943.

[10] Stramel, R. D.; Thomas, J. K. *J. Colloid Interface Sci.* 1986, **110**, 121.

[11] Fukasawa, T.; Iwatsuki, M.; Kawakubo, S.; Miyazaki, K. *Anal. Chem.* 1980, **52**, 1784.

[12] Faust, B. C.; Bahnemann, D. W.; Hoffmann, M. R. *J. Phys. Chem.*, submitted October 1988.

[13] Gerischer, H. in *Solar Energy Conversion*, Seraphin, B. O., Ed., Springer Verlag: Heidelberg, 1979.

[14] Kormann, C.; Bahnemann, D. W.; Hoffmann, M. R. *Environ. Sci. Technol.* 1988, **22**, 798.

[15] Brus, L. *J. Phys. Chem.* 1986, **90**, 2555.

[16] Bahnemann, D. W.; Kormann, C.: Hoffmann, M. R. *J. Phys. Chem.* 1987, **91**, 3789.

[17] Bielski, B. H. J.; Cabelli, D. E.; Arudi, R. L.; Ross, A. B. *J. Phys. Chem. Ref. Data* 1985, **14**, 1046.

[18] Stumm, W.; Morgan, J. J *Aquatic Chemistry*; Wiley: New York, 1981.

[19] Ollis, D. F. *Environ. Sci. Technol.* 1985, **19**, 480.

[20] Matthews, R. W. *Wat. Res.* 1986, **20**, 569.

[21] Pruden, A. L.; Ollis, D. F. *Environ. Sci. Technol.* 1983, **17**, 628.

[22] Kormann, C.; Bahnemann, D. W.; Hoffmann, M. R., in preparation.

[23] Waite, T. D.; Torikov, A.; Smith, J. D. *J. Colloid Interface Sci.* 1986, **112**, 412.

[24] Grätzel, M.; Kiwi, J.; Morrison, C. L.; Davidson, R. S.; Tseung, A. C. C. *J. Chem. Soc. Faraday Trans. 1*, 1985, **81**, 1883.

[25] Cotton, F. A.; Wilkinson, G. *Advanced Inorganic Chemistry*; Wiley: New York, 1980.

[26] Conklin, M. H.; Hoffmann, M. R. *Environ. Sci. Technol.* 1988, **22**, 899.

[27] Kraft, J.; v. Eldik, R. *Inorg. Chem.*, submitted 1988.

[28] Hatchard, C. G.; Parker, C. A. *Proc. R. Soc. Lond.* 1956, **A235**, 518.

[29] Balzani, V.; Carassiti, V. *Photochemistry of Coordination Compounds*, Academic Press, London: 1970.

[30] Baxendale, J. H.; Bridge, N. K. *J. Phys. Chem.* 1955, **59**, 783.

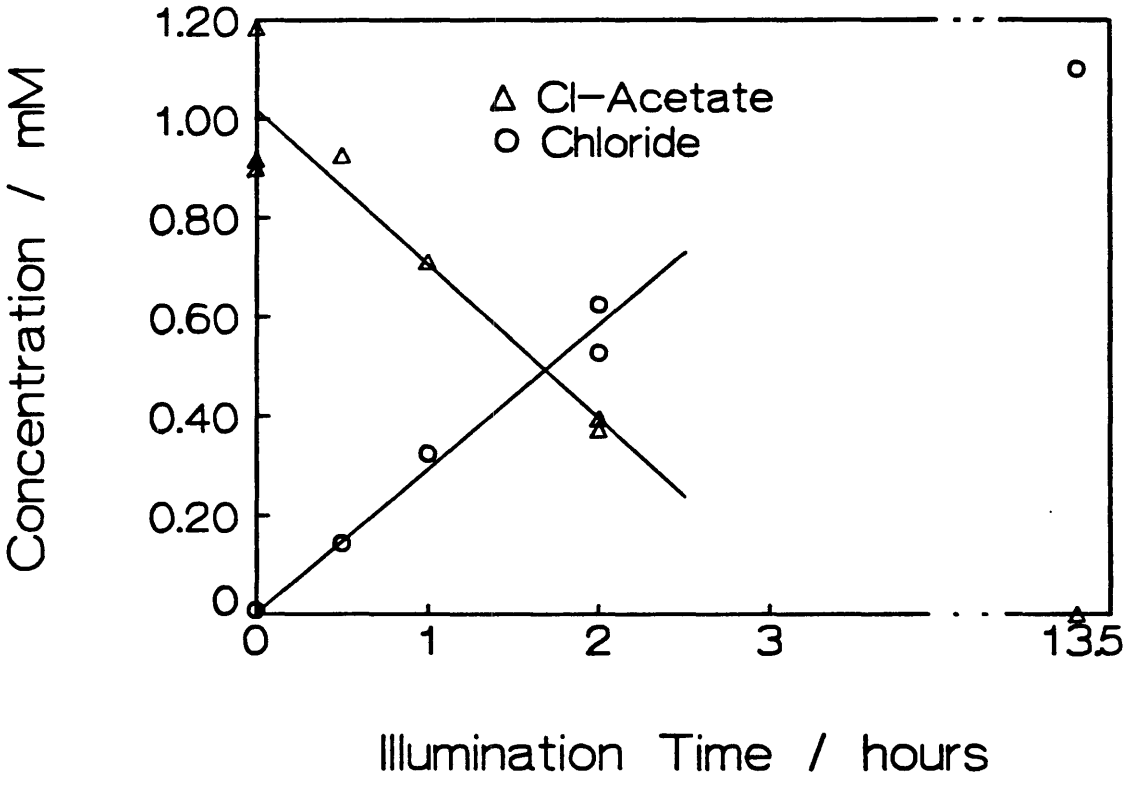
1.20
1.00
0.80
0.60
0.40
0.20
0
Concentration / mM
Δ Cl–Acetate
o Chloride
0
1
2
3
13.5
Illumination Time / hours

Figure 1a

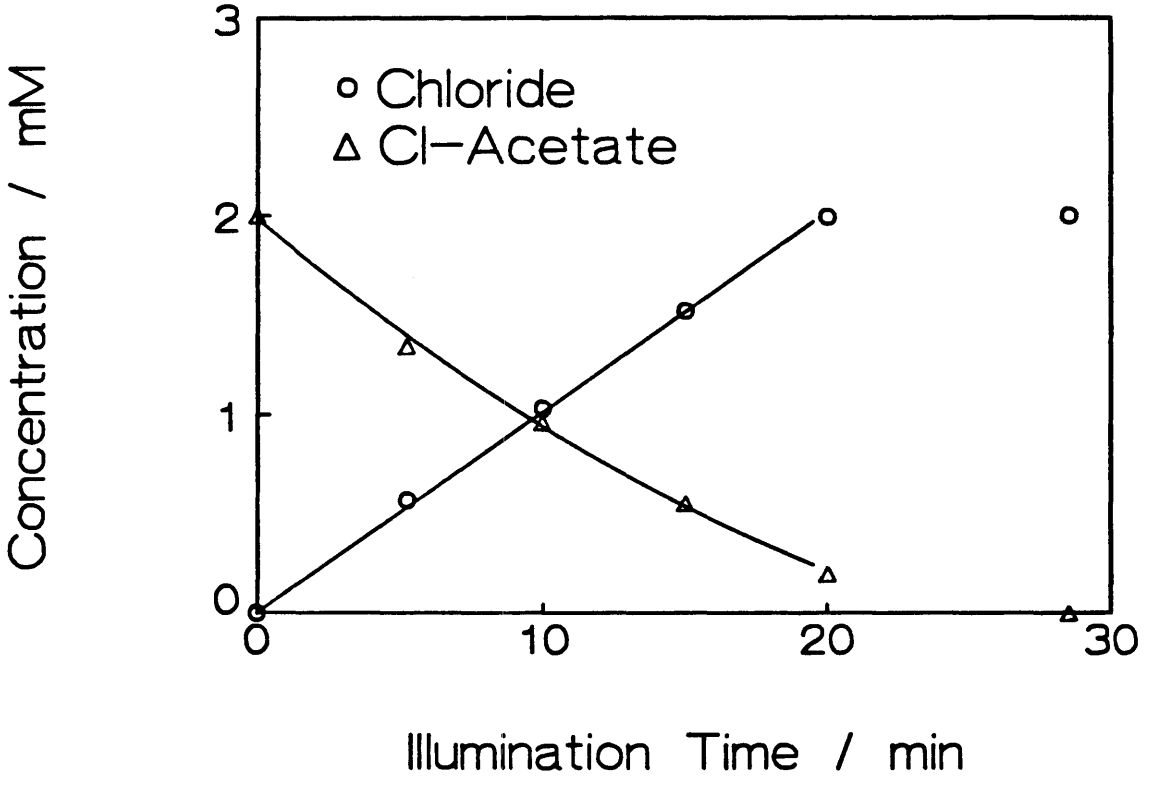
Concentration / mM
3
2
1
0
o Chloride
Δ Cl–Acetate
0
10
20
30
Illumination Time / min

Figure 1b

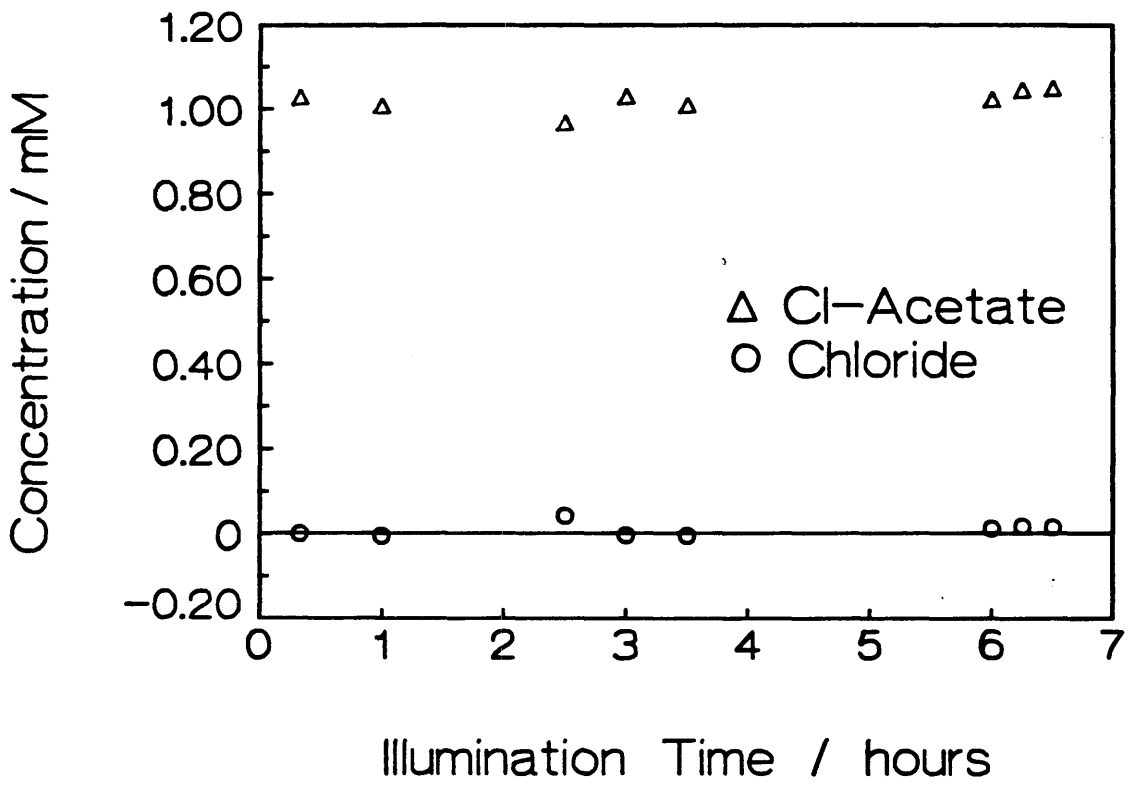
1.20
1.00
0.80
0.60
0.40
0.20
0
−0.20
Concentration / mM
0
1
2
3
4
5
6
7
Illumination Time / hours
Δ Cl−Acetate
o Chloride

Figure 1c

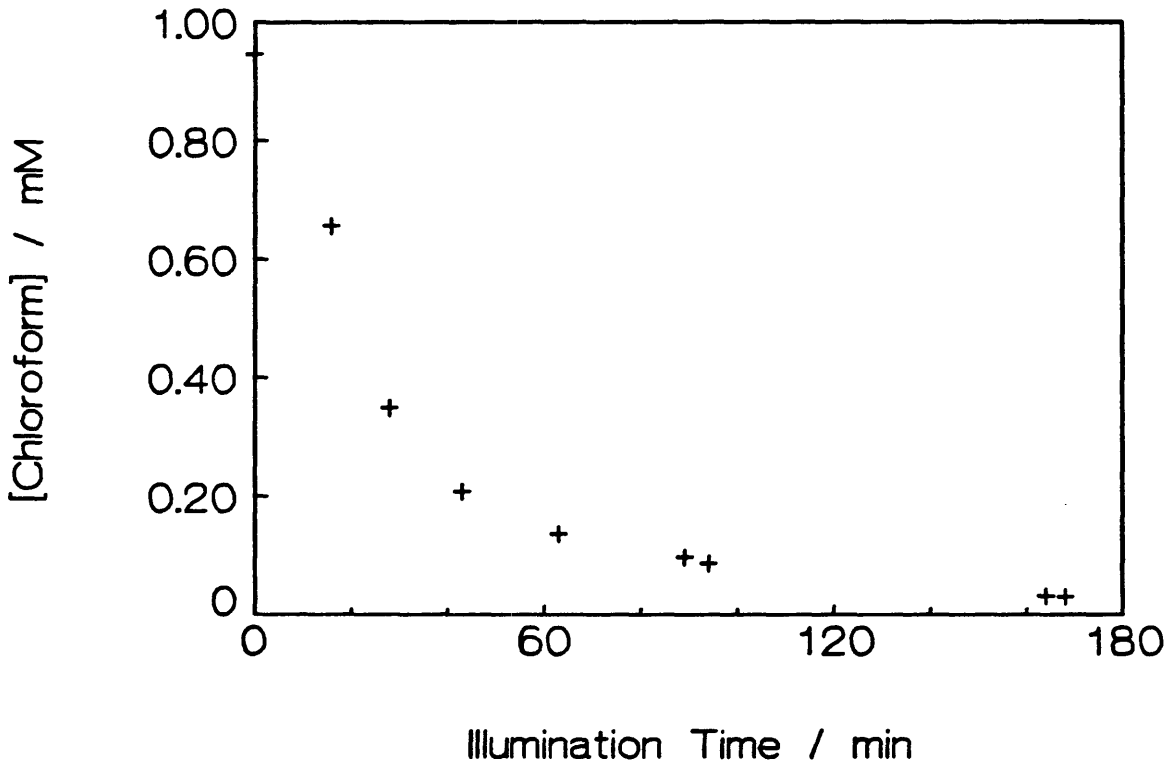
1.00
0.80
0.60
0.40
0.20
0
[Chloroform] / mM
0
60
120
180
Illumination Time / min

Figure 2

Chapter 7

ON THE REACTIVITY OF THE OXIDIZING SPECIES GENERATED BY PHOTOEXCITED TiO_2 PARTICLES IN AQUEOUS SUSPENSION.

INTRODUCTION

Over the past 15 years there has been an active interest in the photoelectrochemistry of small semiconductor oxide particles (cf. references in the preceding chapters). While the photo–reduction process is thought to occur through electrons from the conduction band or from trapped states, there is still an ongoing controversy about the nature and reactivity of the oxidation process. To distinguish between oxidation of solute molecules by photogenerated holes or by intermediate $OH^{\bullet}$ radicals is a subtle point in the discussion of the photoelectrochemistry of metal oxide particles. So far, only few studies concentrated on the mechanistic details of photo–oxidations by these materials. Some authors have obtained evidence for direct hole transfer,[1–2] others have postulated that the active species is the $OH^{\bullet}$ radical.[3–4] The $OH^{\bullet}$ radical may be generated from a hole reacting with surficial hydroxide, ≡TiOH, which involves subsequent substitution of the $OH^{\bullet}$ by OH^- at the Ti center.

$$OH^- + h^+_{vb} \longrightarrow OH^{\bullet} \qquad (1)$$

Alternatively, an outer–sphere electron transfer may occur between an oxidized $\equiv TiO^{\bullet}$ site and hydroxide concentrated within the electrical double layer, $\equiv TiOH_2^+ : OH^-$, adjacent to the charged metal oxide surface. In addition $OH^{\bullet}$ radicals may be generated by reduction of O_2 with conduction band electrons. In this reaction O_2^-/HO_2 and H_2O_2 are expected intermediates. However, H_2O_2 was found to be efficiently degraded by oxidation (formation of O_2).[5,6] It was found to inhibit the oxidation of organic molecules such as methyl orange as it is oxidized itself.[6] Hence, the formation of $OH^{\bullet}$ radicals by reduction of O_2 appears to be unlikely.

Research in this laboratory has provided strong evidence for oxidations occurring by $OH^{\bullet}$ radicals at pH > pH_{zpc} (pH of zero point of charge) but it cannot rule out that some of the observed oxidation rate is due to direct electron transfer from the organic donor molecule, e.g. acetate, to the hole at the particle surface.

We decided to study the oxidative degradation of acetate molecules in illuminated aqueous suspensions of TiO_2. Acetate is an ideal molecule because it can undergo two different reaction pathways depending on whether it is oxidized by an $OH^{\bullet}$ radical or whether its carboxylate moiety transfers an electron to a valence band hole.

We furthermore studied the rate of oxidation of organic anions and cations as a function of pH. While the oxidative degradation of anions such as acetate as a function of pH has been reported several times [1,7] the oxidative degradation of cations has not been examined in detail. The observed pH dependence of the rate of acetate oxidation was explained in terms of band shifting of the valence band $E_{vb} = +2.79 - 0.059 \cdot pH$ [V *vs.* NHE].[7] The effect of surface adsorption was ignored, however. Bahnemann et al. who studied the oxidation of MV^{2+} (methylviologen) obtained evidence for $OH^{\bullet}$ radical reactivity at pH 11.5.[4]

Our experimental findings cannot be explained with the conventional electrochemical and solid state expressions (e.g., the Nernst equation of the flat band potential). It is found that the effect of surface adsorption of the reactant molecules to the oxide surface is a predominant factor in the electrochemical reactivity of TiO_2 particles.

Background

The reaction of acetate with $OH^{\bullet}$ radicals has been studied by Neta et al.[8] and by von Sonntag and co–workers[9] using gamma– and pulse–radiolysis. The $OH^{\bullet}$ radicals react with acetate only [9] via abstraction of a hydrogen atom:

$$CH_3CO_2^- + OH^{\bullet} \longrightarrow {}^{\bullet}CH_2CO_2^- \xrightarrow{O_2} \xrightarrow[\text{fragmentation}]{\text{dimerisation}} \text{products} \qquad (2)$$

In aerated solutions oxygen adds rapidly to the ${}^{\bullet}CH_2CO_2^-$ radicals to give the corresponding peroxyl radicals which then react with each other to yield the final products. A complete material balance has been achieved for the $OH^{\bullet}$ reactions with acetate and the resultant products.[9] Glyoxylate and glycolate were found to be the principal products in a ratio of 2.7 : 0.7 at pH 7.8; formation of formate was not observed.

On the other hand, acetate can be selectively oxidized by electron transfer from the carboxylate group:[10]

$$CH_3CO_2^- \xrightarrow{ox} CH_3CO_2^{\bullet} \xrightarrow{O_2} \xrightarrow[\text{fragmentation}]{\text{dimerisation}} \text{products} \qquad (3)$$

As a consequence, a different product spectrum is obtained.[12] In this case formate is produced but no glyoxylate or glycolate.

In conclusion, it can be stated that the product spectrum for $CH_3CO_2^-$ photo–oxidation on semiconductor surfaces will depend on the reaction pathways that are actually followed (i.e. either reaction with $OH^{\bullet}$ or h^+_{vb}).

EXPERIMENTAL

Materials, experimental methods and instruments, e. g. the irradiation apparatus have been described previously (cf. preceding Chapters). Trichloro-acetic acid (Mallinckrodt) and chloroethylammonium hydrochloride (Aldrich) were used as received. The photo–degradation of acetate was performed by illuminating 2mL aliquots in a 1cm quartz cuvet with light $\lambda > 300$ nm.

A pH–stat titration technique was employed to determine the rates of degradation of organic molecules via the rates of OH^- consumption. The quantitative degradation (oxidation) of chlorinated hydrocarbon molecules $C_xH_yCl_z$ according to

$$C_xH_yCl_z + (x + \tfrac{y-z}{4})\, O_2 \longrightarrow x\, CO_2 + z\, HCl + (\tfrac{y-z}{2})\, H_2O \qquad (4)$$

leads to the formation of z protons which tend to decrease the pH. The autotitration system adds precisely z molecules of OH^- to keep the pH constant, while a computer records the derivative of the amount z with respect to time. The Radiometer autotitration system consisted of a pHM84 pH meter, a TTT80 titrator, and a ABU80 autoburet which was interfaced with an IBM PC–AT computer (An 8253–5 programmable timer on a MBC DASH–8 card was used to count pulses from the ABU80). The titrant solution (0.2 N NaOH) was kept under Ar gas and was calibrated with 0.100 N HCl (Baker Analyzed). The pH–stat reactor contained 100 mL of TiO_2 suspension (0.5 g/l) which was stirred and bubbled with oxygen; the actinometry (300 nm $< \lambda <$ 400 nm) was $I \simeq 10^{-4}$ M $h\nu$ min^{-1}. At pH$\geq$9 a low rate of hydroxide consumption was observed when suspensions of TiO_2 were illuminated in the absence of added organic molecules or when suspensions containing electron donors were stirred in the dark (or in

yellow light λ>500 nm). This was due to CO_2 scavenging; its contribution has been factored into the analysis. At pH<9 no hydroxide consumption due to oxidation of organic molecules was observed in suspensions of TiO_2 in the dark (or in yellow light λ>500 nm).

Ion exclusion chromatography was achieved with a Dionex 2000i HPIC equipped with a HPICE–AS1 separator column, a Ag/AgCl suppressor, and a conductivity detector. The eluent was 2.5 mM HCl.

RESULTS AND DISCUSSION

When suspensions of TiO_2 particles ([TiO_2] = 0.5 g/l, pH 11, [acetate] = 2 mM, [chloroacetate] = 1 mM) are illuminated with near UV light in the presence of air the quantitative degradation of the organic molecules can be observed readily (initial quantum yield: ca. 0.6%). The disappearance of chloroacetate has been shown to occur with a concomitant release of chloride ions in a 1 : 1 ratio (Chapter 6). The overall reaction stoichiometry is:

$$CH_3CO_2^- + 2\ O_2 \xrightarrow[h\nu]{TiO_2} 2\ CO_3^{2-} + 3\ H^+ \qquad (5)$$

and

$$CH_2ClCO_2^- + 1^1/_2\ O_2 + H_2O \xrightarrow[h\nu]{TiO_2} 2\ CO_3^{2-} + Cl^- + 4\ H^+ \qquad (6)$$

Glyoxylate, glycolate, and formate were found in a ratio 1 : 1 : 5 with an overall quantum yield of ≃0.3%. The production of glyoxylate and glycolate is taken as evidence for oxidation via $OH^\bullet$. However, the production of formate does not indicate unambiguously that some oxidation occurs via h^+_{vb}, because formate can also be formed via the oxidation of formaldehyde (which is a by–product in the reaction sequence of eqn 2).

Since the quantum yield of product formation is lower than the quantum yield of acetate degradation and the ratio of glyoxylate to glycolate is 1 : 1 instead of 2.7 : 0.7, it must be concluded that other mechanisms than those outlined in eqns 2–3 are operative. One likely possibility is that the intermediate peroxyl radicals are stabilized on the particle surface where they are

photodegraded before they can dimerize and fragment:

$$CH_3CO_2^- + OH^{\bullet}_{surf} \longrightarrow {}^{\bullet}CH_2CO_{2surf}^- \quad (7)$$

$${}^{\bullet}CH_2CO_{2surf}^- + O_2 \longrightarrow {}^{\bullet}O_2CH_2CO_{2surf}^- \quad (8)$$

$${}^{\bullet}O_2CH_2CO_{2surf}^- + 3\ OH^{\bullet}_{surf} \longrightarrow 2\ HCO_3^- + H^+ + H_2O \quad (9)$$

Similar surface stabilization effects have been observed previously in related systems.[12]

It is surprising that the photodegradation of acetate and chloroacetate occurs at all at pH 11. At this pH the particle surfaces are negatively charged due to the following surficial acid–base equilibria:[13–14]

$$\equiv TiOH_2^+ \rightleftharpoons \equiv TiOH + H^+ \qquad pK_{a1} = 4.5 \quad (10)$$

$$\equiv TiOH \rightleftharpoons \equiv TiO^- + H^+ \qquad pK_{a2} = 8.0 \quad (11)$$

Since pH 11 > pH_{zpc} (pH of zero point of charge; $pH_{zpc} = \frac{1}{2}\ (pK_{a1}+pK_{a2})$; TiO_2: $pH_{zpc} = 6.25$) the particle surfaces will be negatively charged and electrostatic repulsion will prevent the adsorption of acetate molecules. Adsorption to the particle, however, is a prerequisite for hole scavenging. Using the SURFEQL computer code described below the concentration of the Ti–acetate surface species is calculated to be less than 10^{-12} M. Matthews who studied the hydroxylation of benzoate in illuminated suspensions of TiO_2 found enhanced rates of oxidation at alkaline pH where benzoate is not expected to be bound to the surface.[13] It must be concluded that an oxidizing agent (i.e. the

$OH^{\bullet}$ radical) diffuses away from the surface and oxidizes acetate in the homogeneous solution.

At pH < pH_{zpc} this argument does not hold. When an aerated suspension of TiO_2 is illuminated in the presence of acetate at pH 5.6 only low concentrations of formate (quantum yield ca 0.4%) are formed. Thus a different mechanism appears to be operative, e.g. oxidation of acetate by holes and/or a very efficient degradation of the surface stabilized intermediates of eqns 2–3.

The rate of photo–oxidation of organic molecules in illuminated oxygenated suspensions of TiO_2 can be studied conveniently using the pH–stat titration technique. The oxidation of trichloroacetate (pK_a = 0.66), for instance, leads to the quantitative formation of CO_2, protons and chloride according to:

$$CCl_3CO_2^- + {}^1/_2\ O_2 + H_2O \xrightarrow[h\nu]{TiO_2} 2\ CO_2 + 2\ H^+ + 3\ Cl^- \qquad (12)$$

Quantitative degradation of chlorinated hydrocarbons in illuminated suspensions of TiO_2 yielding CO_2 and chloride has been shown to occur in a large number of cases.[15–16] The CO_2 will be present as HCO_3^- at 6.3 < pH < 10.3 and as CO_3^{2-} at pH> 10.3 Thus, depending on the pH of the suspension n(pH) = 2–6 molecules of OH^- need to be added for each molecule of $CCl_3CO_2^-$ that is oxidized in order to maintain the pH constant:

$$n(pH) = 2 + \frac{2}{1+10^{(6.3-ph)}} + \frac{2}{1+10^{(10.3-ph)}} \qquad (13)$$

The rate of chloroacetate degradation is then given by the rate of hydroxide consumption divided by n(pH).

Likewise, the rate of oxidation of chloroethylammonium ions according to

$$CH_2ClCH_2NH_3^+ + 4\tfrac{1}{2}\ O_2 \xrightarrow[h\nu]{TiO_2} 2\ CO_2 + 3\ H^+ + Cl^- + NO_3^- + 2\ H_2O \quad (14)$$

can be studied at pH < 9 ($pK_a \simeq 9$ is the estimated stability constant for the chloroethylammonium ion in water).

Figure 1 shows the rates of degradation of trichloroacetate and of chloroethylammonium ions (10 mM concentrations, respectively) as function of the pH. The rate of degradation of trichloroacetate is highest at low pH. Contrary to acetate and the other chloroacetates, the rate of oxidation of the trichloro derivative approaches zero as the pH $\longrightarrow$ pH_{zpc} (6.2) of TiO_2. This observation yields further evidence for the hypothesis that $OH^\bullet$ radicals diffuse away from the negatively charged TiO_2 surface to oxidize anions in the bulk of the solution. All acetates with a CH bond are susceptible to hydrogen abstraction by the $OH^\bullet$ radical. $CCl_3CO_2^-$ has no CH bond and does not react with the $OH^\bullet$ radical. On the other hand, at low pH the trichloroacetate molecule is bound to the oxide surface via its carboxylate moiety which can donate its electron to a photogenerated valence band hole according to

$$CCl_3CO_2^- + h_{vb}^+ \longrightarrow CCl_3CO_2^\bullet \longrightarrow CCl_3^\bullet + CO_2 \quad (15)$$

The carboxyradical will loose CO_2 yielding the $CCl_3^\bullet$ radical that is susceptible to further degradation reactions.

The rate of degradation of the cation (chloroethylammonium) is zero at pH 3. It reaches a maximum at pH$\simeq$ 8. At pH$\geq$9 a substantial release of acidity due to a dark reaction of the molecule –presumably an intramolecular cyclization associated with the deprotonation of the amino group– becomes

noticeable. The observed rate of oxidation at pH 9 is corrected for this dark effect (≃25 %). Only a negligible release of acidity is observed when a solution (10 mM) of chloroethylammonium hydrochloride is illuminated in the absence of TiO_2 at pH 7.7.

The enhanced rate of oxidation of cations at alkaline pH cannot be explained by a shift of the Fermi level of the semiconductor particles. In fact, the opposite behavior would be expected (i.e., lower rates of oxidation at high pH). Surface adsorption of the electron donor to the oxide particles appears to play a dominant role in the photoactivity of the catalyst.

Under our experimental conditions only one photon is absorbed per particle per ≃4 milliseconds,

$$TiO_2 + h\nu \xrightarrow{\tau = 4 \text{ msec}} h^+_{vb} + e^-_{vb} \qquad (15)$$

hence no significant accumulation of minority carriers (holes or surface $OH^\bullet$) will occur. Fast trapping of valence band holes as surficial hydroxl radicals ($OH^\bullet_{surf}$) has been postulated:[6]

$$h^+_{vb} + OH^-_{surf} \longrightarrow OH^\bullet_{surf} \qquad (16)$$

Regardless of whether the excited state is described in terms of an electron–hole pair or an electron–surface hydroxl radical pair, it is likely to be very short lived due to the well established reducing properties of the electron [17] and the strongly oxidizing properties of both the hole or the surface state.[6] The net result is that recombination will be first order for the minority carriers. The

half life of the electron hole pair has been found to be (30±15) ns for TiO_2 particles:[18]

$$h^+_{vb} + e^-_{vb} \xrightarrow{k_{rec}} \text{heat} \qquad k_{rec} \simeq 3 \cdot 10^7\ s^{-1} \qquad (17)$$

It is assumed that the rate determining step in the photo oxidation of organic molecules is the initial irreversible electron transfer/ hydrogen abstraction at the surface of the particle according to

$$h^+_{vb} \text{ or } OH^{\bullet}_{surf} + D_{surf} \xrightarrow{k_{ox}} D^+ \qquad (18)$$

In this treatment photo oxidations of the donor will be efficient if $k_{ox} \cdot [D_{surf}] > k_{rec}$. On the other hand, if the concentration of organic molecules at or near the surface is too low because of electrostatic repulsion between a charged surface and the charged donor, the catalyst will become deactivated before oxidizing the donor.

The observed rate dependence of the oxidation of anions or cations in illuminated suspensions of TiO_2 particles can be modeled using the SURFEQL computer code that was developed to perform equilibrium calculations of surface speciation.[19]

Figure 2a shows the surface speciation and the concentration of the complex between the TiO_2 surface and trichloroacetate as a function of pH assuming the following stoichiometry:

$$\equiv TiOH + H^+ + Ac^- \overset{K_{ac}}{\rightleftharpoons} \equiv TiAc + H_2O \qquad (19)$$

where $K_{ac} \simeq 10^4$ M^{-2} [20]. The concentration of the surface complex increases steadily below pH 5 in agreement with the observed increase of the rate of degradation of the molecule (cf Figure 1). At pH 11 the concentration of the surface complex is found to be 10^{-12} M.

Figure 2b shows the surface concentration of the complex between the TiO_2 surface and the organic ammonium ion according to

$$\equiv TiOH + H^+ + RNH_2 \overset{K_{am^+}}{\rightleftharpoons} \equiv TiRNH_2^+ + H_2O \qquad (20)$$

where $K_{am^+} = 10^{9.5}$ M^{-2}.[20]

The concentration of the surface complex increases at pH > 4 and reaches a maximum at pH $\simeq$ 9 corresponding to the pK_a of the ammonium ion. Comparison with the experimental rate of oxidation of the molecule in an illuminated suspension of TiO_2 (cf. Figure 1) shows good qualitative agreement.

A quantitative agreement is not expected since the photo–oxidation process depends on additional factors such as the efficiency of the charge separation process, that are likely to depend on the pH and on the surface charge. For instance, Bahnemann et al.[21] have found that hole scavenging becomes less efficient at low pH as repulsion of the hole from the positively charged surface leads to an enhanced recombination with the electron in the interior of the particle.

REFERENCES

1. Kraeutler, B.; Bard, A. J. *J. Am. Chem. Soc.* 1978, **100**, 5985.
2. Duonghong, D.; Ramsden, J.; Grätzel, M. *J. Am. Chem. Soc.* 1982, **104**, 2977.
3. Hair, M. L.; Harbour, J. R. *Adv. Chem. Ser.* 1980, **184**, 173.
4. Bahnemann, D. W.; Fischer, Ch.–H.; Janata, E.; Henglein, A. *J. Chem. Soc., Faraday Trans. 1*, 1987, **83**, 2559.
5. Hong, A. P., Bahnemann, D. W.; Hoffmann, M. R. *J. Phys. Chem.* 1987, **91**, 2109.
6. Brown, G. T.; Darwent, J. R. *J. Phys. Chem.* 1984, **88**, 4955.
7. Sakata, T. in "*Homogeneous and Heterogeneous Photocatalysis*", Pelizetti, E.; Serpone, N., Eds., Reidel, Boston: 1986.
8. Neta, P.; Simic, M.; Hayon, E. *J. Phys. Chem.* 1969, **73**, 4207.
9. Schuchmann, M. N.; Zegota, H.; von Sonntag, C. *Z. Naturforsch.* 1985, **40b**, 215.
10. Braun, W.; Rajbenbach, L.; Eirich, F. R. *J. Phys. Chem.* 1962, **66**, 1591.
11. Schuchmann, H.–P.; von Sonntag, C. *Z. Naturforsch.* 1984, **39b**, 217.
12. Bahnemann, D. W.; Mönig, J.; Chapman, R. *J. Phys. Chem.* 1987, **91**, 3782.
13. Stumm, W.; Morgan, J. J. *Aquatic Chemistry.*
14. Wehrli, B. Dissertation ETH Nr.8232, Zürich: 1987.
15. Ollis, D. F. *Environ. Sci. Technol.* 1985, **19**, 480.
16. Matthews, R. W. *Wat. Res.* 1986, **20**, 569.
17. Brown, G. T.; Darwent, J. R.; Fletcher, P. D. I. *J. Am. Chem. Soc.* 1985, **107**, 6446.

18. Rothenberger, G.; Moser, J.; Grätzel, M.; Serpone, N.; Sharma, D. K. *J. Am. Chem. Soc.* 1985, **107**, 8054.

19. Faughnan, J. SURFEQL – *An Interactive Code for the Calculation of Chemical Equilibria in Aqueous Solution.* W. M. Keck Laboratories, California Institute of Technology: Pasadena, CA, 1981.

20. Schindler, P.; Stumm, W. in *Aquatic Surface Chemistry*, Wiley–Interscience, New York, 1987, pp 83–110.

21. Bahnemann, D.; Henglein, A.; Spanhel, L. *Faraday Discuss. Chem. Soc.* 1984, **78**, 151.

FIGURE CAPTIONS

Figure 1 pH Dependence of the rate of degradation of trichloroacetate (+) and chloroethylammonium (Δ) ions in illuminated suspensions of TiO_2 (0.5 g/L). Actinometry (300 nm– 400nm) I $\simeq 10^{-4}$ Einstein l^{-1} min^{-1}.

Figure 2 Surface speciation of TiO_2 particles (P25, 0.5 g/L) in the presence of 10 mM concentrations of

a) trichloroacetate, solid line: $\equiv Ti{-}CO_2CCl_3$

b) chloroethylamine, solid line: $\equiv Ti^{\pm}NH_2CH_2CH_2Cl$

Calculated using the SURFEQL computer code (diffuse layer model, ionic strength: 0.01, pK_{a1}=4.5, pK_{a2}=8.0, surface area = 50 m^2g^{-1}). For further details see text.

+ : $\equiv TiOH_2^{\pm}$

○ : $\equiv TiOH$

Δ : $\equiv TiO^-$

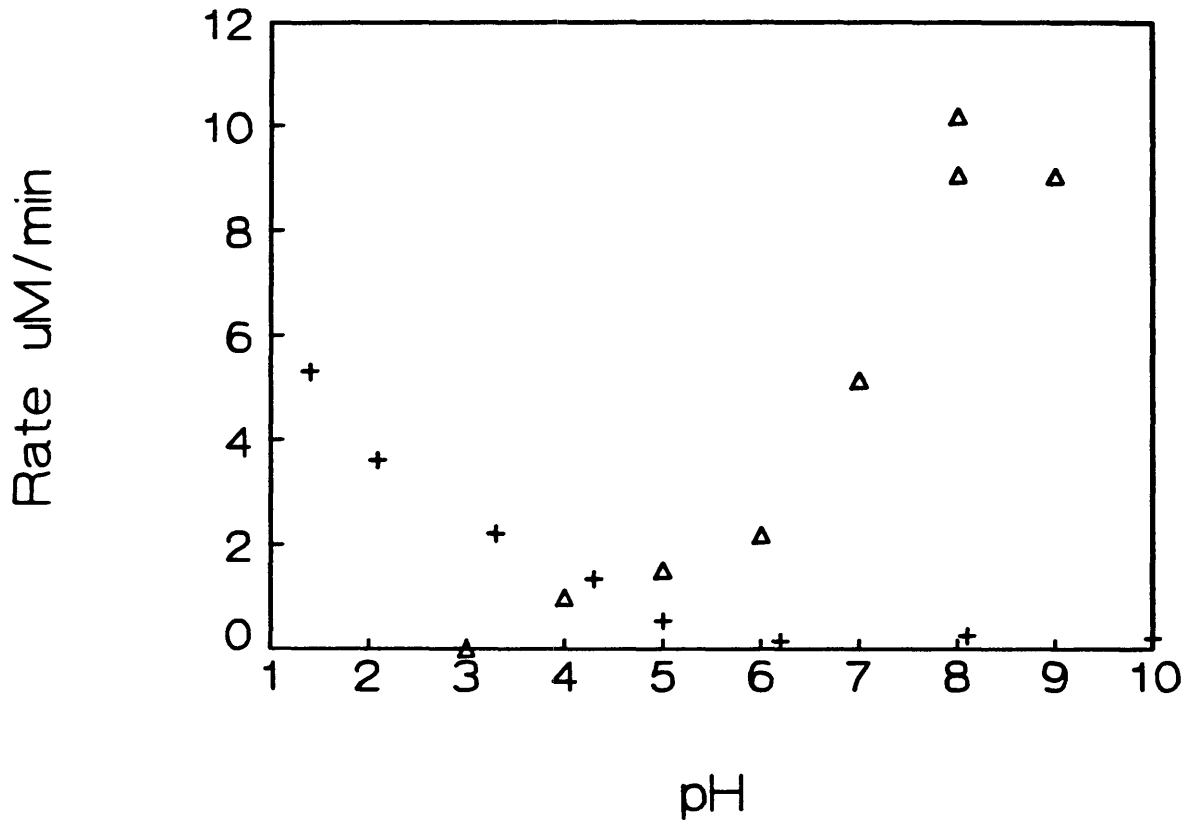

Figure 1

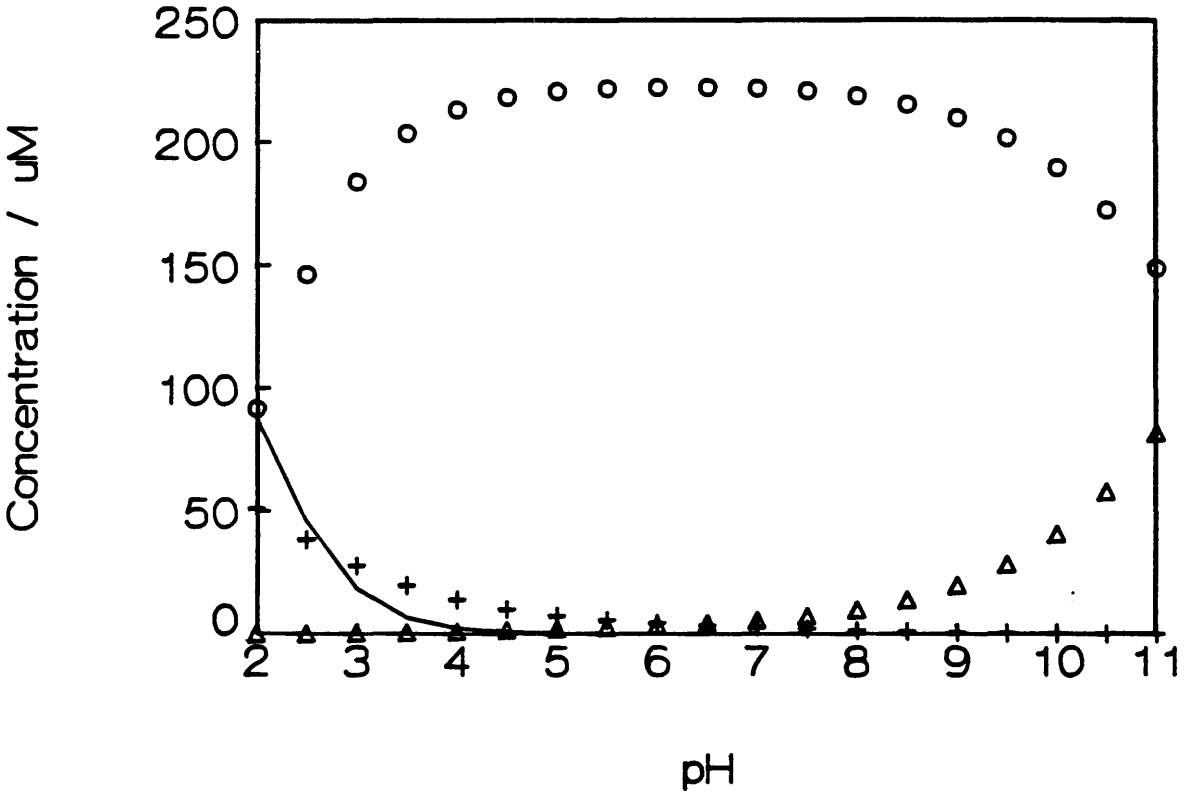

———: ≡Ti–CO_2CCl_3

\+ : ≡$TiOH_2^+$

o : ≡TiOH

Δ : ≡TiO^-

Figure 2a

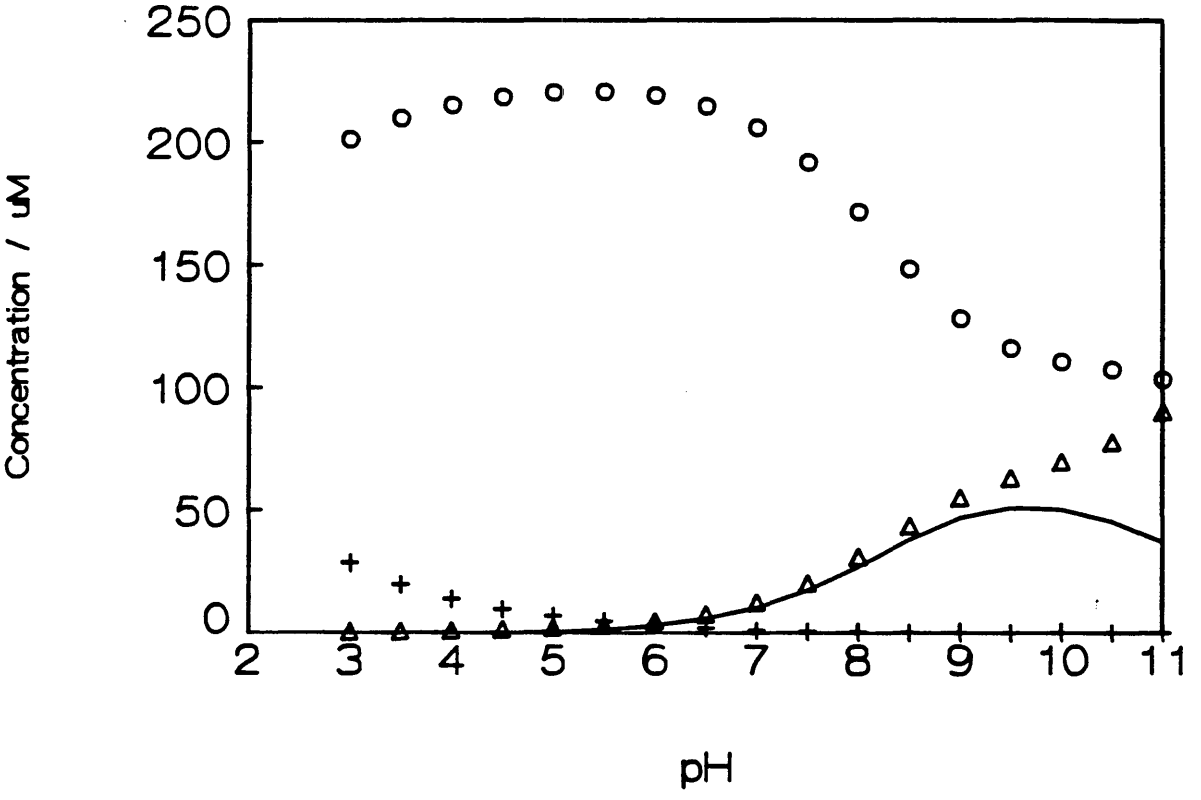

———: $\equiv Ti^{\pm}NH_2CH_2CH_2Cl$

\+ : $\equiv TiOH_2^{\pm}$

o : $\equiv TiOH$

Δ : $\equiv TiO^-$

Figure 2b

Chapter 8

RECOMMENDATIONS FOR FUTURE RESEARCH

In this thesis synthetic methods have been described to prepare ultrasmall colloidal oxide particles of ZnO, TiO_2, and α–Fe_2O_3. Other oxide materials can also be prepared in a highly dispersed form. Two recent articles have pointed out the necessity to synthesize novel ceramic materials that encompass not only advantageous properties such as chemical resistivity, hardness, wear resistance, high melting temperature, low density, low price, but also plasticity and ductility.[1–2] Karch et al. observed substantial plasticity, at 80–180 °C, of "nanocrystalline"* TiO_2 (made by oxidation of nanocrystalline titanium, average crystal size: ≈ 8 nm).[1] This could be explained by diffusion creep. Cations and anions diffuse from the compressed to the stretched side of each grain, round an intergranular circuit, thereby changing the shape of the grain. The authors estimated that the reduction of the crystal size from 10 μm (in conventional ceramics) to ≈ 10 nm improves the strain rate by a factor of 10^9, and the self–diffusivity by a factor of 10^3.[1]

While the common method of preparation of nanocrystalline ceramic materials is costly and energy intensive, as inert gas atmospheres, high vacuum, and very low temperatures (77K) are required, alternative syntheses of substantial quantities (g to kg amounts) of nanocrystalline material at fairly low cost (see, for example, Chapter 3 of this thesis) can be achieved.

*A nanocrystalline material is defined as a polycrystalline material whose crystal size is of the order of a few (1–10) nm.[1]

This thesis has also described numerous photochemical experiments: the photocatalytic formation and degradation of H_2O_2 and organic peroxides, the degradation of chlorinated hydrocarbons using aqueous suspensions of TiO_2 and ZnO. One of the most promising applications of these catalysts is the degradation of toxic molecules (e. g. chlorinated hydrocarbons, or even NO_3^-) by using inexpensive sunlight. Several workers have already made important contributions to this field,[3–4] yet there need to be further studies to unravel mechanistic details of these photodegradation reactions and subsequent demonstrations of practicable feasibility. The transparent colloidal materials prepared as a part of this thesis research lend themselves ideally to mechanistic studies using fast optical techniques.

The efficiency of photocatalytic and photosynthetic reactions of metal oxide particles is dependent on and limited by the rather short lifetime of the excited state. Efficient relaxation channels are provided by fluorescence and radiationless transitions (ZnO, bandgap fluorescence: $\tau_{\frac{1}{2}}<50$ ps, surface fluorescence $\tau_{\frac{1}{2}}<20$ ns (Chapter 2); TiO_2 lifetime of an electron hole pair $\tau_{\frac{1}{2}}\simeq 20$ ns [5]).

Recently Hong et al. described a catalyst based on TiO_2 particles to which an electron relay (Co–Tetrasulfophtalocyanine) was covalently bound (Caltech Thesis, Andrew P. Hong, 1987; see also Chapter 5 of this thesis). A significant enhancement of the rate of electron transfer to oxygen was found, and enhanced rates of oxidation were postulated. It thus appears very promising to modify the colloidal catalysts prepared in this thesis research in a similar fashion in order to obtain more efficient charge separation. In view of the fact that $OH^\bullet$ radicals are generated upon photoexcitation of TiO_2 particles (Chapter 7), the attached electron relay must be resistent to oxidation by this species. It is anticipated that by preparing perchlorinated or perfluorinated electron relays, this problem can be solved.

REFERENCES

[1] Karch, J.; Birringer, R.; Gleiter, H. *Nature* 1988, **330**, 556.

[2] Cahn, R. W. *Nature* 1988, **332**, 112.

[3] Ollis, D. F. *Environ. Sci. Technol.* 1985, **19**, 480.

[4] Matthews, R. W. *Wat. Res.* 1986, **20**, 569.

[5] Rothenburger, G.; Moser, J.; Grätzel, M.; Serpone, N.; Sharma, D. K. *J. Am. Chem. Soc.* 1985, **107**, 8054.